FACULTY OF ENGINEERING
AND ARCHITECTURE

Structural Health Monitoring for Bridges Using Metaheuristic Optimization Algorithms Combined with Artificial Neural Network

Ngoc Hoa Tran

Doctoral dissertation submitted to obtain the academic degree of

Doctor of Civil Engineering

Supervisors

Prof. Magd Abdel Wahab, PhD* - Prof. Tien Thanh Bui, PhD** - Prof. Em. Guido De Roeck, PhD***

* Department of Electromechanical, Systems and Metal Engineering
Faculty of Engineering and Architecture, Ghent University

** Department of Bridge Engineering and Underground Infrastructure
Faculty of Civil Engineering, University of Transport and Communications, Vietnam

***Department of Civil Engineering
Faculty of Engineering Science, KU Leuven

February 2022

GHENT
UNIVERSITY

FACULTY OF ENGINEERING AND ARCHITECTURE

Structural Health Monitoring for Bridges Using Metaheuristic Optimization Algorithms Combined with Artificial Neural Network

Ngoc Hoa Tran

Doctoral dissertation submitted to obtain the academic degree of
Doctor of Civil Engineering

Supervisors

Prof. Magd Abdel Wahab, PhD* - Prof. Tien Thanh Bui, PhD** - Prof. Em. Guido De Roeck, PhD***

* Department of Electromechanical, Systems and Metal Engineering
Faculty of Engineering and Architecture, Ghent University

** Department of Bridge Engineering and Underground Infrastructure
Faculty of Civil Engineering, University of Transport and Communications, Vietnam

***Department of Civil Engineering
Faculty of Engineering Science, KU Leuven

February 2022

GHENT UNIVERSITY

ISBN 978-94-6355-570-8
NUR 955, 956
Wettelijk depot: D/2022/10.500/11

Members of the Examination Board

Chair

Prof. Patrick De Baets, PhD, Ghent University

Other members entitled to vote

Samir Khatir, PhD, Ghent University
Yong Ling, PhD, Ghent University
Prof. Timon Rabczuk, PhD, Bauhaus Universität-Weimar, Germany
Yunlai Zhou, PhD, Xi'an Jiaotong University, China

Supervisors

Prof. Magd Abdel Wahab, PhD, Ghent University
Prof. Tien Thanh Bui, PhD, University of Transport and Communications, Vietnam
Prof. Em. Guido De Roeck, PhD, KU Leuven

Research Institute
Ghent University
Faculty of Engineering and Architecture
Department of Electromechanical, Systems and Metal Engineering.
Laboratory Soete http://www.soetelaboratory.UGhent.be
Technologiepark 46, B-9052 Zwijnaarde, Belgium
Tel: +32 9 331 0477
Email: hoa.tran@ugent.be; ngochoa@utc.edu.vn

I would like to dedicate this thesis to my loving parents, family

For their endless love, support and encouragement

Acknowledgements

First, I would like to express my deep gratitude to Professor Magd Abdel Wahab, Professor Bui Tien Thanh, and Professor Guido De Roeck who gave me a great opportunity to participate in this wonderful research project (VLIR-UOS project) and to study at Ghent University. Thanks to their patient guidance and valuable advice through my research process. I feel extremely fortunate to have the chance to meet and work with them. To be honest, I have learned a lot from them, not only about knowledge but also about kindness and passion for science. Indubitably, without their dedicated help, I would not be able to complete this thesis. I also would like to thank committee members for supporting me in my defense and giving me brilliant suggestions.

I sincerely express my special appreciation to my colleagues at the University of Transport and Communications (UTC) and especially my colleagues at the Department of Bridge Engineering and Underground Infrastructures, who have facilitated and helped me throughout my research.

I am truly grateful to the VLIR-UOS project and the Bijzonder Onderzoeksfonds (BOF) scholarship of Ghent University. Without their financial support, it would be difficult for me to cover the costs of the research process.

I would like to thank my colleagues at Laboratory Soete, Department of Electrical Energy, Systems and Automation, Faculty of Engineering and Architecture, Ghent University for their friendly help and encouragement. I would like to extend my sincere thanks to Mrs. Georgette D'Hont for her patience to help me deal with all administrative problems. In particular, I would especially like to thank Dr.Samir Khartir, MSc. Le Xuan Thang, Dr. Yong Ling, Ph.D. Ho Viet Long, Dr. Nguyen Huong Duong, Ph.D. Nguyen Tran Hieu, Ph.D. Nguyen Ngoc Lan…and other members of my research team for their discussions, advice, and encouragement.

I also sincerely thank my best friends Nguyen Van Binh, Ho Khac Hanh, Pham Hong Tuyen, Nguyen Thanh Do, Nguyen My Yen, Luong Ngoc Quang, Nguyen Hoang Yen, Dinh Tien Dung, Giang Pham... and other friends in Vietnam, and in Belgium for always encouraging and helping me overcome the most difficult times in the research process.

I would also like to thank Prof Edwin Reynders, a researcher at the Department of Civil Engineering, KU Leuven University, Belgium, and Dr. Leqia He, a researcher at Sustainable and Innovative Bridge Engineering Research Center College of Civil Engineering, Fuzhou University, PR China for providing the data of the measurement campaign used in my thesis.

Finally, I would like to express my deepest gratitude to my family, parents (Tran Van Tan, Ta Thi Thuan), brothers (Tran Ngoc Dung), sisters (Tran Thi Tuyet, Tran Thi Nhung, Tran Thi Huong), brothers-in-law (Nguyen Manh Chien, Pham Van Thanh, Ngo Xuan Thi), sister-in-law (Vu

Thi Oanh), and nephews. They love me unconditionally, always trust and encourage me to have more motivation to complete my Ph.D. program.

Hoa Tran

Ghent, 06 January 2022

Contents (ALT+X)

Summary

During service life, engineering infrastructures are inevitably subjected to loads of devastating effects, such as earthquakes, storms, extreme weather, overload or accidental loads, etc., all of which can significantly reduce the operational effectiveness and lifespan. Therefore, during recent decades, Structural Health Monitoring (SHM) systems have been widely deployed and captured much attention from researchers around the world. The task of the SHM system is to detect damages as early as possible based on the obtained data. This plays a crucial role in assessing structural behavior most accurately before arriving at any repair decision.

The objective of this thesis is to deal with the shortcomings of traditional Metaheuristic Optimization (MO) algorithms and Artificial Neural Network (ANN), develop strong tools to increase the accuracy and effectiveness of SHM. Specifically, this thesis conducts SHM for bridges using MO algorithms combined with ANN, which can be summarized in the following main points.

Firstly, the thesis deals with an inverse problem to update and identify the stiffness conditions of typical joints of a large-scale truss bridge using Particle Swarm Optimization (PSO) and Genetic Algorithm (GA). For steel truss bridges, connections of truss members are the most complicated unknown parameters. The assumption of rigid or pinned joints has little effect on the result of static analysis. However, the result of dynamic analysis is extremely sensitive to this assumption. Most of the researchers have employed pin and rigid connections when predicting structural dynamic behavior. The results of this thesis demonstrate that both kinds of this connection cannot reflect exactly the dynamic characteristic of the bridge, because while rigid links overestimate the stiffness of the joint, pin links omit its stiffness. By contrast, the assumption of semi-rigid links (using rotational springs) can provide a good agreement between the numerical model and measurement.

To overcome the drawbacks of traditional PSO, an Improved Particle Swarm Optimization (IPSO) is applied. PSO is a popular metaheuristic algorithm applied successfully in numerous fields over the last decades. However, since PSO applied fixed parameters directly relating to the velocity of particles, this may decrease its efficiency in tackling optimization problems.

The thesis proposes coupling Orthogonal Diagonalization (OD) with IPSO (ODIPSO) to deal with the huge computational cost of PSO. The application of PSO and other MO algorithms is time-consuming since these algorithms employ all populations to seek the best solution through

iterations. This makes them difficult to apply for optimization problems of large-scale structural models. For ODIPSO, OD is applied to arrange the position of particles and to select only particles with the best solution for the next iterations, which helps to reduce the computational cost dramatically. There are several significant features of ODIPSO: (1) IPSO is employed to make particles more flexible during the process of looking for the best solution; (2) only one guide is used to update the velocity of particles instead of utilizing both guides, consisting of the local best and the global best; and (3) in each iteration, only the velocity and the position of the best particles are updated. The results show that ODIPSO not only outperforms PSO, IPSO and OD combined with PSO (ODPSO) in terms of accuracy but also dramatically reduces the computational time compared to PSO and IPSO.

This thesis also introduces the use of Wireless Triaxial Sensors (replacing Classical Wired Systems) to obtain structural dynamic characteristics. The appearance of Wireless Triaxial Transducers increases significantly the freedom in designing an Ambient Vibration Test (AVT).

To deal with the local minimum problem of ANN, a novel ANN based on the search capacity of Cuckoo Search (CS) is proposed to detect damages for a truss bridge. With recent ground-breaking advances, ANN has been applied widely in numerous fields currently. However, because of the application of backpropagation algorithms based on Gradient Descent (GD) techniques, the network of ANN may be trapped in local

minima, especially if its starting point is not on the same side of the global best or the network contains too many local minima. This drawback may reduce the accuracy and effectiveness of ANN. To transcend these limitations of ANN, numerous researchers have employed algorithms based on global search techniques to eliminate the initial local minima of the network by looking for a beneficial starting point. Nevertheless, those solutions are only valid under certain circumstances when the network only contains a few local minima, and they are distributed on the same side. With complex problems such as SHM, the network always exists of different error surfaces with numerous widely distributed local minima. The approach of the selection of a good starting position for the network may no longer be useful. In this thesis, CS algorithm based on the global search technique is employed to work parallel with ANN during the process of training the network. This win-win approach has both advantages of GD techniques (fast convergence) and stochastic search techniques (avoiding being trapped in local minima). The core idea of the proposed method is recapped as follows: (1) ANN using the GD technique is first applied to speed up convergence; (2) if the network gets stuck in local minima, CS with global search capability is applied to assist particles in escaping from local minima; (3) the GD technique is applied again to increase the convergence speed. Steps 2 and 3 are repeated until the target is achieved. The results showed that the proposed approach completely outperforms CS, ANN, and other hybrid ANN in terms of accuracy and considerably reduces calculational costs compared to CS.

It is commonly acknowledged that a high computational cost is putting up a major barrier to the real application of optimization algorithms, as well as ANN. Optimization algorithms that rely on stochastic techniques during the searching process are extremely time-consuming, whereas training data of ANN contains millions of matrices that need to be dealt with. Therefore, in this work, a vectorization technique is used for the training data to reduce the dimension of data. Hence, the computational time is significantly reduced.

To consider the effectiveness of the proposed methods, both numerical models and measurements are employed. The proposed methods are evaluated through numerical models and then compared with the results from the experiments in which numerous large-scale bridges, with large Degrees Of Freedom (DOF), are used to evaluate the effectiveness of the proposed methods.

Samenvatting

Tijdens hun levensduur worden bouwkundige infrastructuren onvermijdelijk blootgesteld aan tal van verwoestende effecten (bijv. aardbevingen, storm, extreem weer, overbelasting, accidentele belastingen, enz.), die allemaal de operationele efficiency en levensduur aanzienlijk kunnen verminderen. Daarom zijn de afgelopen decennia systemen voor structurele gezondheidsmonitoring (SHM) op grote schaal ingezet en hebben ze veel aandacht getrokken van onderzoekers over de hele wereld. De taak van het SHM-systeem is om schade zo vroeg mogelijk op te sporen op basis van de verkregen gegevens. Dit speelt een cruciale rol bij het zo nauwkeurig mogelijk beoordelen van het structurele gedrag in voorbereiding van een mogelijke reparatie ingreep.

Het doel van dit proefschrift is om de tekortkomingen van traditionele optimalisatie-algoritmen en machine-learning aan te pakken, en tevens sterke tools te ontwikkelen om de nauwkeurigheid en effectiviteit van SHM te vergroten. Dit proefschrift focust op SHM voor bruggen met behulp van Metaheuristic Optimization (MO) algoritmen in combinatie met artificieel neuraal netwerk (ANN), wat kan worden samengevat in de volgende hoofdpunten.

Allereerst behandelt het proefschrift een invers probleem om de stijfheidseigenschappen van typische verbindingen van een grootschalige vakwerkbrug aan te passen en te identificeren met behulp van deeltjeszwermoptimalisatie (PSO) en genetisch algoritme (GA). Voor

stalen vakwerkbruggen zijn verbindingen van vakwerkdelen de moeilijkst te modelleren onderdelen. De aanname van starre of scharnierende verbindingen heeft relatief weinig effect op het resultaat van een statische analyse. Het resultaat van een dynamische analyse is echter uiterst gevoelig voor deze aanname. De meeste onderzoekers hebben scharnierende of starre verbindingen gebruikt bij het voorspellen van het structureel dynamisch gedrag. De resultaten van dit proefschrift laten zien dat beide soorten verbindingen niet precies de dynamische eigenschappen van de brug kunnen weergeven, omdat starre verbindingen de rotatiestijfheid van de verbinding overschatten in tegenstelling tot scharnierende verbindingen die deze stijfheid volledig negeren. Daarentegen kan de aanname van halfstijve verbindingen (met behulp van rotatieveren) in het rekenmodel een goede overeenkomst tussen numerieke resultaten en corresponderende metingen opleveren.

Om de nadelen van traditionele PSO te overwinnen, An IPSO wordt voorgesteld. PSO is een bekend metaheuristisch algoritme dat de afgelopen decennia met succes op tal van gebieden is toegepast. PSO heeft echter grote nadelen die de efficiëntie bij het aanpakken van optimalisatieproblemen kunnen verminderen. Een mogelijk nadeel van PSO is voortijdige convergentie, wat leidt tot een laag convergentieniveau, met name bij complexe zoekproblemen met meerdere optima. Anderzijds hangt PSO niet alleen in grote mate af van de kwaliteit van de initiële populaties, maar is het bovendien onmogelijk om de kwaliteit van nieuwe generaties te verbeteren. Als de posities van de initiële deeltjes ver

verwijderd zijn van het globale beste, kan het moeilijk zijn om de beste oplossing te vinden.

Het proefschrift stelt voor om orthogonale diagonalisatie (OD) te koppelen aan IPSO (ODIPSO) om de zeer hoge rekenkosten van PSO aan te kunnen. Naast het probleem van voortijdige convergentie, is de toepassing van PSO en andere EA's tijdrovend omdat deze algoritmen alle populaties gebruiken om via iteraties de beste oplossing te zoeken. Dit maakt ze moeilijk toepasbaar voor optimalisatieproblemen van grootschalige structuurmodellen. Voor ODIPSO wordt OD toegepast om de positie van deeltjes te rangschikken en om alleen deeltjes met de beste oplossing te selecteren voor de volgende iteraties, wat helpt om de rekenkosten drastisch te verlagen. Er zijn verschillende belangrijke kenmerken van ODIPSO: (1) IPSO wordt gebruikt om het probleem van voortijdige convergentie van PSO aan te pakken; (2) Er wordt slechts één richtlijn gebruikt om de snelheid van deeltjes bij te werken in plaats van beide richtlijnen, bestaande uit de lokale beste en de globale beste; en (3) In elke iteratie worden alleen de snelheid en de positie van de beste deeltjes bijgewerkt. De resultaten laten zien dat ODIPSO niet alleen beter presteert dan PSO, IPSO en OD in combinatie met PSO (ODPSO) in termen van nauwkeurigheid, maar ook de rekentijd drastisch vermindert in vergelijking met PSO en IPSO.

Dit proefschrift illustreert ook het gebruik van draadloze triaxiale sensoren (ter vervanging van klassieke bekabelde systemen) om structurele dynamische eigenschappen te verkrijgen. Het inzetten van

draadloze triaxiale sensoren vergroot aanzienlijk de vrijheid van ontwerp bij een operationele trillingstest (Ambient Vibration Test: AVT).

Om het lokale minimumprobleem van ANN aan te pakken, wordt een nieuw ANN voorgesteld gebaseerd op de zoekcapaciteit van koekoek-zoeken (Cuckoo Search: CS) om schade in en een vakwerkbrug te detecteren. Dank zij recente baanbrekende ontwikkelingen wordt ANN tegenwoordig op veel gebieden en op grote schaal toegepast. Vanwege de toepassing van achterwaartse propagatiealgoritmen op basis van gradiëntafdaling (GD)-technieken, kan het netwerk van ANN echter vastzitten in lokale minima, vooral als het startpunt niet aan dezelfde kant van het globale beste ligt of als het netwerk te veel lokale minima bevat. Dit nadeel kan de nauwkeurigheid en effectiviteit van ANN verminderen. Om deze beperkingen van ANN te overstijgen, hebben talrijke onderzoekers algoritmen gebruikt die gebaseerd zijn op globale zoektechnieken om de initiële lokale minima van het netwerk te elimineren via het zoeken naar een gunstig startpunt. Desalniettemin zijn die oplossingen alleen geldig onder bepaalde omstandigheden wanneer het netwerk slechts enkele lokale minima bevat en ze aan dezelfde kant worden verspreid. Bij complexe problemen zoals SHM bestaat het netwerk altijd uit verschillende fout oppervlakken met talrijke wijdverspreide lokale minima. De aanpak van het selecteren van een goede uitgangspositie voor het netwerk is dan wellicht niet meer zinvol. In dit proefschrift wordt een CS-algoritme, gebaseerd op de globale zoektechniek, gebruikt om parallel met ANN te werken tijdens het

trainingsproces van het netwerk. Deze win-win-benadering heeft zowel de voordelen van GD-technieken (snelle convergentie) als van stochastische zoektechnieken (voorkomen om vast te zitten in lokale minima). Het kernidee van de voorgestelde methode wordt als volgt samengevat:
(1) ANN met behulp van de GD-techniek wordt eerst toegepast om deconvergentie te versnellen;

(2) Als het netwerk vastloopt in lokale minima, wordt CS met globale zoekmogelijkheid toegepast om deeltjes te helpen ontsnappen uit lokale minima;

(3) De GD-techniek wordt opnieuw toegepast om de convergentiesnelheid te verhogen. Stappen 2 en 3 worden herhaald totdat het doel is bereikt. De resultaten toonden aan dat de voorgestelde aanpak CS, ANN en andere hybride ANN overtreft in termen van nauwkeurigheid en bovendien de rekenkosten aanzienlijk verlaagt in vergelijking met CS.

Het wordt algemeen erkend dat hoge rekenkosten een grote barrière vormen voor de echte toepassing van optimalisatie-algoritmen en ook ANN. Optimalisatie-algoritmen waarvan het zoekproces gebaseerd is op stochastische technieken, zijn extreem tijdrovend, terwijl trainingsgegevens van ANN miljoenen matrices bevatten waarmee moet gewerkt worden. Daarom wordt in dit proefschrift voor de trainingsgegevens een vectorisatietechniek gebruikt om de

gegevensdimensie te verkleinen. Hierdoor wordt de rekentijd aanzienlijk verkort.

Om de effectiviteit van de voorgestelde methoden te beoordelen, worden zowel numerieke modellen als metingen gebruikt. De voorgestelde methoden worden geëvalueerd door middel van numerieke modellen en vervolgens vergeleken met de resultaten van de experimenten. Tal van grootschalige bruggen, met een groot aantal vrijheidsgraden (DOF) worden gebruikt om de effectiviteit van de voorgestelde methoden te evalueren.

List of Figures

List of Tables

Nomenclature & Abbreviation

SHM	Structural Health Monitoring
FVT	Forced Vibration Test
AVT	Ambient Vibration Test
OMA	Operational Modal Analysis
FEM	Finite Element Model
GA	Genetic Algorithm
IPSO	Improved Particle Swarm Optimization
OD	Orthogonal Diagonalization
MOVA	Monitoraggio Delle Vibrazioni Ambientali
MOSS	Monitoraggio Dello Stato Di Salute
OMAX	Exogenous Forces
PSO	Particle Swarm Optimization
CS	Cuckoo Search
ML	Machine Learning
ANN	Artificial Neural Network

ODIPSO	OD combined with improved particle swarm optimization IPSO
ODPSO	OD combined with PSO
GD	Gradient Descent
DOF	Degrees of freedom
IGA	Isogeometric Analysis
AC	Ant Colony
MAC	Modal Assurance Criterion
ICS	Artificial Intelligence
OSELM	Online Sequential Extreme Learning Algorithm
MLP	Multi-Layered Perceptron
RBFNN	Radial Basis Function Neural Network
HFS	Hybrid Flow Shop
AI	Artificial Intelligence
FRFs	Frequency Response Functions
WPT	Wavelet Packet Transform
BFG	Bidirectional Functionally Graded

MSE	Mean Square Error
ANN-OWPT	A combination between ANN and the optimal wavelet-packet transform
Eqs	Equations
X_t^i, X_{t+1}^i	The position of element i, at time t and t+1, respectively
V_t^i, V_{t+1}^i	The velocity of element i, at time t and t+1, respectively
c_1 and c_2	The cognition learning factor and social learning factor
w	The inertia weight parameter
G_t^{best}	The global best at the time t
P_t^{best}	The local best at the time t
P_a	Probability
α	The step size
n	The number of population
m	The number of uncertain parameter
$(.)^T$	Transpose operation

λ	Lévy flight
β	The coefficient of Levy flight
δ	Parameter determined based on a random walk
T	The constriction factor
Q	The total number of iterations
w_{start}	The value of initial functional inertia weight
w_{end}	The value of functional inertia weight in the last iteration
$X_0, V_0, P_0, G_0^{best}$	The generation of initial position, velocity, the local best, and the global best of particles at the first step, respectively.
u_1, and u_2	One of the best solution of particles at the first step
q_1, and q_2	Particles after crossover
$f(X)$	The objective function
X_{min} and X_{max}	Lower and upper bound of search space.
m_0	${m_0}^{th}$ iteration
a	Active group

$n-a$	Passive group
$(f_l, \delta_l), and\ (\widetilde{f}_{l,}\ \tilde{\delta}_l\ )$	Calculated and measured natural frequencies and mode shapes
z	The number of mode
l	The modal order
E_0	OD matrix
$p, u, \dots, v$	The particles p, u, v, respectively
M	Eigenvectors of matrix C
C	Square matrix
K_1	Converting matrix
PCA	Principal component analysis
CNN	Convolutional neural networks
$w_{i_1 i_2}^1, w_{i_2}^1$	Weight and bias coefficients connecting the input layer and the hidden layer
f_{i_1}	Input data of the ${i_1}^{th}$ neuron
n_1, and n_2	The number of neuron in the input layer and the hidden layer

$\sum_{i_2}^{1}$	The input of the $i_2{}^{th}$ neuron of the hidden layer
O_{i_2}	Outputs of hidden layer
$\sum_{\boldsymbol{i_3}}^{\boldsymbol{2}}$	The input of the $i_3{}^{th}$ neuron of the output layer
n_3	The number of neuron in the output layer.
O_{i_3}	Outputs of the output layer.
$\dagger(\boldsymbol{w})$	The discrepancy between predicted and real outputs
$O_{i_3}^{k}$ and $\bar{O}_{i_3}^{k}$	Predicted and real outputs of the k^{th} output data
N_k	The number of output data
τ	The learning rate
$\nabla_{\partial} J(\partial)$	The derivative of the objective function at ∂
γ	The gamma function
ANNCS1	ANN work parallel with CS during the process of training the network
ANNCS2	CS only used to determine the training parameters of ANN in the first step.

M_k and $\bar{M}_k$	Vectorization matrices employed to reduce the dimension of output matrices $O_{i_3}^k$ and $\bar{O}_{i_3}^k$
α_1 and α_2	The mean of $O_{i_3}^k$ and $\bar{O}_{i_3}^k$, respectively
N_n	The neurons of the network
R_d	The stiffness reduction coefficient
EI_0 and EI	Initial stiffness and damaged stiffness of the structures
N_{input}	The number of input data
R_0	Noise ratio
b	The order of input data.
l_n	The length of span
h_n	The height of the section at the middle span
SSI	Stochastic subspace identification
E_i	Young's modulus
γ_i	Volumetric mass density
ε_i	Poisson's ratio
l_e	Positions on the left main truss

t_e	Positions on the upper chord
NI	National Instruments
n_e	The number of considered element
n_s	The number of damage scenario
N_s	The total damage scenarios
DL	Deep Learning
TLBO	Teaching Learning Based Optimization
SSA	Salp Swarm Algorithm

Chapter 1 Introduction

1.1 Problem outline

Structures may be damaged because of different reasons, e.g., service loads, environmental loads and accidental actions. In particular, bridges endure millions of stress cycles during their service life, and they are expected to be highly vulnerable to fatigue. Any incidents that happen to the bridges may cause economic and life impacts, even threaten the safety of users. Proper SHM programs not only help to avoid or at least to minimize a long out-of-service time, but also enhance operational efficiency in structures [1].

In recent decades, SHM for large-scale bridges has attracted special attention from researchers and the scientific community. Numerous large-scale bridges worldwide are established monitoring systems to assess health conditions and ensure operational safety. Among solutions to SHM, model updating based on vibration measurements seems to bring considerable benefits to the structures because it is non-destructive,

effective, and able to detect damages located deeply in structures. This approach overcomes the drawbacks of other methods, for example, magnet field methods, acoustic methods, ultrasonic methods, and visual inspection, all of which require prior information of damage locations. On the other hand, visual inspection is impossible to detect damages that are invisible to human eyes.

Vibration monitoring consists of field tests to identify structural dynamic characteristics, such as natural frequencies, mode shapes, and damping ratios. This technique is used in numerous fields such as damage detection [2] parameter estimation [3] and structural control purposes [4]. According to the excitation methods, vibration excitation can be subdivided into forced or ambient. A Forced Vibration Test (FVT) requires an artificial excitation force to measure and control. An AVT (or frequently referred to as an Operational Modal Analysis - OMA) relies on ambient (or natural) excitation sources, such as wind or micro-seismicity. Recently, system identification methods have been used for both operational excitation and artificial excitation [5]. This not only helps to conduct the identification of modal scaling factors inexpensively but also provides modal estimates with a very high degree of accuracy. However, using artificial excitation is not always possible, especially when the structure is difficult to access. For long-span bridges, AVT is considered the most effective vibration testing technique because ambient excitation is freely available. By contrast, FVT requires considerable efforts to install

actuators such as shakers to generate measurable responses. Moreover, using FVT not only pushes up the high cost of measurements but also obstructs traffic flow.

On the other hand, nowadays, with the strong development of technology, especially the support of modern computer systems, many tools have been introduced to serve the SHM process. A clear illustration is that, over recent decades, MO algorithms such as GA, PSO, CS, or Machine Learning (ML) methods have been commonly used for SHM. However, traditional optimization algorithms and traditional ML still have fundamental shortcomings that may reduce their effectiveness and accuracy.

Therefore, it is necessary to come up with workable solutions to overcome the drawbacks of traditional MO algorithms as well as traditional ML and make them more effective for SHM. This target has been receiving special attention from the scientific community.

From aforementioned analyzed concerns, this thesis will focus on SHM for large-scale bridges using improved MO algorithms and ML based on structural dynamic behaviors obtained from measurements.

1.2 Objectives and contributions

This thesis focuses on two main objectives that can be summarised as below:

1. Introduce up-to-date approaches to SHM for large-scale bridges using MO algorithms and ANN.
2. This thesis will propose workable solutions to the aforementioned disadvantages of traditional MO methods and ANN, helping them become more effective and applicable to reality. Although both MO algorithms and ANN have demonstrated a high level of competence to deal with optimization problems and SHM over the last decades, they still expose fundamental shortcomings that may reduce their accuracy and restrict their applicability. For ANN, local minima might be the biggest problem that reduces its accuracy and effectiveness, whereas the application of MO is extremely time-consuming because these optimization algorithms rely mainly on stochastic techniques during the process of searching for the best solution.

Based on obtained results, some of the main contributions of the thesis are drawn below.

Firstly, to overcome the drawbacks of traditional PSO, an IPSO is coupled with OD (ODIPSO) to increase the accuracy of obtained results as well as to reduce the computational cost. The proposed method is applied for model updating of a five-span truss bridge.

Moreover, a vectorization technique is used for the training data that plays a vital role in reducing the dimension of data. Hence, the computational time is significantly reduced.

Finally, a significant contribution of this thesis is that a novel ANN based on the search capacity of CS is proposed to deal with the local minimum problem of ANN.

1.3 Thesis outline

Apart from the introduction part (**Chapter 1**), this thesis is split into six chapters organized as follows.

Chapter 2. A literature review of SHM using MO algorithms and ANN is presented.

Chapter 3. This chapter introduces traditional MO algorithms consisting of GA, PSO, CS used for optimization problems. In addition, this chapter also proposes solutions to the shortcomings of traditional MO algorithms.

Chapter 4. In this chapter, the definition, structure, methodology, and shortcomings of ANN are described in detail.

Chapter 5. An efficient approach is proposed to overcome the drawbacks of traditional ANN and CS. The proposed method can deal with the local minimal problem of ANN, increase the accuracy and reduce computational cost compared to CS.

Chapter 6. The proposed methods are applied to real bridges, with large DOF. Both numerical and experimental models are used. The structures are modelled and uncertain parameters are identified. In addition, damage identification problems are also evaluated.

Chapter 7. Conclusions and recommendations for future work are provided in this chapter.

Chapter 2 Literature review on SHM using MO algorithms and ANN

2.1 Introduction

SHM became a central research topic and has received increasing attention from the scientific community in recent decades. Numerous successful applications of SHM have been reported in the literature [7-14].

In recent decades, non-destructive structural damage detection techniques based on s tructural dynamic characteristics, MO algorithms, and ANN have been developed. The application of MO algorithms and ANN to SHM provides enormous benefits such as reducing costs, fast process, without traffic suspension, and providing the results with high accuracy. In this case, this solution can provide an accurate assessment of structural behaviors, detect damages, predict the remaining life, and assure the safety of the structure in the operation process. Hence, over recent decades, MO algorithms and ANN have been commonly used for SHM that will be introduced in detail in sections 2.2 and 2.3.

2.2 SHM- based on MO algorithms

The appearance of MO algorithms has extremely enhanced the efficiency of SHM [15-22]. Those algorithms help to minimize the differences of results between numerical model and measurements. Afterward, the calibrated model can predict the behaviors of the considered structures more accurately. Over the recent decades, numerous researchers have employed OM algorithms for SHM. For example. Jung *et al*. [23] applied a hybrid GA to update a small-scale bridge. The objective function included static deflections, mode shapes, and natural frequencies. However, the process of looking for the best solution of GA is time-consuming because this algorithm has to adjust too many parameters through each iteration. Moreover, GA does not possess an effective global search capacity as other MO algorithms. Zare Hosseinzadeh *et al*. [24] applied CS algorithm for damage identification in structures using an objective function of static displacement. Yildiz [25] employed CS to tackle manufacturing optimization problems. In order to compare with CS in terms of solving milling optimization problems, other optimization algorithms consisting of PSO, Ant Colony (AC) algorithm, and immune algorithm were applied. The results showed that CS was superior to the aforementioned algorithms.

Na *et al*. [26] used GA to determine damages in a large-scale building. The proposed approach could identify damage locations and severity in the considered structures exactly, even though measured data was

incomplete. Khatir *et al*. [27] employed both PSO and GA to identify damage locations and severity in unidirectional graphite-epoxy composite beams based on measured vibration data. The results showed that PSO surpassed GA with regard to convergence rate and accuracy. Khatir *et al*. [28] combined PSO with measured natural frequencies to detect damages in beam-like structures. Qin *et al*. [29] updated a complex railway bridge by using GA combined with the Kriging model. While the Kriging model acted as a surrogate to reduce the deviation between structural parameters and responses, GA provided the opportunity for obtaining the global best solution. Liu *et al*. [30], Zordan *et al*. [31], and other authors also employed the mathematical power of optimization algorithms to update large-scale bridges. Khatir *et al*. [32] applied CS algorithm to determine the discrepancy of natural frequencies between experimental and theoretical analysis of Timoshenko beams based on Isogeometric Analysis (IGA). The outcomes indicated that CS provided a very high degree of accuracy to identify the best IGA parameters of Timoshenko beams. Xu *et al*. [33] used CS to identify damage locations and severity of a dual-span supported beam and a truss structure based on a nonlinear objective function of natural frequencies and Modal Assurance Criterion (MAC). The results demonstrated that CS could detect damages in the considered structures accurately even when the effect of noise was fully assessed. Perera *et al*. [34] employed GA derived from Pareto optimality to identify damage in structures. Panigrahi *et al*.

[35] applied the residual force vector along with GA to determine the damage of multistory shear structures. While the input of the model was natural frequencies of modes without and with corresponding mode shapes, the outputs were damage location and level.

Although MO algorithms have demonstrated their effectiveness in handling optimization problems, especially SHM problems, they still expose some fundamental shortcomings. For example, since PSO applied fixed parameters directly relating to the velocity of particles, this may decrease its efficiency in tackling optimization problems. Therefore, a creative solution to the aforementioned limitations of the traditional PSO is strictly necessary. On the other hand, PSO relies heavily on the quality of initial populations. If the positions of initial particles are far away from the global best, it may be difficult to find the most optimal solution.

Over the recent decades, numerous researchers have proposed distinct types of IPSO used to tackle the drawbacks of PSO. Løvbjerg *et al*. [36] proposed an IPSO based on the theory of reproductive and subpopulations making a significant contribution to the increase in the accuracy of the standard PSO. The gaussian mutation was employed to increase the search capacity of particles influencing convergence speed and accuracy of PSO [37]. Baskar *et al*. [38] adopted a new approach using two particle swarms that exchanged information and worked in parallel to remedy the shortcomings of PSO due to premature convergence. Clerc [39] increased the convergence rate of PSO by adding a constriction factor

taking the swarm gravity center into account. Wang *et al*. [40] enhanced the efficiency of the standard PSO by combining it with a simulated annealing algorithm. Parsopoulos *et al*. [41] proposed a nonlinear method derived from the initialization technique of PSO to expand the global search capacity of particles. Qin *et al*. [42] combined PSO algorithm with a surrogate model to update higher vibration modes for a continuous railway concrete bridge in Spain. They pointed out that combining PSO algorithm and a surrogate model could reduce the computational time.

Shirazi *et al*. [43] proposed an adaptive multi-stage optimization derived from a modified PSO to determine multiple damage cases of the tested structures. Tran-Ngoc *et al*. [44] proposed a novel approach to SHM of a truss bridge using IPSO coupled with OD. IPSO was employed to make particles of PSO more flexible, whereas OD based on optimal selection was used to eliminate poor quality population and to reduce the dimension of the model. The results showed that the proposed method not only increased the accuracy of the model but also drastically decreased computational costs.

The traditional CS algorithm also exists main drawbacks. The accuracy of CS is low if the initial position of populations is far away from the best solution. This algorithm does not possess crossover and mutation operators such as GA to improve the quality of the next generations. On the other hand, since CS look for the best solution based on stochastic techniques, this leads to a massive increase in computational cost.

Recently, many researchers have proposed different types of Improved Cuckoo Search (ICS) to deal with the issues of shortcomings. Mohapatra *et al.* [45] combined ICS with ML to classify medical datasets. ICS was employed to determine training parameters of ML consisting of input weights and hidden biases. In order to compare with the proposed approach, other algorithms including Online Sequential Extreme Learning Algorithm (OSELM), Multi-Layered Perceptron (MLP), and Radial Basis Function Neural Network (RBFNN) were also employed. The results demonstrated that the proposed approach outperformed OSELM, MLP, and RBFNN in terms of accuracy. Marichelvam *et al.* [46] employed ICS to deal with the multistage Hybrid Flow Shop (HFS) scheduling problems. ICS was applied to minimize the discrepancy between the start time and finish time of sequential tasks for the HFS scheduling problems. Simulations and comparisons indicated that ICS was superior to simulated annealing, GA, PSO, and AC algorithms in terms of accuracy. Zhou *et al.* [47] used ICS applying swap and inversion strategy, and greedy strategy to solve planar graph coloring problems. The results showed that ICS provided a higher correction to the coloring rate and required less computational time than PSO.

2.3 SHM- based on ANN

ANN is a sub-branch of Artificial Intelligence (AI) designed to mimic the way that the human brain processes information. With recent notable

advances, ANN has been commonly employed in a wide variety of fields [48-51]. For example, Nguyen-Thanh *et al*. [52] used neural networks combined with a high-dimensional model to generate a surrogate model for computational homogenization of elastostatics. Chau *et al*. [53] proposed employing Chebyshev polynomials for the activation function of neural networks to increase convergence speed when optimizing cross-sections for truss structures. Hyeon-JongHwang *et al*. [54] employed ANN to predict the bond performance of tension lap splices. The obtained results showed that the proposed method provided a higher level of accuracy compared to existing design equations.

Sujith Mangalathu *et al* [55] presented a multi-parameter fragility methodology based on ANN to create fragility curves for skewed concrete bridges. This approach could determine uncertain parameters on the fragility curves. The results showed that the column longitudinal reinforcement ratio, the ground motion intensity measure, and span length made the main impact on the seismic fragility of the considered bridges. Eissa Fathalla *et al* [56] employed ANN to assess the remaining life of in-service bridge decks. The input data consisted of crack patterns and their widths. Although the obtained results could predict the remaining life of the structure, the risk of wrong assessment may be happened because of overfitting problems of the trained network. Ulrike Dackermann *et al* [57] identified damages in a two-storey framed structure using ANN combined with Frequency Response Functions

(FRFs). To verify the obtained results, measurement was also employed. The results showed that the proposed method was reliable and accurate in determining damages in the considered structure.

ANN and time-modal features were employed to identify damages for simply supported beams and free–free beams in the work of [58]. The damage identification consisted of two phases, in which the first one was to monitor damages based on time-domain features and the second one was to estimate damages based on modal-domain features. Eui-YoulKim *et al* [59] combined ANN and Wavelet Packet Transform (WPT) to detect the fault in a moving transfer robot. WPT was used for feature extraction and ANN was used for fault classification. Input data was an abnormal operating sound occurring when the robots move. The results showed that abnormal operating sound was sufficient and reliable for the fault diagnosis of mechanical components. C.ZANG *et al* [60] employed measured FRFs and ANN to predict the actual state of the considered structure. When input data was measured FRFs, output data was the health state of structure (damaged or intact). To consider the robustness of the proposed approach under the effect of significant experimental noise, 5% random noise was added into the input data.

In the work of [61], a counter-propagation neural network was used to control earthquake-induced vibrations in building structures. The authors concluded that the proposed method possibly determined the required control forces exactly without an unsupervised learning method.

R.M. Di Benedetto *et al* [62] employed ANN to predict the energy absorption capability of thermoplastic commingled composites. The results showed that the proposed method possibly predicted the impact energy with a high level of accuracy. Geng Chen *et al* [63] employed ANN to predict global material strengths of particulate reinforced metal matrix composites. Features obtained from direct method analyses were selected as input data, whereas global material strengths played a role as output data. Tam T.Truong *et al* [64] introduced ANN to optimize the material distribution of Bidirectional Functionally Graded (BFG) beams. In this research, ANN was used to predict responses of BFG beams and a differential evolution approach was applied to deal with optimization problems. A.G. Stamopoulos *et al* [65] used ANN and X-ray Computed Tomography data to assess the quality of porous CFRP specimens. The input data consisted of 30 porosity scenarios used to train the network. The obtained results showed that the predictions of the ANN had a close correspondence with those from measurements. Fabio Rizzo *et al* [66] employed ANN to estimate the flutter velocity of suspension bridges. Uncertain parameters including deck chord length, bridge weight, and structural damping were selected as input data.

Oğuzhan Hasançebi *et al* [67] adopted an efficient approach based on ANN to update a reinforced concrete bridge in Pennsylvania. A field experiment was employed to calibrate the numerical model. After that, both linear and non-linear analyses based on the calibrated numerical

model were used to create datasets to train the network. The outcomes indicated that the proposed method was reliable to predict structural responses under the significant effect of uncertainties that could occur during the service life of structures. Moreover, this study also concluded that non-linear analysis should be taken into account for structural model updating problems. Prasun Chokshi *et al* [68] developed a novel ANN model derived from a phase distribution prediction model to determine the suitable process of hot stamping. Thermal & mechanical history was used to generate datasets for the network, whereas advanced statistical techniques were also employed to deal with overfitting problems that may happen in the process of training the network. The results showed that the performance of the proposed method provided a considerable improvement over most of the existing methods.

Luis García Esteban *et al* [69] employed ANN based on a feedforward multilayer perceptron network to identify the modulus of elasticity of timber structures. Input data consisting of ultrasonic wave propagation velocity, thickness, width, density, moisture content, visual grading, and moisture content used to train the network. Jia Ma *et al* [70] proposed a data-driven modelling framework derived from ANN to analyse the contact process between barrel and bourrelet of complex contacting surfaces. Different initial indentation velocities obtained from measurement were served as datasets for the training process. To gain an optimal network, hyper-parameters including the structure of the

network (the number of neurons in each layer), training parameters (weight and bias) were tuned in the process of training the network. The obtained outcomes provided a good agreement between calculated and real targets. Y.S. Kong *et al* [71] adopted a new approach using Hybrid multilayer perceptron ANN to estimate the fatigue life of automotive coil springs. The measured acceleration signals were selected as input data of the network. The optimized ANN structure was determined by tuning the number of neuron in the hidden layer. The ANN structure that provided the lowest Mean Square Error (MSE) values was selected to train the network. The authors concluded that the proposed method provided a high accuracy and a good correspondence between predicted and experimental values.

Khairul H.Padil [72] developed an efficient ANN based on a non-probabilistic method to identify structural uncertainties. While natural frequencies and mode shapes were chosen as input data, output was the young's modulus that possibly represents changes in the stiffness parameter. To assess the robustness and applicability of the proposed method, the effect of noise on datasets was used. An experimental model was also employed to verify results obtained from the numerical model. In the work of [73], a combination between ANN and the Optimal Wavelet-Packet Transform (ANN-OWPT) was presented to recognize sound quality. ANN model was employed three-layer back-propagation to train the network. To verify the effectiveness of ANN-

OWPT, vehicle noises were used for sound quality recognition. From achieved outcomes, the authors pointed out that the proposed approach was effective and could be utilized to simulate the critical bands in the human hearing system. S.L. Xie *et al* [74] proposed a novel method using the capacity of ANN to identify nonlinear hysteretic systems. All Bouc–Wen model parameters were calculated in one step by utilizing Bouc–Wen model-based ANN. To assess the efficiency of the proposed method, a wire cable experimental system was employed. The obtained results demonstrated that the presented identification approach possibly determined the nonlinear hysteretic systems accurately.

2.4 Conclusion of chapter 2

This chapter introduces approaches to SHM using MO algorithms and ANN. It is acknowledged that numerous important achievements using MO algorithms and ANN for SHM have been represented in the last decades. However, there are still fundamental shortcomings that need to come up with workable solutions that will be introduced in the next chapters.

Chapter 3 MO algorithms

3.1 Introduction

MO algorithms are designed to seek, build and choose heuristics that possibly provide solutions with a higher level of accuracy. Because MO algorithms employ few assumptions, they can be employed to deal with a wide range of optimization problems.

MO algorithms often incorporate some form of randomness to overcome the problems of local minima. However, stochastic techniques may also cause a high computational cost. Hence, to make MO algorithms easy to apply for real-world problems, it is extremely necessary to employ other techniques to reduce computational time.

In this thesis, some popular MO algorithms such as GA, PSO, CS are employed for SHM introduced in section 3.2. On the other hand, proposed approaches introduced in section 3.3 will be employed to remedy the shortcomings and increase the effectiveness of traditional MO algorithms.

3.2 MO algorithms

3.2.1 GA

GA is a MO algorithm commonly applied in numerous fields [75-76]. This algorithm employs a crossover operator to mate initial particles (parents) with each other, and a mutation operator to create the next generations that have better quality than the old ones. Each particle possesses a fitness function used to minimize the difference between the real and calculated results. Relying on the problems that need to tackle, the fitness function could apply to any structures. There are numerous types of GA applying for engineering problems in which real-coded GA is the most popular because of its simplicity and effectiveness.

However, because of the lack of velocity coefficients, the global search capacity of GA is less effective. The accuracy of obtained results also depends crucially on the judicious selection of crossover and mutation operators. Moreover, because there are too many parameters that need to be adjusted through each step, the process of seeking the global best is extremely time-consuming. This makes GA difficult to apply for monitoring the health of large-scale structures that contain a large number of DOF. The use of GA to look for the best solution is depicted in Figure 3-1 and from step 1 to step 6.

Step 1. The generation of initial position (X_0), and the local best (P_0), respectively.

$$X_0 = \left[x_0^1, x_0^2, \ldots, x_0^j\right];\ j = [1; m] \tag{3.1}$$

$$P_0 = [p_0^1, p_0^2, \ldots, p_0^j] \tag{3.2}$$

$$x_0^j = [x_0^{1j}, x_0^{2j}, \ldots, x_0^{nj}] \tag{3.3}$$

$$p_0 = [p_0^{1j}, p_0^{2j}, \ldots, p_0^{nj}] \tag{3.4}$$

m is the number of uncertain parameters that need to be sound.

Step 2. The local best of populations is calculated and put in an increasing order based on the objective function $f(X)$

$$P_0 = [P_0^{max} \ldots P_0^{min}] \tag{3.5}$$

Step 3. Choose the parents from the best particles

$$P_{localbest} = [P_0^{max}] \tag{3.6}$$

Step 4. Crossover

$$P_{t+1} = [P_t^{u_1} + P_t^{u_2}] \tag{3.7}$$

u_1, and u_2 are one of the best solution of particles at the step t.

Step 5. Mutation

$$P_{t+1}^{q_1} + P_{t+1}^{q_2} \tag{3.8}$$

q_1, and q_2 are particles after crossover.

Step 6. Choose the best offspring particles after crossover and mutation for the next iteration

$$P_{localbest} = [P_{t+1}^{max}] \tag{3.9}$$

Repeat steps 4-6 until termination criteria are satisfied (The number of iterations is 100 or the difference between calculated and real results is less than 10^{-6}).

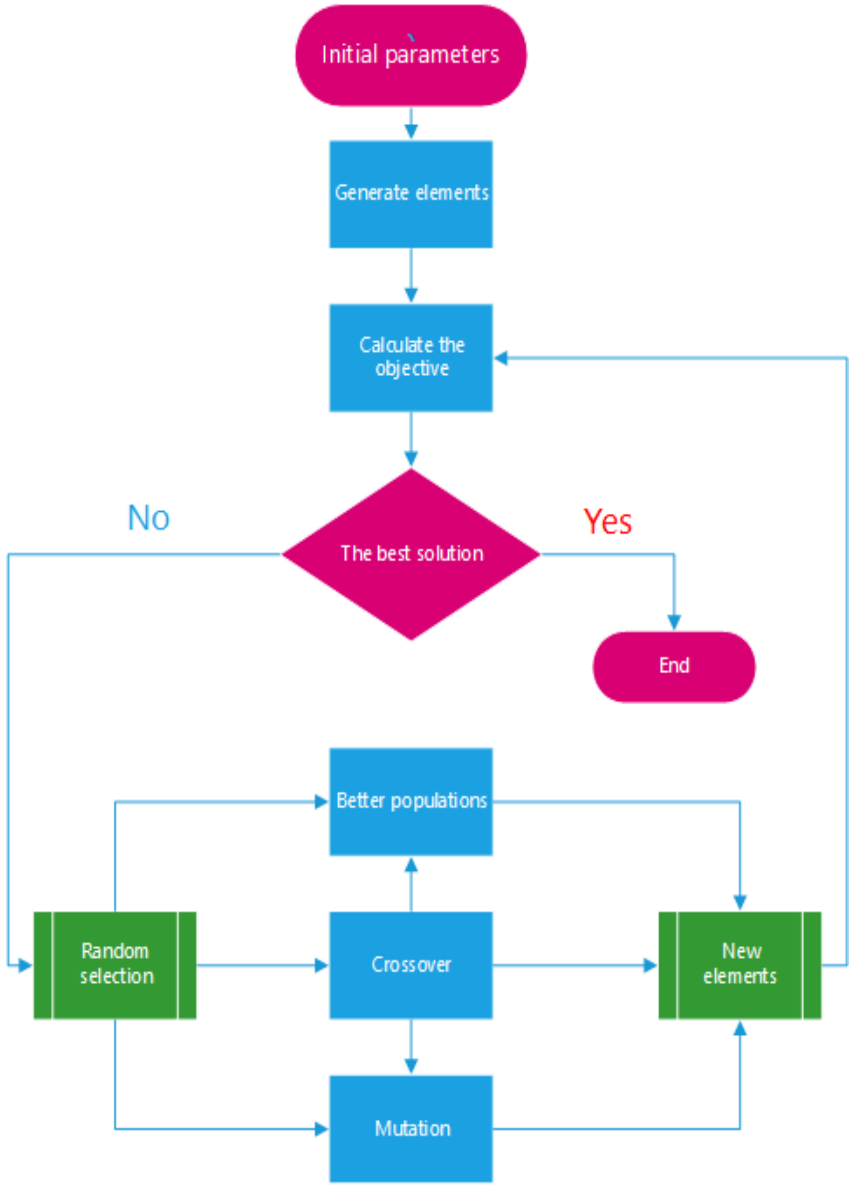

Figure 3-1–The use of GA to look for the best solution

3.2.2 PSO

In 1995, Kennedy developed a MO, namely PSO derived from global search techniques to seek the optimal solution [77]. PSO was initially employed to simulate the process of seeking the food of some animals such as birds and fishes. By observing the behavior of birds and fishes seeking food, researchers found that communicating with each other was advantageous to the search for the optimal solution during evolution. PSO algorithm relies on two equations to seek the best solution.

The first equation is to determine the position of each element:

$$X_{t+1}^{i} = \left(X_{t}^{i} + V_{t+1}^{i}\right); \; ; \; i = [1, n] \tag{3.10}$$

The second one is to determine the velocity of each element:

$$V_{t+1}^{i} = w * V_{t}^{i} + c_1 * rand * \left(P_{t}^{best} - X_{t}^{i}\right) + c_2 * rand * \left(G_{t}^{best} - X_{t}^{i}\right) \tag{3.11}$$

Where X_t^i, X_{t+1}^i indicate the position, V_t^i, V_{t+1}^i represent the velocity of element i at time t and t+1, respectively. n indicates the number of population. c_1 and c_2 are the cognition learning factor and social learning factor, whereas 'rand' denotes random numbers (0 < rand < 1). While w is the inertia weight parameter, G_t^{best} and P_t^{best} represent the global best, and the local best at the time t, respectively. After a step, each element compares its optimal solution with others to find the global best. The best optimal solution will be determined after all iterations are completed.

With the global search capacity and smart strategy for seeking the best solution, PSO has demonstrated its effectiveness to deal with optimization problems. However, since PSO applied fixed parameters directly relating to the velocity of particles, this may decrease its efficiency in tackling optimization problems. Moreover, the process of looking for the best solution is also time-consuming. The use of PSO to look for the best solution is depicted in Figure 3-2.

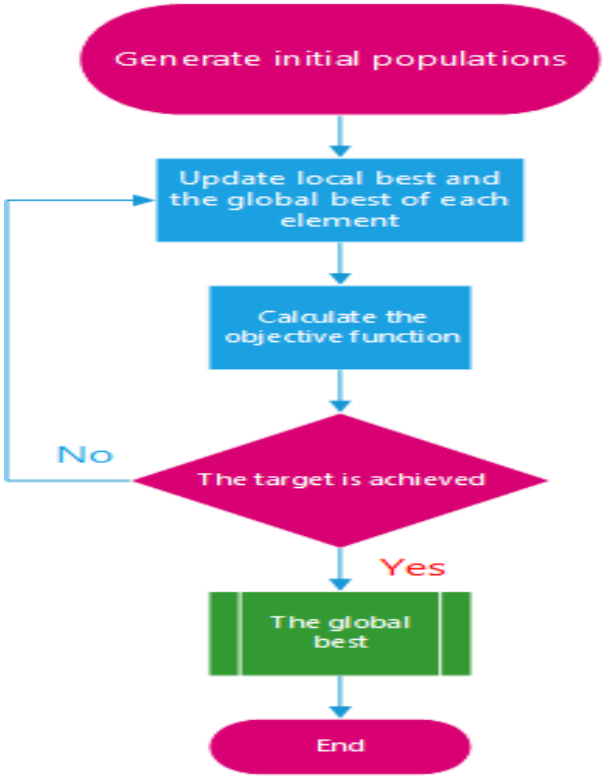

Figure 3-2–The use of PSO to look for the best solution

3.2.3 CS

CS is a kind of bionic optimization algorithm inspired by the obligate brood parasitism of cuckoo birds. Basically, cuckoos often choose the nests of other birds to spawn their eggs. If the host birds discover that the eggs are not their own, they may either leave their nest or throw parasite eggs away. CS algorithm is formed based on the following three idealized rules [96].

1. The cuckoos select a stochastic nest to lay their eggs and only one egg is spawned at a time.
2. The nests with the highest quality of eggs will be carried over into the next steps.
3. The number of available host nests is fixed, whereas there is a 0-100% probability (P_a) that the host possibly discovers the parasite eggs. If the host birds detect parasite eggs, they may either abandon their own nest or throw the eggs away.

The best solution is determined as Eq (3.12):

$$X_{t+1}^{i} = X_{t}^{i} + \boldsymbol{levy}(\boldsymbol{\lambda}) * \alpha \tag{3.12}$$

Where X_t^i and X_{t+1}^i are solutions of cuckoo i at t^{th} and $t + 1^{th}$ iteration, respectively, and α represents the step size. Lévy flight ($\boldsymbol{\lambda}$) is step length drawn from the following probability distribution :

$$\boldsymbol{levy}\ (\boldsymbol{\lambda}) = \frac{1}{\delta^{\beta}} \tag{3.13}$$

β is the coefficient of Levy flight: $1 < \beta < 3$ [78]; parameter (δ) is determined based on a random walk via probability distribution function. Step length (levy (λ)) should be selected according to the scale of the problem of interest. If step length (levy (λ)) is chosen too short, the new generation may be very close to the previous one. If λ is too long, the next generation may jump extremely far from the old one.

It is acknowledged that with the global search competence using Levy flights random walks and cuckoo's breeding strategy, CS has already proved its effectiveness to tackle optimization problems. Nevertheless, the accuracy of CS is low if the initial position of populations is far away from the best solution. This algorithm does not possess crossover and mutation operators such as GA to improve the quality of the next generations. On the other hand, like other swarm intelligence methods based on stochastic techniques, the process of finding the global best of CS is time-consuming. The use of CS to look for the best solution is depicted in Figure 3-3.

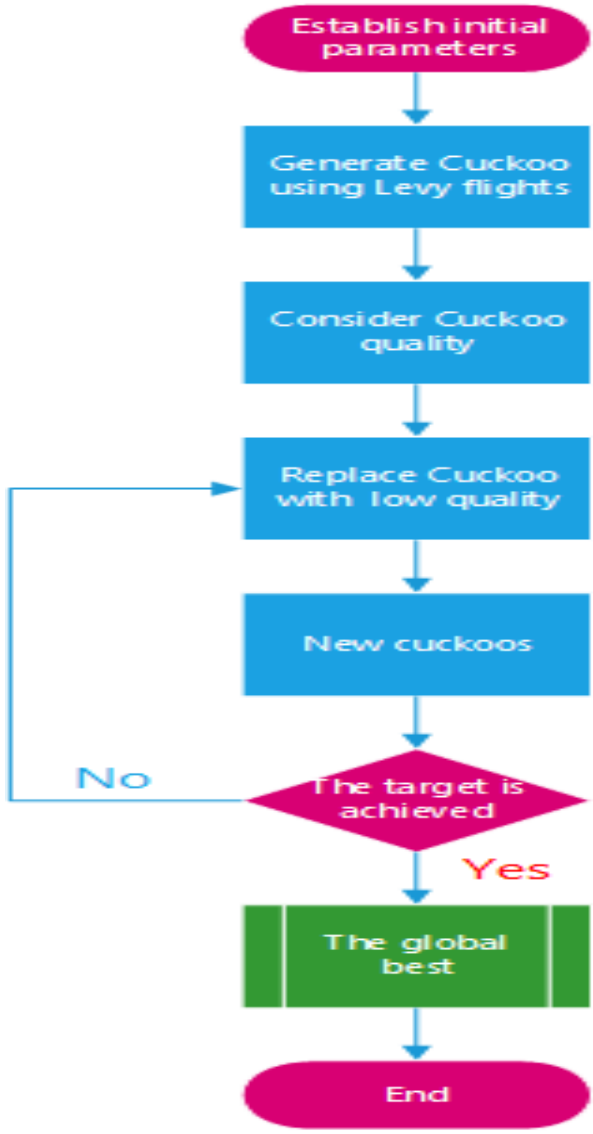

Figure 3-3–The use of CS to look for the best solution

3.3 Improved MO algorithms

3.3.1 IPSO

Due to the capability of dealing with complex constrained issues based on global search capacity, PSO has demonstrated its effectiveness in numerous engineering applications. However, since PSO applied fixed parameters directly relating to the velocity of particles, this may decrease its capability of handling optimization problems. Hence, some improved mechanisms comprising the solution to the premature convergence and the design of a novel formula for updating the velocity of particles should be applied. In this work, the two improved parameters of IPSO consist of functional inertia weight (w) and constant constriction factor (T) are used [79]. They play an integral part in enhancing the effectiveness of the standard PSO. While w creates the biggest impact on the change of the velocity of particles, T influences convergence speed.

- ***Functional inertia weight (w)***

In the search actions, if particles move close to the desired position, w should keep a small value, which assists the elements in maintaining recent velocity for the next steps. If the position of particles is far from the optimal solution, w should keep a larger value. This helps the particles avoid suboptimal regions and look for a better optimal solution. Therefore, the new value of w is expressed in Eqs. (3.14)-(3.15) [79]

$$w = w_{end} + (w_{start} - w_{end})\left(1 - \left(\frac{K}{Q}\right)\right) if(P_i^t \neq X_i^t) \quad (3.14)$$

$$w = w_{end}\,; if(P_i^t = X_i^t) \quad (3.15)$$

- ***The constriction factor (T)***

To keep IPSO away from premature convergence, in the early iterations, the constriction factor (T) needs to choose a convex function and hold a larger value, which assists the elements in looking for the global best in a large area. In the later iterations, T needs to choose a concave function and hold a small value so that T can alter slightly to the minima. This strategy guarantees that PSO can converge to the best solution. According to the mentioned principle, the functional constriction factor (T) needs to follow the rule of a cosine function shown in Eq (3.16) [79].

$$T = \frac{cos(\frac{\Pi}{Q} * K) + \frac{1}{4}}{4} \quad (3.16)$$

The parameters obtained from Eqs (3.14)- (3.16) are put into Eq (3.11). The velocity of IPSO used to seek the new position becomes:

$$V_{t+1}^i = w * V_t^i + c_1 * rand * (P_t^{best} - X_t^i) + c_2 * rand * (G_t^{best} - X_t^i)\,; if(K < Q/2) \quad (3.17)$$

$$V_{t+1}^{i} = T * (w * V_t^i + c_1 * rand * \left(P_t^{best} - X_t^i\right) + c_2 * rand * \left(G_t^{best} - X_t^i\right)); if (K \geq Q/2) \quad (3.18)$$

Q indicates the total number of iterations, whereas K represents K^{th} iteration, $K \in (0, Q)$; w_{start} is the value of initial functional inertia weight; w_{end} indicates the value of functional inertia weight in the last iteration.

3.3.2 ODIPSO

In this thesis, to increase the accuracy and reduce the computational cost of traditional PSO, a novel algorithm referred to as ODIPSO is proposed in this section. OD is applied to arrange the best local position of particles in the form of an OD matrix and only select particles providing better solutions (located on the diagonal line of the OD matrix) for the next iterations. The populations (n) are split into two groups including active group (a) and passive group $(n - a)$. The active group comprises the better solution of (a) particles, whereas the passive group includes the results of $(n - a)$ remaining ones. This algorithm is developed based on the idea that only particles of the active group are selected for the next step. By contrast, particles of the passive group are not updated since their contributions to the search for the optimal solution are insignificant [80]. This strategy helps to decrease the dimension of the model extremely, and the computational time is also reduced. In each step, matrix (C) is constructed from particles of the active

group. After that OD matrix (E_0) is determined. The objective function $f(X)$ is applied to reduce the differences between calculated and real results. The process of searching for the best solution using OD combined with IPSO is given as follows:

Step 1: . The generation of initial position (X_0), velocity (V_0), the local best (P_0), and the global best of particles (G_0^{best}), respectively.

$$X_0 = \left[x_0^1, x_0^2, \ldots, x_0^j\right];\ j = [1; m] \tag{3.19}$$

$$V_0 = [v_0^1, v_0^2, \ldots, v_0^j] \tag{3.20}$$

$$P_0 = [p_0^1, p_0^2, \ldots, p_0^j]\,; G_0^{best} \tag{3.21}$$

$$x_0^j = [x_0^{1j}, x_0^{2j}, \ldots, x_0^{nj}] \tag{3.22}$$

$$v_0^j = [v_0^{1j}, v_0^{2j}, \ldots, v_0^{nj}] \tag{3.23}$$

$$p_0 = [p_0^{1j}, p_0^{2j}, \ldots, p_0^{nj}] \tag{3.24}$$

m is the number of uncertain parameter that needs to be sound.

Step 2: Select the objective function $f(X)$ for model updating of the considered structures including natural frequencies and mode shapes.

$$f(X) = \sum_{l=1}^{z} \frac{(\widetilde{f}_l - f_l)^2}{(\widetilde{f}_l)^2} + \sum_{l=1}^{z} \left[1 - \frac{(\tilde{\delta}_l^T . \delta_l)^2}{(\delta_l^T . \delta_l) * (\tilde{\delta}_l^T . \tilde{\delta}_l)}\right] \tag{3.25}$$

While $(f_l,\ \delta_l), and\ (\tilde{f}_{l,}\ \tilde{\delta}_l\ )$ denote calculated and measured natural frequencies and mode shapes, z represents the number of mode. "l" is the modal order.

Step 3: Calculate the values of the objective function $f(X)$ of particles at the iteration t^{th}

Step 4: Arrange the local best of particles in an increasing order based on $f(X)$

Step 5: Construct matrix K_1 consisting of the best local solution of particles in which each row keeps the local best of each particle based on the results obtained from step 4.

$$K_1 = X_t^i \tag{3.26}$$

$$f\left(X_t^p\right) < f(X_t^u) \dots < f(X_t^v) \tag{3.27}$$

$p, u, \dots, v$ are the particles p, u, v, respectively.

Step 6: Convert matrix K_1 to square matrix C with the size $a * a$.

$For\ k = 1{:}\,a;\ q = 2{:}\,a$

$$C(1,k) = K_1(1,k) \tag{3.28}$$

$$C(k,1) = K_1(1,k) \tag{3.29}$$

$$C(q,k) = K_1(q,k) \tag{3.30}$$

End

For $k = 2: a$

$$C_1(q,k) = C(q,k) \tag{3.31}$$

$$C(k,q) = C_1(q,k) \tag{3.32}$$

End

Step 7: Calculate OD matrix E_0 from matrix C

$$E_0 = M^{-1} * C * M \tag{3.33}$$

Where: Matrix M includes eigenvectors and matrix E_0 consists of the corresponding eigenvalues of matrix C.

Step 8: Control the search areas of particles: (X_{min}, X_{max})

Step 9: Update the position and velocity of particles at $t + 1^{th}$ iteration

$$V_{t+1}^i = K * \left(w * V_t^i + c_1 * rand * \left(E_0 - X_t^i\right)\right) \tag{3.34}$$

$$X_{t+1}^i = (X_t^i + V_{t+1}^i) \tag{3.35}$$

$$If(X_{t+1}^i > X_{max}) \tag{3.36}$$

$$X_{t+1}^i = X_{min} + rand * X_{min} \tag{3.37}$$

$$If(X_{t+1}^i < X_{min}) \tag{3.38}$$

$$X_{t+1}^{i} = X_{min} + rand * X_{min} \tag{3.39}$$

Step 10: Update the locally optimal position of each element and the globally optimal position to use for the next iterations based on the objective function $f(X)$.

$$If\ f\left(X_{t+1}^{i}\right) < f\left(X_{t}^{i}\right) \tag{3.40}$$

$$f\left(X_{t+1}^{i}\right) = f\left(X_{t+1}^{i}\right) \tag{3.41}$$

$$Otherwise\ \ f\left(X_{t+1}^{i}\right) = f\left(X_{t}^{i}\right) \tag{3.42}$$

Step 11. Repeat the process steps 3-10 until termination criteria are satisfied.

Step 12: The iteration is completed and the best solution is obtained.

$$f(G^{best}, m_0) = min\ \ f(X) \tag{3.43}$$

$$G^{best} = X^{m_0} \tag{3.44}$$

The combination of IPSO and OD used for model updating is shown in Figure 3-4

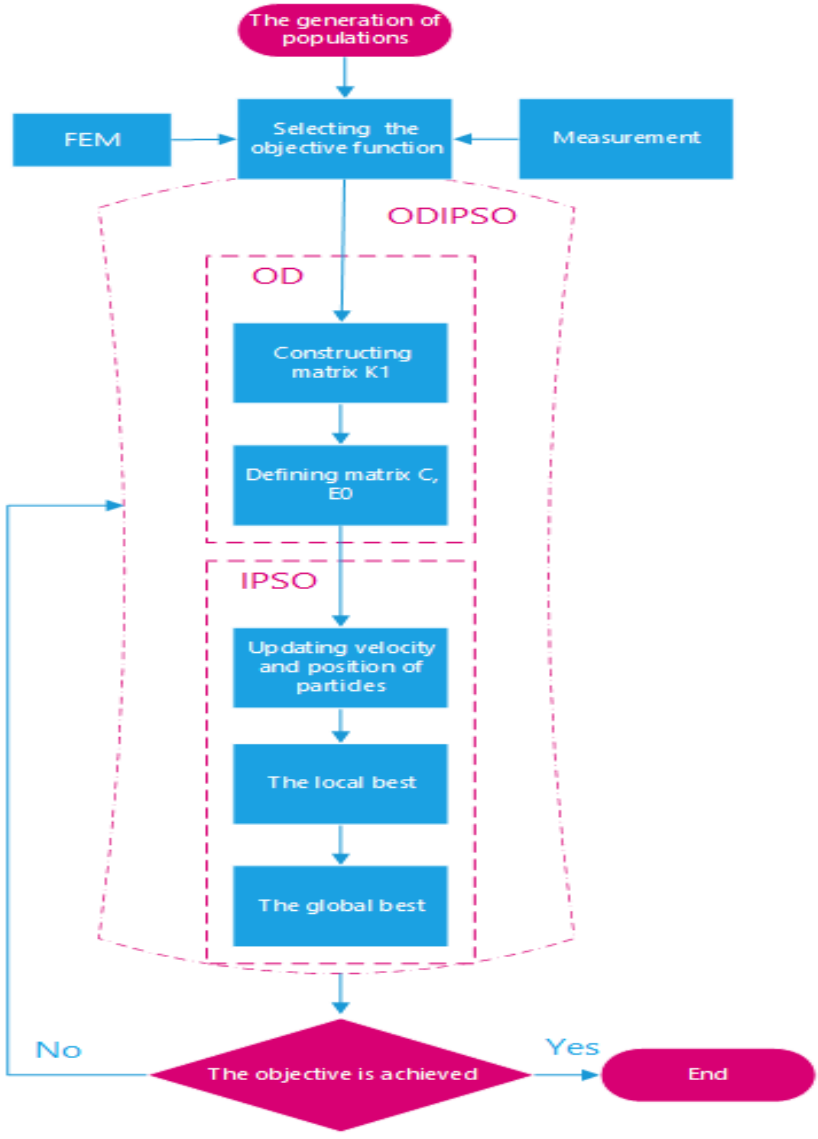

Figure 3-4– Methodological approach to model updating utilizing ODIPSO

3.4 Conclusion of chapter 3

In this chapter, common MO algorithms such as GA, PSO, CS are introduced in detail. Although those algorithms have demonstrated their capacity to deal with many optimization problems, they still have some fundamental shortcomings. To remedy those shortcomings and increase the effectiveness of traditional MO algorithms, some algorithms consisting of IPSO, and ODIPSO are introduced. These algorithms will be used for SHM of large-scale structures that are introduced in section 6.

Chapter 4 ANN

4.1 Introduction

ANN is a sub-branch of AI that has been commonly applied for SHM in the last decades. Zhou and Abdel Wahab [81] employed an auto-associative neural network combined with transmissibility to identify damage location and severity in a ten-floor building structure. In their study, the effect of noise (2%) on natural frequencies was assessed. Maity and Saha [82] applied the change of static properties (strain and displacement) for damage detection in a simple cantilever beam using a back-propagation algorithm in ANN. Nguyen *et al*. [83] proposed a method using Principal Component Analysis (PCA) combined with residual FRFs to identify damage in a concrete arch bridge. Damage features were obtained from PCA and FRFs used as input data for the network. They demonstrated that the proposed approach successfully identified damage location and level in the considered bridge. Janssens *et al*. [84] applied a feature learning model based on Convolutional Neural Networks (CNN) for bearing fault diagnosis. Elshafey *et al*. [85] proposed a method based on the feed-forward backpropagation, and the radial basis neural networks to predict crack width for both thick and thin concrete elements. Cascardi *et al*. [86] used ANN to estimate the strength of FRP-confined concrete. The study showed that the proposed model

could provide a good agreement between the numerical model and measurement.

4.2 ANN structure

ANN methodology has been built in the shape of parallel distributed network models inspired by biological nervous systems. One of the outstanding properties of ANN is the ability to learn identification from experience to improve its performance. Therefore, the trained network can be utilized to classify and examine new data sets that are similar to the characteristics of trained data sets. Because of the potential capability of ANN for modeling both simple linear and complex nonlinear functions, this algorithm can be applied to tackle a wide range of complex issues, whose solutions are difficult to obtain by only applying common methods. These applications consist of identification, classification, pattern recognition, control system, and image processing. With ANN, setting up the network have dramatic effects on the obtained results. A network of ANN includes three main components, namely the input layer, the hidden layer, and the output layer. Each layer consists of sets of neurons connected by training parameters (weight and bias). Each neuron comprises a processing element with synaptic input connections based on the number of the processing neuron in the previous layer. Among the different types of neural networks, multilayer perceptron neural networks are the most commonly used models. Multilayer perceptron neural networks include one or more hidden layers of cells (or neurons)

connected between the input and output layers. The number of neurons in each hidden layer, and the number of hidden layers in a network create significant influences on the generalization capability of the network. The question of how to choose the number of nodes in the hidden layer and the number of hidden layers in a network to obtain optimal results is still an open topic today. For numerical data, there is no persuasive evidence that the network of ANN with two or more hidden layers may outperform networks with one hidden layer. By contrast, using more hidden layers may lead to a higher computational cost. Therefore, only one hidden layer is utilized for ANN in this work, and the structure of a three-layer neural network is shown in Figure 4-1.

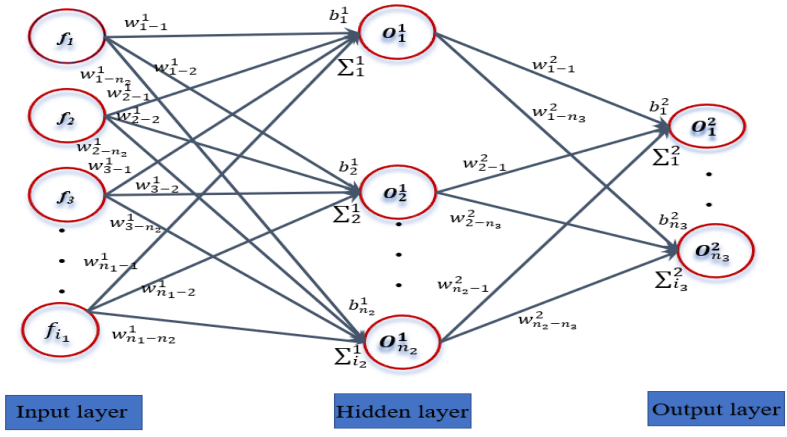

Figure 4-1– Three-layer neural network architecture

4.3 Methodology

Figure 4-1 shows the signal transmission process between neurons in layers. The input layer receives input patterns and then transmits the signal to the hidden layer. The hidden layer includes a certain number of neurons playing a vital role as a bridge between the input layer, and the output layer. Each neuron in the preceding layers is fully connected to the following ones, and the connections are based on training parameters (weight and bias). The signal transmission is based on two Eqs.

The first equation is a summation function computed as the sum of bias, weight ratios, and output signals of the previous layers.

$$\sum_{i_2}^{1} = \sum_{i_1,i_2}^{n_1,n_2} \boldsymbol{w}_{i_1 i_2}^{1} * f_{i_1} + \boldsymbol{b}_{i_2}^{1} \; ; i_1 = (1{:}\, n_1); i_2 = (1{:}\, n_2) \tag{4.1}$$

$\boldsymbol{w}_{i_1 i_2}^{1}, \boldsymbol{b}_{i_2}^{1}$ are weight and bias coefficients connecting the input layer and the hidden layer, whereas f_{i_1} indicates input data of the ${i_1}^{th}$ neuron; n_1, and n_2 are the number of neuron in the input layer and the hidden layer, respectively; $\sum_{i_2}^{1}$ denotes the input of the ${i_2}^{th}$ neuron of the hidden layer.

After the summation function (4.1) is conducted. The second equation is an activation function (4.2) applied to limit the value range of the output. The activation function can be a monotonically increasing

linear or nonlinear function. In this study, in order to deal with nonlinear problems, a sigmoid activation function is employed.

$$O_{i_2} = \frac{1}{1 + e^{-\Sigma_{i_2}^1}} \tag{4.2}$$

This process of transmitting signal is similar to that between the hidden layer and output one shown in Eqs (4.3)-(4.4).

$$\sum_{\boldsymbol{i_3}}^{\boldsymbol{2}} = \sum_{i_2,\, i_3}^{n_2,\, n_3} \boldsymbol{w}_{i_2 i_3}^2 * O_{i_2} + \boldsymbol{b}_{i_3}^2;\ i_3 = (1{:}\, n_3) \tag{4.3}$$

$\sum_{\boldsymbol{i_3}}^{\boldsymbol{2}}$ denotes the input of the ${i_3}^{th}$ neuron of the output layer; n_3 indicates the number of neuron in the output layer.

$$O_{i_3} = \frac{1}{1 + e^{-\Sigma_{\boldsymbol{i_3}}^{\boldsymbol{2}}}} \tag{4.4}$$

The discrepancy between predicted and real outputs is determined.

$$\dagger(\boldsymbol{w}, \boldsymbol{b}) = \sum_{\mathrm{k}=1}^{N_k} \frac{1}{2} \frac{(O_{i_3}^k - \bar{O}_{i_3}^k)^2}{N_k} \tag{4.5}$$

$O_{i_3}^k$ and $\bar{O}_{i_3}^k$ in turns are predicted and real outputs of the k^{th} output data, respectively; N_k is the number of output data. To minimize the difference between calculated and real outputs $\dagger(\boldsymbol{w}, \boldsymbol{b})$, training

parameters are turned applying a backward process based on GD techniques described in Eqs (4.6)-(4.14).

$$\frac{\partial \sum_{i_3}^{2}}{\partial w_{i_2 i_3}^{2}} * \frac{\partial O_{i_3}}{\partial \sum_{i_3}^{2}} * \frac{\partial \dagger(\boldsymbol{w}, \boldsymbol{b})}{\partial O_{i_3}} = \frac{\partial \dagger(\boldsymbol{w}, \boldsymbol{b})}{\partial w_{i_2 i_3}^{2}} \tag{4.6}$$

$$\frac{\partial \sum_{i_3}^{2}}{\partial b_{i_3}^{2}} * \frac{\partial O_{i_3}}{\partial \sum_{i_3}^{2}} * \frac{\partial \dagger(\boldsymbol{w}, \boldsymbol{b})}{\partial O_{i_3}} = \frac{\partial \dagger(\boldsymbol{w}, \boldsymbol{b})}{\partial b_{i_3}^{2}}$$

$$\frac{\partial \dagger(\boldsymbol{w}, \boldsymbol{b})}{\partial O_{i_3}} = -(\overline{O_{i_3}} - O_{i_3}) \tag{4.7}$$

$$\frac{\partial O_{i_3}}{\partial \sum_{i_3}^{2}} = \frac{e^{-\sum_{i_3}^{2}}}{(1 + e^{-\sum_{i_3}^{2}})^2} \tag{4.8}$$

$$\frac{\partial \sum_{i_3}^{2}}{\partial w_{i_2 i_3}^{2}} = O_{i_2}; \frac{\partial \sum_{i_3}^{2}}{\partial b_{i_3}^{2}} = 1; \tag{4.9}$$

New training parameters connecting the hidden layer and the output layer are obtained.

$$w_{i_2 i_3}^{2}{}^{+} = w_{i_2 i_3}^{2} - \tau * \frac{\partial \dagger(\boldsymbol{w}, \boldsymbol{b})}{\partial w_{i_2 i_3}^{2}} \tag{4.10}$$

$$b_{i_3}^{2}{}^{+} = b_{i_3}^{2} - \tau * \frac{\partial \dagger(\boldsymbol{w}, \boldsymbol{b})}{\partial b_{i_3}^{2}}$$

Training parameters connecting the input layer and the hidden layer are also adjusted; τ is the learning rate.

$$\frac{\partial \sum_{i_2}^{1}}{\partial \boldsymbol{w}_{i_1 i_2}^{1}} * \frac{\partial O_{i_2}}{\partial \sum_{i_2}^{1}} * \frac{\partial \dagger(\boldsymbol{w}, \boldsymbol{b})}{\partial O_{i_2}} = \frac{\partial \dagger(\boldsymbol{w}, \boldsymbol{b})}{\partial \boldsymbol{w}_{i_1 i_2}^{1}} \tag{4.11}$$

$$\frac{\partial \sum_{i_2}^{1}}{\partial \boldsymbol{b}_{i_2}^{1}} * \frac{\partial O_{i_2}}{\partial \sum_{i_2}^{1}} * \frac{\partial \dagger(\boldsymbol{w}, \boldsymbol{b})}{\partial O_{i_2}} = \frac{\partial \dagger(\boldsymbol{w}, \boldsymbol{b})}{\partial \boldsymbol{b}_{i_2}^{1}}$$

$$\frac{\partial O_{i_2}}{\partial \sum_{i_2}^{1}} = \frac{e^{-\sum_{i_2}^{1}}}{(1 + e^{-\sum_{i_2}^{1}})^2} \tag{4.12}$$

$$\frac{\partial \sum_{i_2}^{1}}{\partial \boldsymbol{w}_{i_1 i_2}^{1}} = f_{i_1}; \frac{\partial \sum_{i_2}^{1}}{\partial \boldsymbol{b}_{i_2}^{1}} = 1; \tag{4.13}$$

$$\boldsymbol{w}_{i_1 i_2}^{1}{}^{+} = \boldsymbol{w}_{i_1 i_2}^{1} - \tau * \frac{\partial \dagger(\boldsymbol{w}, \boldsymbol{b})}{\partial \boldsymbol{w}_{i_1 i_2}^{1}} \tag{4.14}$$

$$\boldsymbol{b}_{i_2}^{1}{}^{+} = \boldsymbol{b}_{i_2}^{1} - \tau * \frac{\partial \dagger(\boldsymbol{w}, \boldsymbol{b})}{\partial \boldsymbol{b}_{i_2}^{1}}$$

The process of training the network shown in Eqs (4.1)-(4.14) is repeated until the objective is achieved or the number of iteration is finished.

4.4 Shortcomings of traditional ANN

GD algorithms are local optimization techniques applying the principle of a downward slope to reduce the difference between real and

desired outputs. Although this deviation is significantly reduced after each iteration, GD algorithms still have drawbacks. The global best of GD algorithms is the solution of the differential equation of the objective function (loss function). However, seeking the global best of the objective function in ANN is complicated or even impossible in some cases. This is due to the complexity of the form of the objective function. The most common approach for seeking the best solution in ANN is that the network starts from a random point and then iteratively moves closer to the target. The search process ends when the target is achieved (the derivative of the objective function at the obtained point goes to 0). The methodology of GD algorithms is described below.

- Select a starting point $\partial = \partial_0$
- Update ∂ using Eq (4.15) until the derivative goes to 0

$$\partial = \partial - \tau \nabla_{\partial} J(\partial) \tag{4.15}$$

With $\nabla_{\partial} J(\partial)$ is the derivative of the objective function at ∂.

The obtained results of ANN rely heavily on whether or not the network gets stuck in local minima. A clear illustration is given in Figure 4-2 that describes the process of training the network to determine the best solution. In Figure 4-2 (a), if the network only contains just one global best ($\boldsymbol{A_0}$), whether the starting point is $\boldsymbol{A}$ or $\boldsymbol{B}$, the best solution is always obtained. In Figure 4-2 (b), the network contains both local best and global best. If the starting point is $\boldsymbol{B}$, the network can determine the global

best ($\boldsymbol{A_0}$). By contrast, if the starting point is $\boldsymbol{A}$, the network is trapped in the local best ($\boldsymbol{A_1}$). Nevertheless, a network often contains a large number of local minima, especially for complex problems as shown in Figure 4-2 (c). In this case, even the network starts from $\boldsymbol{A}$ or $\boldsymbol{B}$, it still gets stuck in local minima during the training process. Therefore, the approach of the selection of good starting positions may no longer be useful.

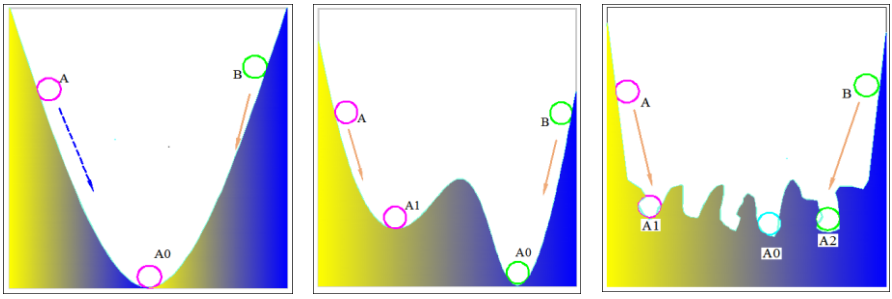

(a) (b) (c)

Figure 4-2– The process of looking for the global minima of GD technique (a) the network with only global best; (b) the network with both local best and global best; (c) the network with numerous local minima.

In fact, some researchers have also proposed methods to overcome the local minimum drawbacks and improve the efficiency of ANN. The core idea of these approaches is to choose beneficial starting points to remove initial local minima. For example, Khatir *et al.* [87] employed Teaching-Learning-Based Optimization to determine training parameters (weight

and bias coefficients) of ANN used to detect damages for a laboratory beam with free-free boundary conditions. Rajendra *et al*. [88] employed GA to evaluate the fitness of training function in ANN when predicting optimized parameters to reduce free fatty acids of sunflower oil. Yazdanmehr *et al*. [89] also coupled GA with ANN to look for the optimal chemical composition used to produce a nanocrystalline powder with minimum coercion. Tran-Ngoc *et al*. [90] used CS to improve ANN by determining initial training parameters consisting of weight and bias. The results showed that this combination outperformed ANN alone and other optimization algorithms in terms of accuracy. Nevertheless, because CS was only applied to determine initial training parameters, the network may be still trapped in local minima during the training process. With the same approach, Samir *et al.* [91] combined PSO with ANN to detect damages in a laminated composite. In their research, PSO was employed to determine an optimal starting point for the training network. This strategy assisted the network in avoiding local minima in the first steps of the training process. Azadeh *et al*. [92] used a flexible algorithm based on GA and ANN (GA-ANN) to evaluate and optimize complex production units. They pointed out that GA-ANN was superior to GA alone and conventional ANN in terms of optimizing machine productivity. However, this combination was time-consuming because GA had to adjust too many parameters in the training process. Moreover, the global search

capacity of GA is also less superior than other MO algorithms such as PSO, CS.

It is easily seen that the above-mentioned approaches applied solutions to local minima by choosing a beneficial starting position based on the global search capability of other algorithms. This strategy may help the network to avoid the first local minima (first valley). However, a network often has many local bests distributed everywhere, especially if the network contains a complex error surface. Hence, the particles of the network may be still trapped into other local minima (other valleys) during the process of training the network.

4.5 Conclusion of chapter 4.

The structure and methodology of ANN are presented clearly in this chapter. Moreover, the fundamental shortcoming of ANN relating to local minima is analysed in detail. Over the last decades, some researchers have proposed some solutions to local minimum problems of ANN by choosing a good starting point. However, this solution seems to be infeasible if the network contains many local minima and is distributed at different sides of the network. This acts as a premise to come up with workable solutions introduced in the next section.

Chapter 5 A novel ANN based on the global search techniques

5.1 Motivation

To overcome the drawbacks of those mentioned approaches, this thesis proposes a novel ANN based on the global search techniques of CS that is referred to as ANNCS1. ANNCS1 is employed to deal with the problems of local minima during the process of training the network rather than only depending on the luck of having a good starting point. The proposed approach is depicted in Figure 5-1.

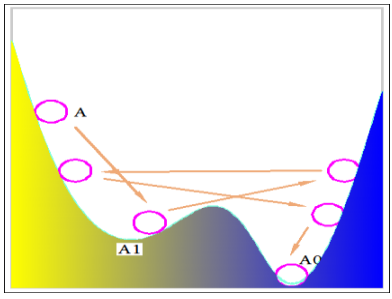

Figure 5-1– Escaping the network from local minima using CS.

The core idea of ANNCS1 is that the network firstly applies the GD technique to increase the speed of convergence. Figure 5-1. shows that if

the network is trapped in local minima (A_1), CS based on the global search technique is employed to escape elements from local minima. After that, the GD technique is applied again. This parallel working process is repeated until the objective function is reached. This win-win approach provides the network with the highest opportunity for obtaining the global best.

To consider the effectiveness of the proposed method, this thesis will compare the results obtained from ANNCS1 with traditional ANN and approaches mentioned in ref [87-92] which is referred to as ANNCS2.

5.2 Methodology of ANNCS1

Normally, the outputs of ANN obtained from the forward process are then propagated backward using backpropagation algorithms. Nevertheless, since backpropagation algorithms employ GD techniques, ANN may face a high risk of getting stuck in local minima if the network creates complex error surfaces with too much of the local best. To deal with this problem, CS based on global search techniques is employed to escape elements from local minima. This means that CS replaces backpropagation algorithms to determine training parameters (weight and bias).

Training parameters ($w_{i_1 i_2}^1$, $b_{i_2}^1$, $w_{i_2 i_3}^2$ and $b_{i_3}^2$) are transferred to a form of a single vector that then becomes initial population (X_0) of CS.

$$X_0 = \left[w_0^1,\ w_0^2, \cdots,\ w_0^j\right], j = [1{:}m] \tag{5.1}$$

$$w_0^j = \left[w_0^{1j},\ w_0^{2j}, \cdots,\ w_0^{nj}\right]^T \tag{5.2}$$

n denotes the number of population; m denotes the number of training parameters ($w_{i_1 i_2}^1, b_{i_2}^1, w_{i_2 i_3}^2$ and $b_{i_3}^2$).

The objective function is chosen as Eq. (5.3).

$$f(X) = \sqrt{\sum_{k=1}^{N_k} (M_k)^2 - (\bar{M}_k)^2} \tag{5.3}$$

M_k and $\bar{M}_k$ are vectorization matrices employed to reduce the dimension of output matrices $O_{i_3}^k$ and $\bar{O}_{i_3}^k$

$$M_k = \frac{1}{N_k - 1} \sum_{k=1}^{N_k} |O_{i_3}^k - \alpha_1|^2 \tag{5.4}$$

$$\bar{M}_k = \frac{1}{N_k - 1} \sum_{k=1}^{N_k} |\bar{O}_{i_3}^k - \alpha_2|^2 \tag{5.5}$$

α_1 and α_2 are the mean of $O_{i_3}^k$ and $\bar{O}_{i_3}^k$, respectively

$$\alpha_1 = \frac{1}{N_k} \sum_{k=1}^{N_k} O_{i_3}^k \tag{5.6}$$

$$\alpha_2 = \frac{1}{N_k}\sum_{k=1}^{N_k} \bar{O}_{i_3}^{k} \tag{5.7}$$

Get cuckoos randomly based on Levy flights

$$X_1 = X_0 + \boldsymbol{levy}(\boldsymbol{\lambda}) * \alpha_n \tag{5.8}$$

Where α_n is the step size

$levy(\lambda)$ is identified from Levy flight [78].

$$levy\ (\lambda) = \theta^{\beta^{-1}} \tag{5.9}$$

θ is calculated using a probability distribution function.

$$\theta = \left(\frac{\gamma(1+\beta) * sin\left(\frac{\Pi * \beta}{2}\right)}{\gamma\left(\frac{1+\beta}{2}\right) * \beta * 2^{\frac{(\beta-1)}{2}}}\right)^{\frac{1}{\beta}} \tag{5.10}$$

Where $\boldsymbol{\gamma}$ is the gamma function used for both positive integers and complex numbers. With complex numbers, γ is identified in a form of an integral function.

$$\gamma(d) = \int_0^{\infty} q^{d-1}e^{-q}dq \tag{5.11}$$

With positive integers (j_0), γ is determined in the form of a factorial

$$\gamma(j_0) = (j_0 - 1)! \tag{5.12}$$

Apply the upper and lower bound of the search area

$$If\ X_1 > X_{max} \tag{5.13}$$

$$X_1 = X_{min} + rand * X_{min} \tag{5.14}$$

$$Else\ if\ X_1 < X_{min} \tag{5.15}$$

$$X_1 = X_{min} + rand * X_{min} \tag{5.16}$$

Identify the best nest based on the objective function $f(X)$

$$f(X_1) < f(X_0) \tag{5.17}$$

$$f(X_1) = f(X_1); X_1 = X_1 \tag{5.18}$$

Otherwise

$$f(X_1) = f(X_0); X_1 = X_0 \tag{5.19}$$

Determine new solutions based on selective random walks

$$\boldsymbol{K} = rand\ (X_1) > P_a \tag{5.20}$$

Where P_a is the probability that the host can detect the parasite eggs

Get cuckoos based on Levy flights at t^{th} iteration

$$X_{t+1} = X_t + \alpha_n * K \tag{5.21}$$

$$If\ X_{t+1} > X_{max} \tag{5.22}$$

$$X_{t+1} = X_{min} + rand * X_{min} \tag{5.23}$$

$$\text{Else if } X_{t+1} < X_{min} \tag{5.24}$$

$$X_{t+1} = X_{min} + rand * X_{min} \tag{5.25}$$

Calculate $f(X)$ of particles at t^{th} iteration

Identify the best nest

$$f(X_{t+1}) < f(X_t) \tag{5.26}$$

$$f(X_{t+1}) = f(X_{t+1}); X_{t+1} = X_{t+1} \tag{5.27}$$

$$f(X_{t+1}) = f(X_t); X_{t+1} = X_t \tag{5.28}$$

Determining the best solution.

$$f(G^{best}) = \min(f(X)) \tag{5.29}$$

$$\boldsymbol{X} = G^{best} \tag{5.30}$$

The best solution determined by CS is converted into training parameters to train the network by using pseudocode (Figure 5-2) .

k_0=0;

$w_{i_1 i_2}$=zeros (n_1, n_2);

for i_1=1: n_1

  for i_2=1: n_2

  k_0=k_0+1; $w_{i_1 i_2}$ (i_1, i_2)= X(k_0);

  End

end

$w_{i_2 i_3}$=zeros (n_2, n_3);

for i_2=1: n_2

  for i_3=1: n_3

  k_0=k_0+1; $w_{i_2 i_3}$ (i_3, i_2)= X(k_0);

  end

end

b_{i_2}=zeros (n_2, 1);

for i_2=1: n_2

  k_0=k_0+1; b_{i_2} (i_2, 1)= X(k_0);

end

b_{i_3}=zeros (n_3,1);

for i_3 =1: n_3

  k_0=k_0+1; b_{i_3} (i_3, 1)= X(k_0);

end

Assigning new weight and bias parameters for the network of ANN

net.IW{1,1}=$w_{i_1 i_2}$; % weight ratios connecting the input – hidden layer

net.LW{2,1}=$w_{i_2 i_3}$; % weight ratios connecting the hidden – ouput layer

net.b{1,1}=b_{i_2}; % bias ratios connecting the input – hidden layer

net.b{2,1}=b_{i_3}; % bias connecting the hidden – ouput layer

Figure 5-2– Pseudocode is used to convert the best solutions of CS to weight, bias ratios of ANN.

k indicates neuron order of the neurons of the network (N_n). k $\in$ (1; N_n).

$$N_{\mathrm{n}} = n_1 * n_2 + n_2 * n_3 + n_2 + n_3 \tag{5.31}$$

Where n_1, n_2, n_3 indicate the number of neuron in the input layer, the hidden layer, and the output layer, respectively.

This process is repeated until the objective function is achieved or the number of iteration is completed. The proposed approach is also described in detail in Figure 5-3

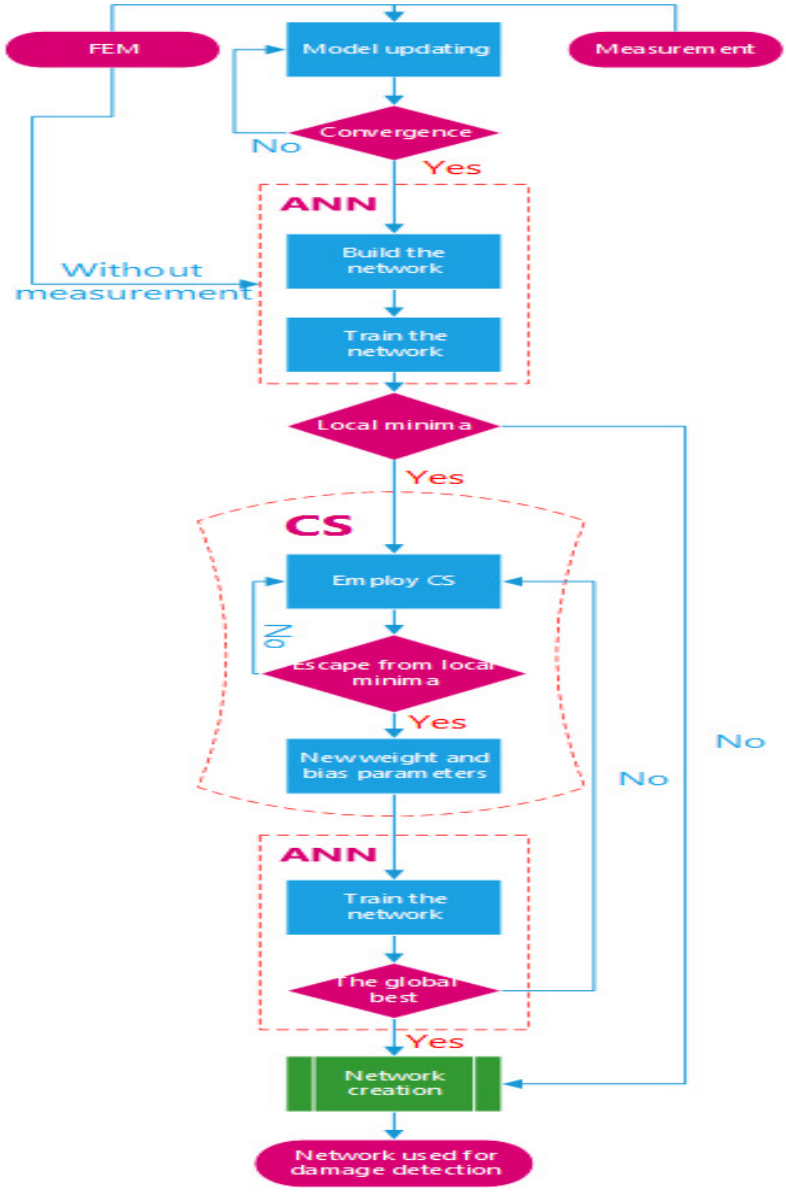

Figure 5-3– The diagram of ANNCS1

The damages are used as the output of the network. Damage locations are determined using the stiffness reduction coefficient (R_d) as in Eq. (5.32) [93].

$$R_d = (1 - \frac{EI * EI_0}{EI_0}) * 100\% \quad (5.32)$$

Where EI_0 and EI denote initial stiffness and damaged stiffness of the structures.

To consider the effect of noise on input data, Gaussian white noise is applied [94].

$$\text{Noise} = \sqrt{10^{10*log_{10}\frac{\sum_{b=1}^{N_{input}}(f_i)^2}{N_{input}}-R_0}} * \text{Rand}\ (0 < \text{Rand} < 1) \quad (5.33)$$

$$\text{Input\_data}_{\text{new}} = \text{Input\_data}_{\text{old}} + \text{Noise} \quad (5.34)$$

N_{input} is the number of input data; f_i is input data; R_0 is the noise ratio; b is the order of input data.

5.3 Conclusion of chapter 5.

This chapter proposes a novel approach (ANNCS1) to deal with local minimum problems of ANN. ANNCS1 employs both advantages of ANN (gradient descent technique) and CS (global search technique) to look for

the best solution. This win-win approach provides the network with the highest opportunity for obtaining the global best. The effectiveness of ANNCS1 will be considered by applying it for damage detection of a large-scale bridge in section 6.

Chapter 6 Applications to Bridges

6.1 Introduction

In this section, proposed algorithms will be applied for model updating, damage detection for a wide range of bridges as shown in Table 6.1.

Table 6.1. List of bridges applying the proposed algorithms.

Order	Bridge	Problems	Applied method
1	Nam O Bridge	Model updating	PSO and GA
2	Guadalquivir Bridge	Model updating	ODIPSO
3	Chuong Duong Bridge	Damage detection	ANNCS1

6.2 Nam O Bridge

6.2.1. Bridge description

The Nam O Railway Bridge is a large-scale steel truss bridge, located in Da Nang city in the middle of Vietnam. The bridge plays a vital role in connecting train traffic from the North to the South. The Nam O Bridge was constructed in 2011, with funding from the Hanoi – Ho Chi Minh City Line Bridge Safety Improvement Project. The bridge includes 4 simply supported spans of equal length (75 m). The rail track is placed directly on the stringers of the bridge deck. The abutment on the Hai Van side is referred to as ***A*0**, whereas the three piers are numbered as ***P*1**, ***P*2**, ***P*3**, starting from the ***A*0** side. The last (fourth) span goes from ***P*3** to the abutment ***A*1** on the Da Nang city side. Some views of the bridge are given in Figure 6.1.

(a) (b)

Figure 6-1–Some views of Nam O Bridge: (a) Upstream side; (b) Downstream side

Truss members were made from steel with a variety of section types such as *I*, *L*, Box (Figure 6-2), and connected to each other by bolts.

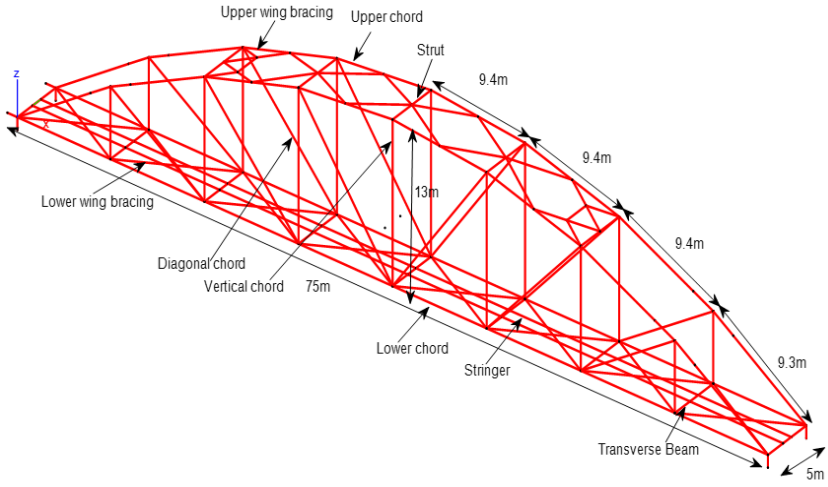

Figure 6-2– Main structural elements

The measured span (the first span from the Hai Van side) is put on rocker and pin bearings. Rocker bearings permit translation and rotation in one direction, while pin bearings only allow rotational movement. The characteristics of rocker and pin bearings (size, stiffness) are collected from catalogues of manufacturers to calculate the parameters of the equivalent springs.

6.2.2. FEM

In order to predict structural dynamic behaviors, and compare them with those obtained from measurement, a FEM of Nam O Bridge was built by using the MATLAB toolbox StaBil [95] (see Figure 6-3).

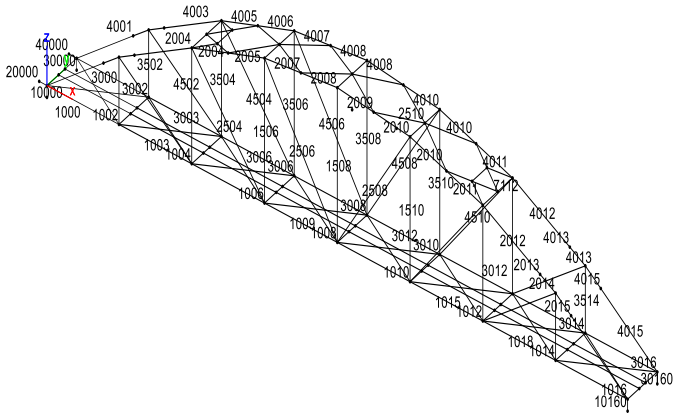

Figure 6-3–FEM of the Nam O Bridge

The following details describe the FEM:

- The bridge is modeled by 137 nodes, 227 elements, and 9 section types of truss members are used (see Table 6.2).

- Main structural members are shown in Figure 6-2: upper chords, lower chords, vertical chords, diagonal chords, stringers, upper wind bracings, lower wind bracings, and struts, are modeled using three dimensional ($3D$) beam elements. The beam element is based on Timoshenko beam theory. The element provides options for unrestrained warping and restrained warping of cross-sections. This element has six DOFs at each node including translations in the x, y, and z directions and rotations around the x, y, and z directions. The transverse girders (of the deck system) are also modeled using beam elements.

- The global X-axis is in the longitudinal direction of the bridge; the Y-axis is in the transverse direction (to the river flow direction) and the Z-axis is in the vertical direction. The left main truss is on the downstream side. Likewise, the right main truss is on the upstream side. Both trusses represent the side view of the bridge (Figure 6-1).

- Bearings are modeled by using spring elements.

- Section and material properties of structural members are listed in Table 6.2 and Table 6.3

Table 6.2 – Cross-sectional properties of truss members

Members	Area(m^2)	Moment of Inertia I_y (m^4)	Moment of Inertia I_z (m^4)
Upper chord	0.056	6.70×10^{-04}	3.1×10^{-03}
Lower chord	0.020	2.10×10^{-04}	6.30×10^{-04}
Vertical chord	0.010	5.49×10^{-05}	1.15×10^{-04}
Diagonal chord	0.014	1.24×10^{-04}	2.78×10^{-04}
Stringer	0.020	2.07×10^{-04}	6.27×10^{-04}
Transverse Beam	0.026	2.03×10^{-04}	3.61×10^{-03}
Strut	0.020	6.25×10^{-04}	2.80×10^{-03}
Upper wind bracing	0.0036	8.00×10^{-06}	1.09×10^{-05}
Lower wind bracing	0.0049	2.38×10^{-06}	4.38×10^{-06}

Note: I_y is the moment of inertia of the weak axis (the same direction with global Y), I_z is the moment of inertia of the strong axis (the same direction with global Z).

Table 6.3 – Material properties of truss members

Components	Value	Unit
Young's modulus	2×10^{11}	N/m^2
Volumetric mass density	7850	Kg/m^3
Poisson's ratio	0.3	/

- The connection between truss joints: due to the uncertainty of the actual joint stiffness, three possible models of link types are considered: a) pin, b) rigid, and c) semi-rigid. This process can be considered as a trial step to analyze and determine some unknown parameters (material properties, section properties, or joint conditions and so on.).

Case 1: Pin connection

In order to simplify the calculation, researchers as Duerr [96], Saka [97] assumed truss members linked to each other by pin connections (Figure 6-4 a). In this case, the influence of rotational stiffness is neglected, and no moments are transferred between truss members. In the static analysis of truss structures, this link is often applied for node joints, which has little effect on the result of the force of truss members because moment transfer is rather insignificant with dominant axial forces (compression and tension).

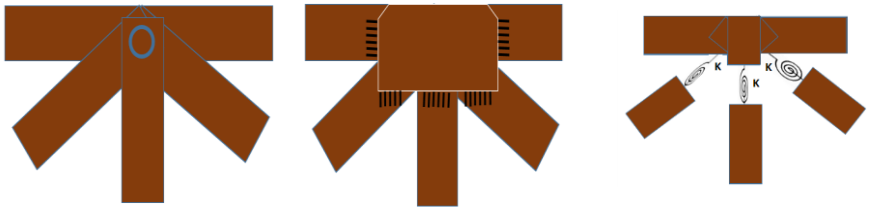

(a) (b) (c)

Figure 6-4–Connection types of truss joints: (a) Pin connection; (b) Rigid connection; (c) Semi-rigid connection (rotational springs)

Case 2: Rigid connection.

Duerr [98], and other authors have also applied rigid links (Figure 6-4 b) for truss joints. Basically, a rigid joint can transfer axial forces (compression, tension) as well as moments between members.

Case 3: Semi-rigid connection.

This link type has recently been applied by many researchers. Luong *et al* [98] determined the stiffness of node joints, when updating a truss structure in the laboratory, and found that a semi-rigid connection represents the most accurately the dynamic characteristics of the considered truss structure. Dubina *et al.* [99], Csébfalvi [100], and other researchers applied semi-rigid links (rotational springs) for truss structures. However, most of the aforementioned authors only applied this type of joint in the static analysis, whereas a few others employed it to analyze the dynamic analysis of scale models in the laboratory.

Rotational springs (Figure 6-4 c) are often used to present semi-rigid links at truss joints.

This study also applies the aforementioned three scenarios of joint conditions to predict the structural dynamic behaviors of the Nam O Bridge. Linear elastic rotational springs with three DOFs at each node: rotations around the x, y, and z directions are used for vertical chords and diagonal chords as Figure 6-4 c. The original stiffness of rotational springs is estimated according to reference [98]. The results are given in Table 6.4 and Figure 6-5.

Table 6.4 – The natural frequencies from the FEM for three connection cases, and from measurement.

Mode	Pin connection (Hz)	Rigid connection (Hz)	Semi-rigid connection (Hz)	Measurement (Hz)	Mode types
1	1.18 (18.6%)	2.05 (29%)	1.47 (1.4%)	1.45	First lateral
2	2.76 (11.3%)	4.36 (29%)	3.14 (1%)	3.11	First torsion
3	3.11 (5.18%)	4.44 (26%)	3.32 (1.2%)	3.28	Second lateral
4	3.79 (17.7%)	7.18 (36%)	4.80 (3.7%)	4.62	First vertical bending
5	3.94 (34.9%)	8.15 (26%)	6.96 (13%)	6.05	Second torsion

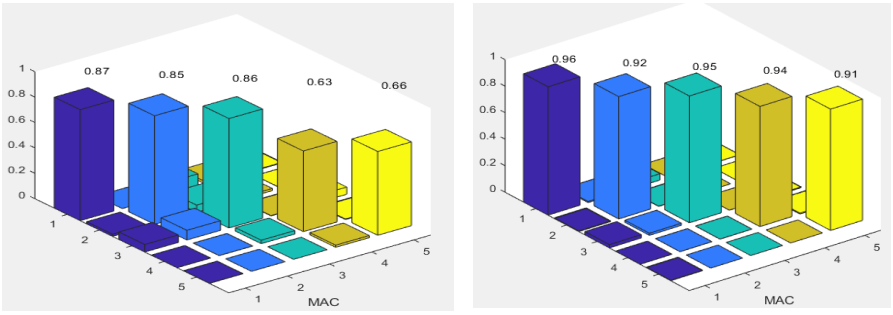

(a) (b)

Figure 6-5–MAC values of mode shapes before model updating: (a) Rigid connection, (b) Semi-rigid connection

Table 6.4 demonstrates that the FEM of the bridge with pinned connection does not predict the behaviors of the bridge properly. Natural frequencies of the first five modes are lower than those of measurement. The result of the FEM with rigid connection is also not satisfactory in comparison to the experimental one. Specifically, there are deviations between natural frequencies calculated from FEM and measurement (from 26% to 36%). Natural frequencies from the FEM are higher than those from the experiment. Rigid links make the structure stiffer than in reality, while the truss members in Nam O Bridge are linked with each other by bolts. Additionally, MAC values (Figure 6-5 a) lower than 0.9 indicate the significant difference between mode shapes of FEM and measurement. The model with a semi-rigid connection provides improved simulated modal results in comparison to the experimental ones. There is a small deviation between natural frequencies calculated

from FEM and measurement (around 1%, apart from mode 5 having 13%). The MAC values (Figure 6-5 b) higher than 0.9 indicate consistent correspondence between the numerical model and measurement [101-102]. However, it is necessary to update some uncertain parameters such as Young's modulus, the stiffness of springs at bearings and truss joints to get the best correspondence between theoretical and experimental results.

6.2.3. Experimental measurements

6.2.3.1. The AVT

6.2.3.1.1. Test description

The modal identification test was performed on the first span between abutment $A0$ and pier $P1$. Span length is l_n=75 m, maximum height at mid-span h_n=13 m. In total, there were 32 truss connections. The dynamic response was due to ambient wind forces or the free vibration of the bridge after train passage. In order to obtain sufficient data for vibration-based system identification as well as to be compatible with FEM analysis, ideally, all nodes and all directions (longitudinal- x, transversal- y, and vertical- z) from the bottom to the top of the arch-truss type should be included in the measurement grid. However, by neglecting deformation due to normal forces, several displacement components (DOFs) can be linked (slaved nodes) to DOFs of other (master) nodes. Therefore, in the measurement layout 64 (= 32 x 2) DOFs

are configured in either of two directions (x and y or y and z depending on measurement positions: see Figure 6-6), of which 40 DOFs were real measurements and 24 DOFs virtual (slave) results. An overview of the sensor layout is shown in Figure 6-6.

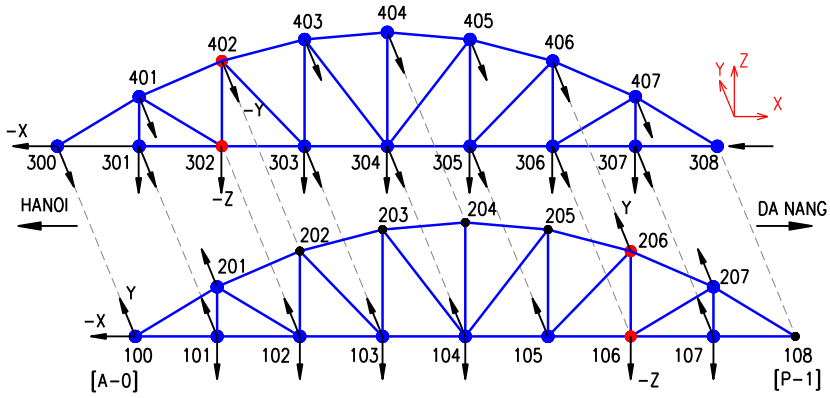

Figure 6-6–The measurement grid: accelerometers at 40 DOFs; red: reference points-106, 206, 302 and 402; blue: roving points.

6.2.3.1.2. Sensors placement

On the bridge, ten accelerometers (PCB-393B12) with high sensitivity from 965 to 1,083 mV/m/s^2, were employed for response signal acquisition. However, the sensitivity of accelerometers need to be carefully considered in this case. It is well known that modal properties, especially the natural frequencies, are influenced by environmental conditions, mainly temperature. Hence, the calibration was valid for the (constant) temperature during the AVT. If the measurements would be

repeated as part of an SHM program (to detect structural damages) definitely, this dependency has to be taken into account. In practice, this kind of bridge will have a high amplitude vibration during the train passage. Therefore, using a high sensitivity sensor can lead to distortion or clipping the response. For this reason, besides the ambient response measurement, the vibration of the bridge was only considered after a train passage.

The vibration measurement grid was divided into 8 setups; each setup included a maximum of 10 accelerometers as in Table 6.5. From these 10 ones, 4 served as references while the remaining accelerometers were roving over the bridge. The 4 reference sensors were presently placed at the lower and upper nodes of the two bays (see Figure 6-6). An optimal reference was a sensor where all lower modes of vibration were present. Therefore, modelling the structure beforehand was a reliable basis to allocate where the reference sensors should be located. Division of sensors in "reference" and "roving" was necessary when the number of the available sensor was less than the number of DOF that need to be measured. In this case, a multi-setup measurement campaign was employed. Reference sensors were placed in nodes where all lower vibration modes had non-zero modal displacements. The position was selected based on the modal results of a preliminary FEM. It was also possible to generate "optimal positions" of the reference sensors when applying Optimal Sensor Placement algorithms [103]. In practical

measurements (on bridges), there will be as many reference sensors as possible dependent on the existing instrumentation. Preferably, there is more than one reference sensor. In the case of multiple setups, the other (roving sensors) cover all the remaining positions in the measurement grid.

Table 6.5 – Overview of setups used for data acquisition and corresponding DOFs

Setup	Reference channels				Roving channels					
setup 1	106z	206y	302z	402y	101z	103z	301z	303z	305z	
setup 2	106z	206y	302z	402y	102z	104z	107z	304z	306z	307z
setup 3	106z	206y	302z	402y	102y	103y	104y	304y	306y	307y
setup 4	106z	206y	302z	402y	101y	105y	107y	301y	303y	305y
setup 5	106z	206y	302z	402y	102y	103y	104y	304y	306y	307y
setup 6	106z	206y	302z	402y	100x	100y	300y	300x	308x	
setup 7	106z	206y	302z	402y	403y	404y	405y	406y		
setup 8	106z	206y	302z	402y	201y	207y	401y	407y		

In order to identify the real operational conditions of the bearings, 5 sensors were placed at bearings. Four sensors at two nodes (100 and 300) in direction x and y, and the remaining one at node 308 in direction

x). As the bearing at node 108 was a fixed one, no sensor was placed at this node.

6.2.3.1.3. Data acquisition process

A 12-channel data acquisition system (Figure 6-7), using three NI 9234 modules from National Instruments was employed to record the voltage signals from the sensors and to convert these analog signals after conditioning to digital data. A portable computer was used to command the data acquisition system and to read and save the digital data.

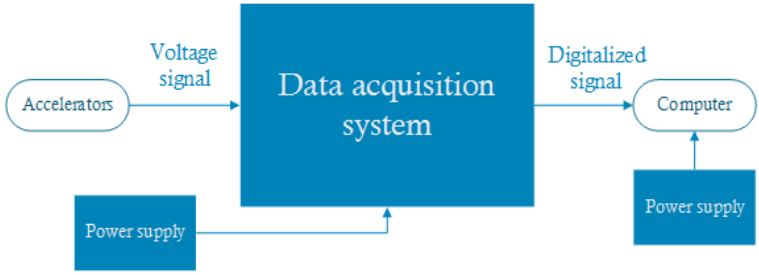

Figure 6-7– Data acquisition process

The total acquisition time was at least ten to twenty minutes (approx. 900 - 1200 s) for one output-only setup at a sampling rate of 1651 Hz. It meant that each channel had 1485900 - 1981200 data points. The envisaged acquisition time was 20 minutes for the AVT. For some setups, this was shortened because of the passage of a train during the measurement. However, a measurement duration of 10 minutes was considered to be sufficient, considering the natural frequencies of the

lowest modes. As the system identification was done for each setup separately, time lengths had not to be identical. The measurement campaign took place on two successive days. Figure 6-8 shows the installation of the equipment on site.

(a) (b)

Figure 6-8–Field measurement instrumentation: (a) DAQ system (Compact DAQ Chassis NI 9178 and 3 vibration modules NI 9234) and portable computer; (b) Transversal accelerometer (PCB-393B12) at truss connection.

6.2.3.2. System identification by MACEC

6.2.3.2.1. Data pre-processing

In this stage, MACEC software developed by Edwin Reynders *et al.* [104] was employed to process the measured data. Some parameters in MACEC had to be set up for treating the acquired acceleration data from

8 setups in a systematic manner. The procedure of data pre-processing is as follows:

- The first step was to construct a grid of measured nodes, then connecting these nodes by lines to create a visualization of the structure.

- Input required parameters include labels, data types, sensitivities, amplification factors, and measurement units, corresponding to each channel.

- A pure ambient response measurement in a period of approximately ten minutes was extracted.

- There was always an offset on the measured signal data, therefore, the DC component needs to be removed from the time series of all channels.

- A "FILT-FILT" function was applied to pass signals with a frequency higher than a cutoff frequency of 0.5 Hz and attenuated signals with frequencies lower than 0.5 Hz. The purpose of this step was to remove low natural frequency blurring or noise by highlighting frequency trends, i.e. higher than 0.5 Hz [105].

- The frequency range of interest in bridge structure often lies between 0-20 Hz. Therefore, to facilitate the System

Identification, first digital filtering was applied to the measurement signals, followed by resampling them to achieve a Nyquist frequency of 20 Hz by the "DECIMATE" function with a decimation factor of 40.

6.2.3.2.2. Covariance based system identification (SSI-COV)

After the pre-processing stage, a measurement model of the structure was identified. The Stochastic Subspace Identification (SSI) method is often employed to perform system identification for the output-only or OMA of structures. There are two implementations of the SSI: the data-driven (SSI-data) option and the covariance (SSI-cov) option. Reynders *et al*. [105] pointed out that the implementation of the SSI-cov was more straightforward, as well as, computationally less expensive than the SSI-data. In comparison with SSI-data, the SSI-cov implementation also obtains a similar accuracy. Therefore, the dynamic system identification of the tested bridge was performed by SSI-cov.

The system identification was started by specifying the number of block that the raw time data was divided into. The number of block was used for computing sample covariance of the output correlation matrices. In general, half the number of block rows i_0, could be chosen based on the relationship between the lowest frequency of interest and the Nyquist-frequency. In practice, the value of i_0 has a significant influence on the quality of the identified system model. Its value should be as large as possible, however, the excessiveness of calculation time and memory

usage should be considered [105]. For this case, the value of i_0 was chosen as 250.

Another parameter that needs to be considered was the maximum system order. In the theoretical aspect, observing the number of non-zero singular value of the block Toeplitz can identify the system order n_s. In practice, it is not easy to inspect this number of non-zeroes because of the noise from modelling inaccuracies, measurement noise…etc., the higher singular values do not equal zero exactly. Therefore, a maximal "gap" between two successive singular values becomes important evidence to find the system order. Peeters *et al* [106] stated that the gap was not clear to find out, especially in large structures. For system identification of the Nam O bridge, the considered system order was ranged from 2 to 140 in increasing steps of 2 i.e., [2:2:140].

6.2.3.3. Modal analysis

To obtain a clear stabilization diagram when model orders ranged from 2 to 140, some criteria need to be specified. The criteria were 1% for frequency stabilization, 5% for damping ratio stabilization, and 1% for mode shape stabilization. These values were selected based on experience with many other similar structures [105]. The stable poles appeared systematically in certain frequency sub-intervals, from 0 to 15 Hz. The stabilization diagram with SSI-cov of setup 1 is shown in Figure 6-9 for illustration purposes.

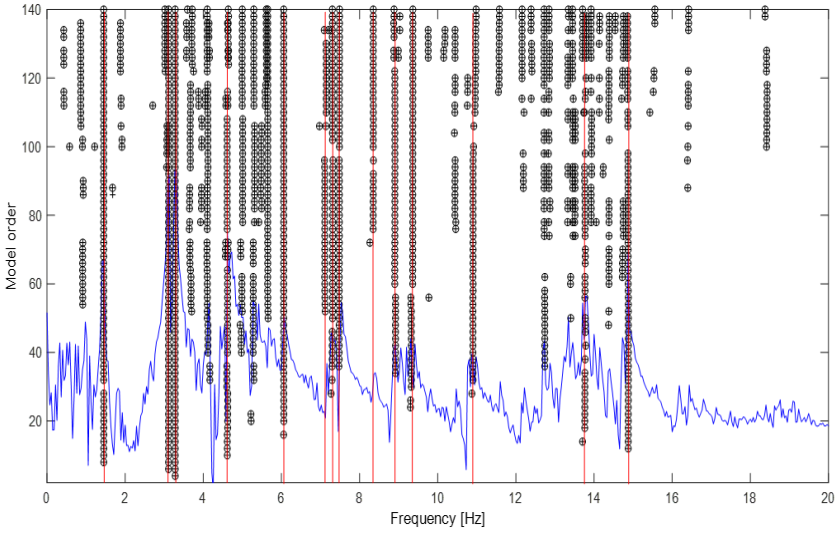

Figure 6-9–The stabilization diagram of setup 1 in the interval from 0 to 20 Hz. The used symbols are: ⊕ for a stable pole, (.v) for a stable frequency and mode shape vectors pole, (.d) for a stable frequency and damping pole and (.f) for a stable frequency pole

Theoretically, a bridge has a multitude of vibration modes. However, all the modes of vibration do not contribute equally to the response of a structure. Normally only the first few modes, which have higher participation factors are considered to get the dynamic response of structures. Those main lower modes are enough to solve the model updating problem. In this case, only the first 5 modes within the frequency interval from 1.45 Hz to 6.05 Hz, as shown in Figure 6-10 were used for model updating. For a detailed explanation about the construction and the

interpretation of the stabilization diagram in Figure 6-9, the reader is referred to [106].

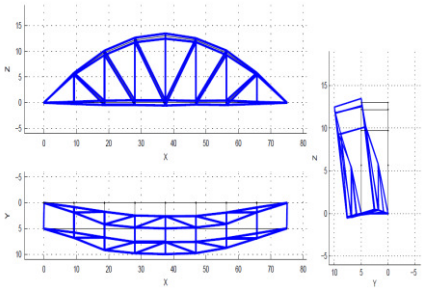

Mode 1, first lateral, $f = 1.45$ Hz, xi=0.82%

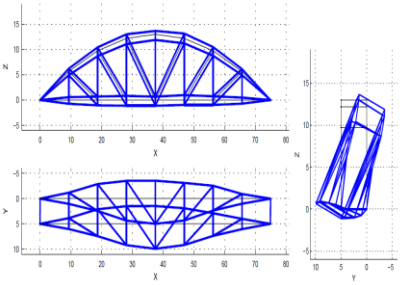

Mode 2, first torsion, $f = 3.11$ Hz, xi =0.19%

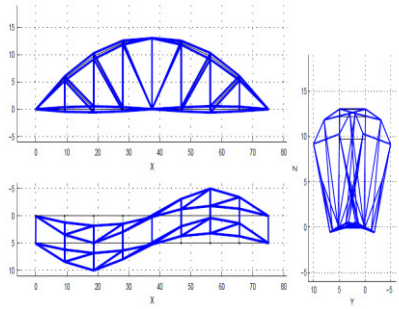

Mode 3, second lateral, $f = 3.28$ Hz, xi =0.27%

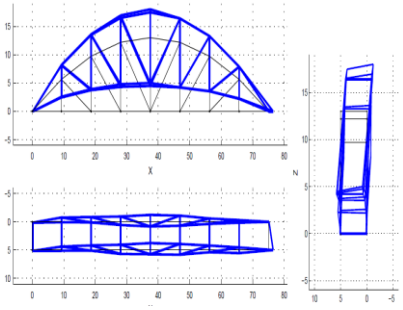

Mode 4, first vertical bending, $f = 4.62$ Hz, xi =2.54%

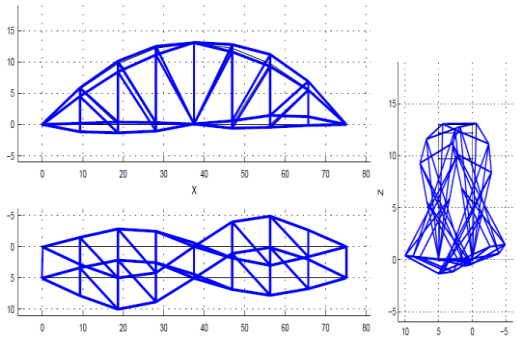

Mode 5, second torsion, $f = 6.05$ Hz, $xi = 0.28\%$

Figure 6-10– identified modes

6.2.4. Model updating

A FEM updating is applied in the Nam O Bridge. Eight uncertain parameters, including Young's modulus of truss members (E), the stiffness of 6 springs under bearings (k_1, k_2, k_3, k_4, k_5, k_6) as shown in Figure 6-11, and the stiffness of rotational springs at truss joints (k_7) are chosen to update. The approach for determining the original stiffness of rotational springs is referred from [98], whereas the stiffness of springs at the bearings is calculated based on bearing types.

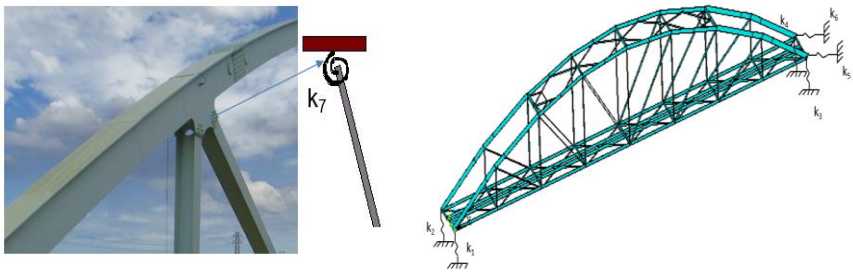

(a) (b)

Figure 6-11–Uncertain structure parameters are selected to update in the model: (a) The springs at truss joints; (b) The springs at bearings.

The objective function is built based on both mode shapes and natural frequencies. PSO and GA algorithms are used to look for the best solution. In PSO, a population size of 50 individuals is used. The inertia weight parameter (w) is 0.3, and the values of the cognition learning factor and the social learning factor are $c_1 = 2$ and $c_2 = 2$. In order to compare with PSO, for GA, the population size of 50 individuals is also applied, crossover and mutation coefficients are 0.8 and 0.1, respectively. The stop criteria of loops in both PSO and GA are established as follows: the deviation of objective function (fitness) value between two consecutive iterations is lower than 10^{-6}, or the maximum number of iterations is 100.

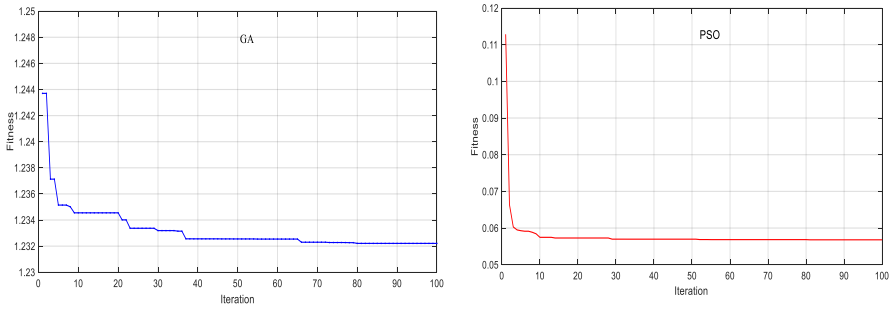

(a) (b)

Figure 6-12–Fitness tolerance (a) GA; (b) PSO

Figure 6-12 shows that the convergence rate of PSO is faster than GA. With the same population, PSO can find the result of the global best (the best solution) after only 30 iterations, Whereas GA needs approximately 80 iterations to obtain the global best. Besides, the convergence level of PSO outperforms that of GA. The tolerance of the objective function of PSO is lower than 0.1, while the result of GA is about 1.2. That means that the deviation between numerical model and measurement after model updating using PSO was lower than GA. This result can be explained based on the approach for finding the best solution in the two algorithms. While in PSO, only the best global position of particles (the best solution) is given out, in GA, information of all particles is shared with each other after each iteration.

A summary of the analysis and the experimental results is given in Table 6.6 and Figure 6-13.

- Apart from mode 5 (the difference of natural frequency between FEM and measurement is 7.6%), the natural frequencies of mode 1, mode 2, mode 3, and mode 4 calculated by FEM and measurement do perfectly match.
- The MAC values from 0.99 to 0.90 (Figure 6-13) demonstrate a close correspondence between the mode shapes of FEM and measurement.
- The results of both calculated frequencies and mode shapes applying PSO are closer to those of the measurement than GA.

After model updating, the FEM is applied to validate higher modes that were not included in the objective function. Table 6.6 and Figure 6-13 show that the model updating also reduces the deviation between the measured and calculated natural frequencies, mode shapes of the higher modes (mode 6 to mode 10).

Table 6.6 – The modal natural frequencies from the FEM after model updating compared to the measurement

Mode	Before model updating (Hz)	Model updating-GA(Hz)	Model updating-PSO(Hz)	Measurement (Hz)
1	1.47 (1.4%)	1.47 (1.3%)	1.45 (0%)	1.45
2	3.14 (1%)	3.06 (1.6%)	3.10 (0.3%)	3.11

3	3.32 (1.2%)	3.29 (0.3%)	3.27 (0.3%)	3.28
4	4.80 (3.7%)	4.70 (1.7%)	4.66 (0.8%)	4.62
5	6.96 (13%)	6.53 (7.3%)	6.55 (7.6%)	6.05
6	7.21 (1.35%)	7.11 (0.2%)	7.15 (0.4%)	7.12
7	7.50 (2.74%)	7.35 (0.7%)	7.33 (0.5%)	7.30
8	8.33 (14,1)	8.21 (10%)	8.10 (8.57%)	7.46
9	9.18 (10.81%)	9.05 (9.2%)	9.00 (7.94%)	8.29
10	9.79 (10.16%)	9.64 (8.5%)	9.57 (7.10%)	8.89

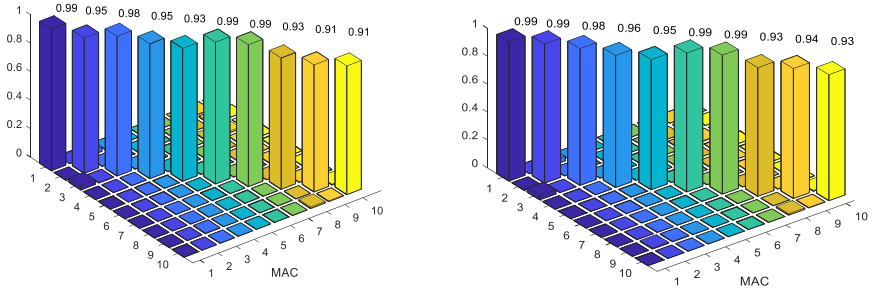

(a) (b)

Figure 6-13–MAC values of mode shapes after model updating: (a) GA; (b) PSO

Table 6.7 gives the range of variation of the uncertain parameters based on experience or estimated according to reference [98]. The model updating process also adjusts uncertain parameters of the bridge (Table 6.8). The changes in Table 6.8 show that the parameters before and after updating are not too much different. This is easy to explain since the Nam O bridge has been in operation for about 7 years. Therefore, the bridge is in a good situation. The stiffness of the bearing and rotational springs $k_1, k_2, k_3, k_4 k_{5,} k_{6,}$ and k_7 have a decreasing trend with lower levels for GA compared to that of PSO. This proves that the stiffness of bearings and rotational springs is overestimated. Therefore, to get consistent correspondence between theoretical and experimental results, the stiffness of bearings and rotational springs should be adjusted.

Table 6.7 – The range of variation of the uncertainty parameters

	k_1	k_2	k_3	k_4	k_5	k_6	k_7	E
Lower	1.0	1.0	1.0	1.0	1.0	1.0	7	1.9
Upper	2.0	2.0	2.0	2.0	2.0	2.0	9	2.2

Table 6.8 – Values of uncertain parameters before and after updating.

	k_1	k_2	k_3	k_4	k_5	k_6	k_7	E
Before	1.3	1.3	1.3	1.3	1.5	1.5	8	2

After(GA)	1.27	1.22	1.19	1.21	1.45	1.38	7.8	1.99
After(PSO)	1.20	1.16	1.12	1.16	1.40	1.33	7.6	1.98

Note: unit of k_1, k_2, k_3, k_4 is 10^{10} N/m, unit of k_5, k_6 is 10^7 N/m, unit of k_7 is 10^5 N.m/rad, unit of E is 10^5 MPa.

6.3 Guadalquivir railway bridge

6.3.1. Bridge description

The Guadalquivir railway bridge (Figure 6-14) located in Seville city (Spain) is a twin steel truss bridge with one rail track in each direction. The bridge includes five continuous truss spans: two side spans 51 m long and three intermediate spans of 50.94 m. While the two abutments are labeled as $E1$ and $E2$, the four piers are referred to as $P1$, $P2$, $P3$, and $P4$. The right main span represents the downstream side of the river, whereas the left main one is located at the upstream side of the river. The bridge was opened to traffic in 1929 and has been reinforced on several occasions by adding reinforcements to its members. It seems that the condition of the bridge is fairly good by visual inspection but several local defects exist in connection bolts and the structural members.

Figure 6-14–The Guadalquivir railway bridge [108].

6.3.2. FEM

A FEM (Figure 6-15) is built using the MATLAB toolbox Stabil [95] based on the geometry obtained from design drawings and site visits and inspections.

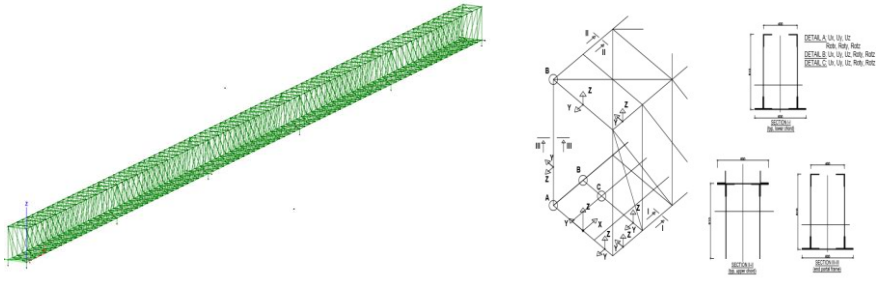

(a) (b)

Figure 6-15–(a) FEM of Guadalquivir railway bridge; (b) Details of beam element cross-sections and connections. XYZ is the global coordinate system, xyz is the local axis system of the beam elements.

The main structural members consist of top chords, bottom chords, stringers, portal frames, verticals modeled using three-dimensional beam elements. The beam element is based on Timoshenko beam theory which includes shear-deformation effects. The element provides options for unrestrained warping and restrained warping of cross-sections. The counter braking truss, the bracing members, and the transverse beams are modeled utilizing a beam element type. The rail track and non-structural components such as handrail, maintenance path, and power line, etc. are included in the model as added mass. The counter braking truss is connected to truss members by translational constraints to the node joints. The global X-axis is in the longitudinal direction of the bridge; the Z-axis is in the vertical direction, and the Y-axis is in the transverse direction (to the river flow direction). Pier $P2$ and abutment $E2$ use pin bearings (fixed bearings), and others apply roller ones. Roller bearings allow translational and rotational displacement in the longitudinal direction, whereas pin ones only permit rotation. Bearings are modeled using spring elements.

Figure 6-16 shows the cross-section of the different beam members. The connection between the transverse floor beams of the portal frames

with the main truss is modeled as fully constrained, i.e., all six DOFs are fixed (detail A in Figure 6-16). The connection between the upper transverse beams of the portal frames with the main truss is also modeled as fully constrained except for the rotation of the upper transverse beam along its beam axis (global Y direction). This choice is based on a visual inspection of the bridge. Likewise, the same type of constraint is used for the connection between other floor beams to the main truss (detail B). The stringer (longitudinal floor beam) is discontinuous at the cross floor beam positions. Its connection with the floor beams also permits the rotation around its local longitudinal axis, which is parallel to the global X direction.

Table 6.9 – Summary of the first twenty-two modes from FEM.

Modes	f (Hz)	Mode types	Modes	f (Hz)	Mode types
1	2.81	1st ↔	12	6.96	5th ↕
2	2.95	2nd ↔	13	7.13	8th ↔
3	3.70	3rd ↔	14	7.35	9th ↔
4	3.91	4th ↔	15	7.85	10th ↔
5	4.38	1st ↕	16	8.18	11th ↔
6	4.49	5th↔	17	8.59	1st ∩
7	4.69	2nd ↕	18	8.65	2nd ∩

8	5.43	3rd ↕	19	8.73	3rd ∩
9	5.70	6th ↔	20	8.96	4th ∩
10	5.96	7th ↔	21	9.72	5th ∩
11	6.31	4th ↕	22	10.02	6th ∩

Note: ↔ transverse; ↑ vertical; ∩ torsion;

The first twenty-two modes within the frequency range from 2.81 Hz to 10.02 Hz as shown in Table 6.9. In this frequency interval, all modes are global, i.e., not localized in a part of the structure. Some modes have very close natural frequencies, which may present a challenge to separate them from the identified modes of the experimental data. Modes 1-4, 6, 9-10, and 13-16 are transverse bending modes. Mode 1 (2.81 Hz) has its main deformation in the first span, whereas mode 2 (2.95 Hz) is similar but has its main deformation in the last span. Modes 5, 7-8, 11, and 12 are vertical bending modes. Most of them exhibit longitudinal modal displacements. Mode 17 and higher modes are torsional modes. In fact, they are rather a combination of transversal and torsional frame deformation. Figure 6-16 shows some selected mode shapes from the FEM.

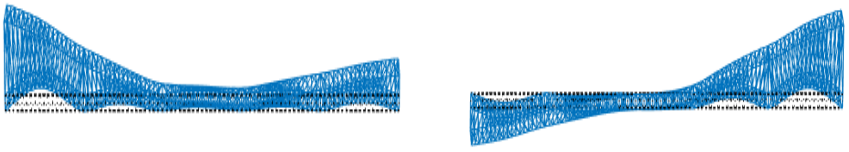

Mode 1 (2.81 Hz)

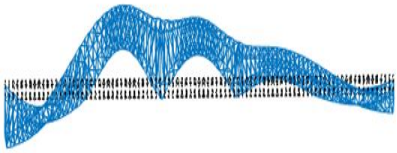

Mode 2 (2.95 Hz)

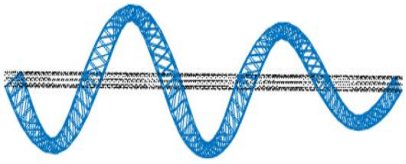

Mode 3 (3.70 Hz)

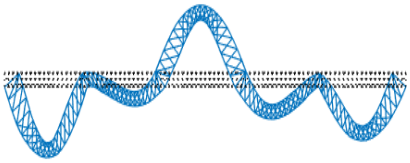

Mode 5 (4.38 Hz)

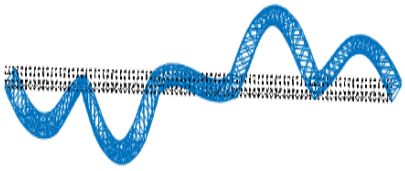

Mode 8 (5.43 Hz)

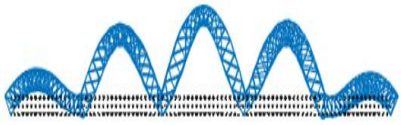

Mode 11 (6.31 Hz)

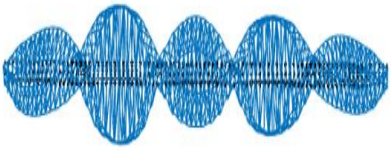

Mode 12 (6.96 Hz)

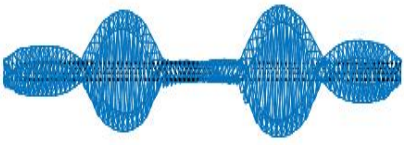

Mode 18 (8.65 Hz)

Mode 21 (9.72 Hz) Mode 22 (10.02 Hz)

Figure 6-16–Selected mode shapes from FEM of the Guadalquivir bridge. Modes 1, 2, 3 are transverse; modes 5, 8, 11, 12 are vertical; modes 18, 21, 22 are torsion.

6.3.3. Measurements

6.3.3.1. Instrumentation and test setup

The AVT was carried out by the Structural Mechanics section of KU Leuven on one of the two bridges located on the upstream side of the river (for train traffic from Alcazar to Seville). In order to speed up the roving process between test setups, wireless triaxial sensors (Figure 6-17) were used instead of a classical wired system.

Figure 6-17. wireless triaxial sensors

Twelve triaxial wireless acceleration sensor units (GeoSIG GMS-18) [109] were connected by a time-synchronous Wi-Fi network. The data quality and operational efficiency make wireless acceleration sensors increasingly common in civil engineering practice. The application of wireless triaxial sensors avoided the use of cables, permitted to cover all the length of this very large structure. This supported the field measurements in becoming more convenient by reduced equipment installation time.

Ideally, this kind of truss structure would have the same measurement grid as the truss joints on the bottom and the top levels. However, due to safety reasons, systematic measurement of the node joint DOFs only performed on the bottom chords. The upper chords only contained a limited number of nodes measured, at portal frames 0; 86, and 90 (see Figure 6-18 for the portal frame numbers). This ideal solution facilitated the organization of the AVT without reducing the quality of the results. The measurements were divided into successive test setups. Four fixed reference sensors were placed on the right main truss at bay numbers 9, 27, 43, and 63. These reference sensors were positioned at locations where most modes with relatively large modal displacements as obtained from the preliminary numerical model. The fifth fixed reference sensor was placed at node 63 on the left main truss. A well-chosen selection of the reference sensors was extremely essential to guarantee a

proper identification of all the vital mode shapes. Figure 6-18 shows the measurement grid design for the AVT.

The remaining seven sensors were employed as roving sensors. Table 6.10 shows the location of the roving sensors among setups on the right main truss. They were distributed in a way that, at each particular setup, there was at least one sensor in each span. Setups 14 to 26 were identical to setups 1 to 13. However, they were situated at the left main truss. There were twenty-seven setups in total. The last setup (setup 27) was designed to measure the vibration of the transversal portal frame and helped afterwards to distinguish between the global modes. In this setup, four sensors were installed on a few accessible upper chord nodes at the bridge ends.

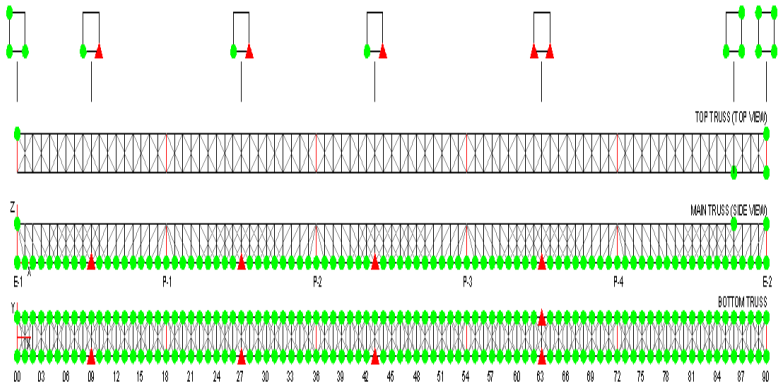

Figure 6-18– The measurement points (●) and the location of the fixed reference sensors (▲).

Table 6.10 – Roving sensor positions for all setups. Superscript l_e indicates positions on the left main truss; superscript t_e indicates positions on the upper chord.

Set ups	Node numbers to be measured						
1	0	1333	266	39	52	65	788
2	1	14	27	40	53	66	79
3	2	15	28	41	54	67	80
4	3	16	29	42	55	68	81
5	4	17	30	43	56	69	82
6	5	18	31	44	57	70	83
7	6	19	32	45	58	71	84
8	7	20	33	46	59	72	85
9	8	21	34	47	60	73	86
10	9	22	35	48	61	74	87
11	10	23	36	49	62	75	88
12	11	24	37	50	63	76	89
13	12	25	38	51	64	77	90
27	$1t_e$	$86l_e$	$86t_e$	$90l_e$	90	$90t_e$	$90t_e$

The sampling frequency was 200 Hz. The measurement duration was about fifteen minutes per setup. It took about 30 minutes on average to complete one setup including the time to relocate roving sensors. Train

traffic operated normally with up to 5 train passages per hour during rush hours. The whole in-situ test was done in less than two working days.

6.3.3.2. Test results

6.3.3.2.1. System identification and modal analysis

A pure ambient measurement period of about 10 to 15 minutes was extracted for each setup. OMA was performed using the MATLAB toolbox MACEC 3.2 [95]. A high pass filter was applied with a cut-off frequency of 0.1 Hz to remove the low drift frequency. Next, low pass digital filtering of the data was employed in both forward and reverse directions and the data was down-sampled to 50 Hz. By applying the reference-based implementation of the Covariance-Driven Stochastic Subspace Identification Method (SSI-cov/ref), a model of the tested structure was determined from the data in the system identification process.

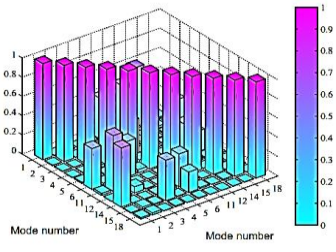

(a)

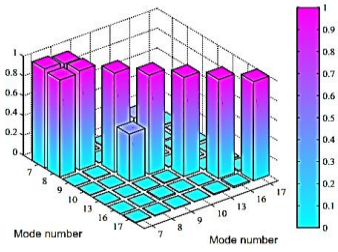

(b)

Figure 6-19–The MAC-values of identified modes. (a) transverse modes; (b) vertical modes.

The reference signals were taken as the pre-processed time histories from the channels connected to the fixed reference sensors. The considered model order range was from 2 to 250 in steps of 2 and half the number of block row was 120. The main stabilization criteria were taken the same as in [105], the differences in two consecutive natural frequencies and damping ratios were $dfi \leq 1\%$ and $d\xi i \leq 5\%$, respectively; MAC values between two successive mode shapes were lower than 1% and the Modal Phase Collinearity (MPC) was larger than 0.5. These values were chosen based on experience with numerous other similar structures. Thirty-seven modes were identified within a frequency range from 2.78 Hz to 14.21 Hz.

The identified modal characteristics are given in Table 6.11. The identified modes are all characterized by a low damping ratio. Most of them have a mode shape that is almost purely real, as evidenced by high MPC and low Mean Phase Deviation (MPD) values, which ensures a very high degree of accuracy. Mode 3 (2.99 Hz) has lower quality (as seen from the lower MPC and higher MPD values), possibly because it was not well stimulated. Its identified frequency is very close to that of mode 2 (2.90 Hz). Another explanation could be that mode 3 has its largest modal displacements in span 5 where no fixed reference sensor was located. Modes 14, 19, 22, 28, 29, 36, and 37 have an MPC value less than 0.85,

indicating a lower accuracy. These modes are either transverse modes or torsional modes of a high order. Modes 15 and 28 also have MPD values that are larger than 10^{o}.

Table 6.11 – Summary of the first thirty-seven modes from the measurement.

Modes	f (Hz)	MPC [-]	MPD [o]	Modes	f (Hz)	MPC [-]	MPD [o]
1 ↔	2.78	0.976	5.7	20↔	7.37	0.791	15.2
2 ↔	2.90	0.985	5.1	21↔	8.46	0.854	12.5
3 ↔	2.99	0.876	13.0	22↔	8.52	0.847	12.1
4 ↔	3.13	0.962	6.5	23∩	8.90	0.945	6.7
5↔	3.24	0.972	5.7	24∩	9.11	0.95	6.4
6↔	3.36	0.912	12.9	25 ∩	9.33	0.933	7.8
7↕	4.36	0.984	3.5	26 ∩	9.44	0.951	7.3
8↕	4.48	0.98	3.8	27 ∩	9.65	0.936	7.5
9 ↔	4.65	0.878	10.6	28 ∩	9.87	0.835	13.9
10↕	4.78	0.89	10.4	29 ∩	10.02	0.837	12.6
11↔	5.16	0.907	12.7	30 ∩	10.48	0.926	8.2
12↔	5.22	0.953	9.8	31 ∩	10.55	0.878	11.1
13↕	5.36	0.961	6.4	32 ∩	10.79	0.935	7.9
14↔	5.51	0.844	9.1	33∩	11.09	0.947	7.1
15↔	5.59	0.842	12.9	34 ∩	11.61	0.914	7.6
16↕	6.06	0.961	6.8	35 ∩	12.02	0.905	8.2
17↕	6.70	0.935	8.5	36 ∩	12.59	0.841	13.0
18↔	7.04	0.921	16.3	37∩	14.21	0.843	11.7
19↔	7.19	0.811	13.4				

Note: ↔ transverse; ↑ vertical; ∩ torsion

All modes with a natural frequency between 2.78 and 3.36 Hz are transverse modes. In the frequency range from 4.36 to 7.37 Hz, eight vertical modes are determined. The other five modes in this frequency range are either transverse modes or transverse modes combined with vertical displacements. Modes of some pairs with closely spaced frequencies can be obtained, which demonstrates that the proposed technique separates the close modes well. The first two modes in the frequency range from 8.46 to 14.21 Hz also belong to the combination mode including vertical mode coupled with transverse modal deformation. Almost all modes from 23 onward (from 8.90 Hz to 14.21 Hz) are torsional modes. Modes 29 and 30 can also be assessed as combination modes. It is reminded that only four sensors were located on the upper chords of the bridge. However, the information provided by these sensors is really useful to identify the modal displacements of the portal frames. With this modal information of the three frames at sections 0 (on top of the abutment $E1$), 86, and 90 (close to and on top of the abutment $E2$), some of the measured modes, for instance, measured modes 2 and 3 in Table 6.11 could be related to known modes from the FEM.

6.3.3.2.2. Discussions on the identified mode shapes

Figure 6-20 shows some of the identified mode shapes. The longitudinal displacements of the nodes at the lower chords (in the X-direction) are fairly small compared to those in other directions. There

are very small modal displacements in the longitudinal direction especially at the bearings since bearings on the pier $P2$ and abutment $E2$ are fixed in the longitudinal direction. It seems that the roller supports permit free longitudinal displacements for the service loads and thermal expansion but restrain longitudinal displacements under small amplitude vibrations.

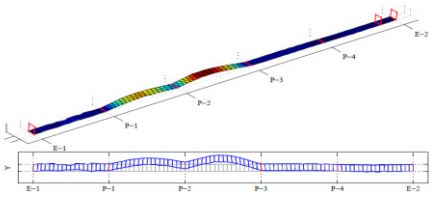

Mode 1 (2.78 Hz)

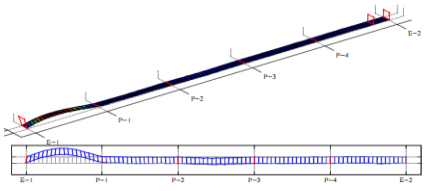

Mode 2 (2.90 Hz)

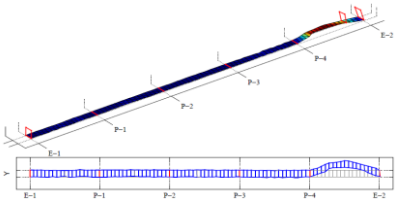

Mode 3 (2.99 Hz)

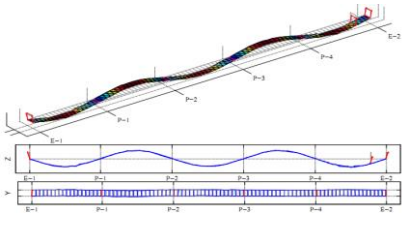

Mode 8 (4.48 Hz)

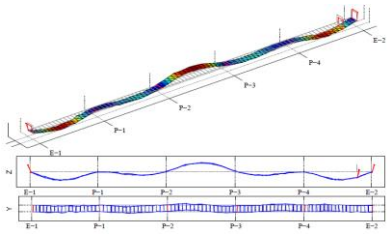

Mode 13 (5.36 Hz)

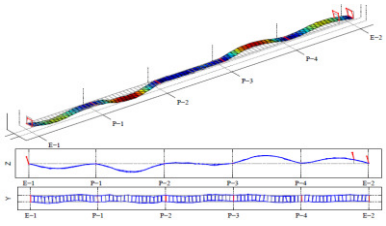

Mode 16 (6.06 Hz)

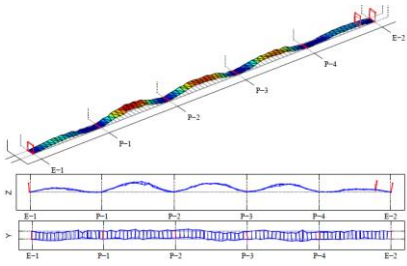

Mode 17 (6.70 Hz)

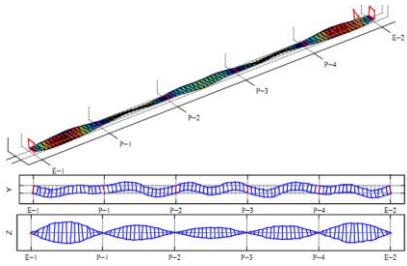

Mode 24 (9.11 Hz)

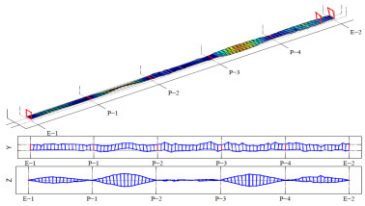

Mode 29 (10.02 Hz)

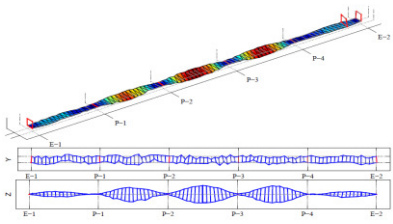

Mode 30 (10.48 Hz)

Figure 6-20–Selected mode shapes identified from the modal test. Modes 1, 2, 3, are transverse; modes 8, 13, 16, 17 are vertical; modes 24, 29, 30 are torsion.

Mode 8 (4.48 Hz) is the second vertical mode having the maximum modal displacement in the fifth span. Figure 6-19 indicates MAC values among different identified transverse and vertical modes, respectively. For the measured vertical modes, the high values of the MAC between modes 7 and 8 are obtained since the linear dependence of the modal displacements in the lower chords of the bridge.

6.3.3.3. Validation of the numerical model

The identified modes are compared with the modes of the numerical model. The modes are separated into three groups including transverse, vertical, and torsional modes.

6.3.3.3.1. Transverse modes

The discrepancy of natural frequencies and MAC-values between numerical and experimental modal analysis results are listed in Table 6.12.

Table 6.12 – Comparison between measured and FEM results for the transverse modes.

Measurement		FEM		Difference (%)	Mac values
Modes	f (Hz)	Modes	f (Hz)		
1	2.78	3	3.70	24.8	0.85
2	2.90	1	2.81	3.20	0.86
3	2.99	2	2.95	1.35	0.87
4	3.13	4	3.91	19.9	0.90
5	3.24	N/A	N/A		
6	3.36	N/A	N/A		
9	4.65	6	4.49	3.56	0.85
11	5.16	N/A	N/A		
12	5.22	N/A	N/A		
14	5.51	9	5.70	3.33	0.90
15	5.59	10	5.96	6.20	0.90
18	7.04	13	7.13	1.26	0.94
19	7.19	N/A	N/A		
20	7.37	14	7.35	0.27	0.94
21	8.46	15	7.85	7.77	0.93
22	8.52	16	8.18	4.15	0.91

Table 6.12 shows that apart from mode 1 and mode 4, numerical and measured natural frequencies have a close correspondence. However, the identified mode shapes do not match very well with the corresponding analysis ones (MAC values of modes 1-3 and mode 9 are lower than 0.9)

6.3.3.3.2. Vertical modes

Table 6.13 compares the identified and the calculated modes. Generally, the quality of the experimental vertical modes is good, which is demonstrated by the MAC- values shown in Figure 6-19 b. The comparison between natural frequencies and MAC-values between numerical and experimental modal analysis results is given in Table 6.13. The MAC values are close to 1 indicating that a good correspondence between FEM and measurement is obtained.

Table 6.13 – Comparison between measured and FEM results for the vertical modes.

Measurement		FEM		Differences (%)	Mac values
Modes	f (Hz)	Modes	f (Hz)		
8	4.48	5	4.38	2.28	0.98
10	4.78	7	4.69	1.92	0.97
13	5.36	8	5.43	1.29	0.96
16	6.06	11	6.31	3.96	0.96
17	6.70	12	6.96	3.73	0.95

6.3.3.3.3. Torsion modes

The identified torsional modes do not match very well with the corresponding analysis modes. This deviation occurs due to several factors, such as the coupling constraints between the stiffness of the members themselves, and the condition of the bearings. Table 6.14 compares the FEM modes 17-22 with the experimental modes 23-26, 29, and 30, respectively. Identified mode 23 is found to be close to FE mode 17. The natural frequencies of those modes almost coincide with each other, whereas the mode shapes are very similar.

Table 6.14 – Comparison of measured and FEM results for the torsion modes.

Measurement		FEM		Differences (%)	Mac values
Modes	f (Hz)	Modes	f (Hz)		
23	8.90	17	8.59	3.61	0.92
24	9.11	18	8.65	5.32	0.94
25	9.33	19	8.73	6.87	0.87
26	9.44	20	8.96	5.36	0.89
29	10.02	21	9.72	3.08	0.94
30	10.48	22	10.02	4.59	0.93

6.3.4. Model updating

In order to update uncertain parameters (m) consisting of the stiffness of 8 springs under bearings ($k_1, k_2, k_3, k_4, k_5, k_6, k_7, k_8$) as shown in Figure 6-21 and Young's modulus of truss members (E), a FEM updating is applied for the Guadalquivir railway bridge.

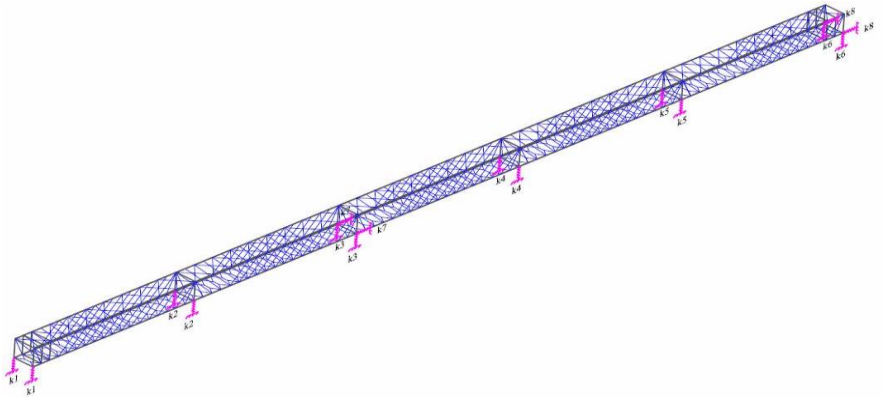

Figure 6-21–Springs under bearings are selected for model updating

ODIPSO coupling IPSO with OD is used for seeking the global best. For IPSO, while the population (n) is 100, the values of the learning factors c_1, and c_2 are 2. To assess the performance of the proposed algorithm, PSO, IPSO, and ODPSO are also applied for model updating of the bridge. The population size, and the values of c_1, and c_2 applying for PSO, IPSO, and ODPSO are the same as those of ODIPSO. The inertia weight w using for PSO and ODPSO is selected equally 0.3. The best solution will be obtained if the discrepancy in two consecutive iterations of the objective function $f(X)$ is lower than 10^{-6} or the maximum number of iterations is 100. The

first ten modes (numerical modes 1-10) are selected for model updating. To assess the effectiveness of the proposed approach, after model updating, the FEM is employed to consider the higher modes (modes 11-22) that were not taken into account for the objective function.

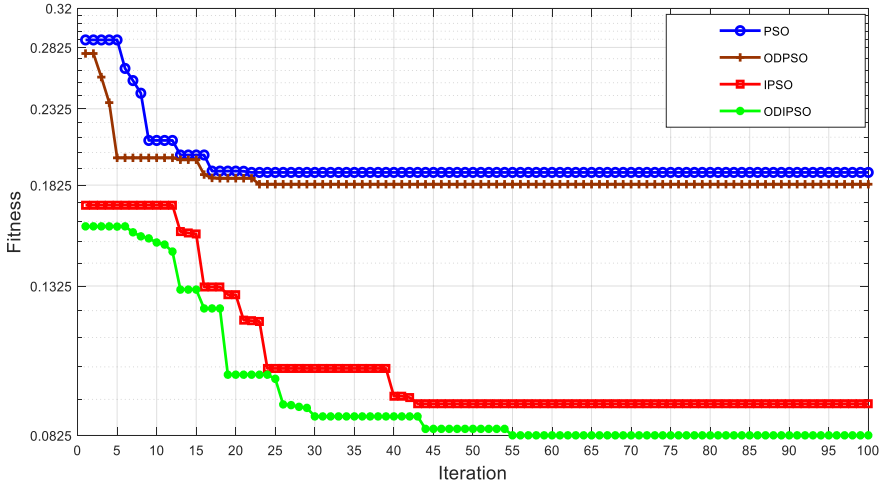

Figure 6-22–Fitness tolerance of PSO, ODPSO, IPSO, and ODIPSO

Table 6.15 – Some evaluation criteria used to compare the considered algorithms

Evaluation criteria	PSO	ODPSO	IPSO	ODIPSO
The number of iteration	100	100	100	100
Speed of convergence	16	23	43	55
Total CPU time (s)	1045623 (12.1 days)	213456 (2.47 days)	1052135 (12.2 days)	214316 (2.48 days)
Convergence level	0.188	0.183	0.091	0.083

From Figure 6-22 and Table 6.15, PSO and ODPSO converge faster than IPSO and ODIPSO. PSO can find the best solution after only 16 iterations, whereas ODPSO, IPSO, and ODIPSO need 23, 43, 55 iterations to look for the best solution, respectively. For convergence level, while the tolerance of objective function of ODIPSO is 0.083, those of PSO, IPSO, and ODPSO are 0.091, 0.183, and 0.188, respectively. In terms of computational cost, PSO and IPSO spend a large amount of time (1045623 s, and 1052135 s on a PC with an Intel I7 Processor 1.91 GHz and 16 GB RAM) to find the best solution. This is a big drawback of applying those algorithms for tackling optimization problems of large-scale structures.

Table 6.16 – Measured and analyzed natural frequencies before and after model updating

Modes	Before model updating (Hz-%)	PSO (Hz-%)	ODPSO (Hz-%)	IPSO (Hz-%)	ODIPSO (Hz-%)	Measurement - modes (Hz)

1	2.81 (3.20%)	2.83 (2.41%)	2.84 (2.11%)	2.86 (1.40%)	2.89 (0.35%)	2.90 (2)
2	2.95 (1.35%)	2.97 (0.67%)	2.98 (0.34%)	2.99 (0.00%)	3.00 (0.33%)	2.99 (3)
3	3.70 (24.8%)	3.51 (20.8%)	3.42 (18.7%)	3.28 (15.2%)	3.21 (13.3%)	2.78 (1)
4	3.91 (19.9%)	3.78 (17.1%)	3.72 (15.8%)	3.58 (12.5%)	3.46 (9.53%)	3.13 (4)
5	4.38 (2.28%)	4.42 (1.38%)	4.43 (1.13%)	4.46 (0.44%)	4.49 (0.22%)	4.48 (8)
6	4.49 (3.56%)	4.52 (2.88%)	4.53 (2.64%)	4.56 (1.97%)	4.57 (1.72%)	4.65 (9)
7	4.69 (1.92%)	4.72 (1.27%)	4.73 (1.05%)	4.77 (0.21%)	4.79 (0.21%)	4.78 (10)
8	5.43 (1.29%)	5.41 (0.92%)	5.40 (0.74%)	5.37 (0.19%)	5.36 (0.00%)	5.36 (13)
9	5.70 (3.33%)	5.67 (2.99%)	5.64 (2.65%)	5.61 (1.95%)	5.58 (1.61%)	5.51 (14)
10	5.96 (6.20%)	5.93 (5.73%)	5.90 (5.25%)	5.83 (4.12%)	5.80 (3.62%)	5.59 (15)
11	6.31 (3.96%)	6.27 (3.34%)	6.25 (3.04%)	6.20 (2.26%)	6.18 (1.94%)	6.06 (16)
12	6.96 (3.73%)	6.93 (3.32%)	6.90 (2.90%)	6.83 (1.90%)	6.80 (1.47%)	6.70 (17)
13	7.13 (1.26%)	7.11 (0.98%)	7.09 (0.71%)	7.05 (0.14%)	7.03 (0.14%)	7.04 (18)
14	7.35 (0.27%)	7.40 (0.41%)	7.42 (0.67%)	7.47 (1.33%)	7.49 (1.60%)	7.37 (20)
15	7.85 (7.77%)	7.91 (6.95%)	7.92 (6.81%)	7.97 (6.15%)	7.99 (5.88%)	8.46 (21)
16	8.18 (4.15%)	8.25 (3.27%)	8.27 (3.02%)	8.32 (2.40%)	8.34 (2.11%)	8.52 (22)
17	8.59 (3.61%)	8.65 (2.89%)	8.67 (2.65%)	8.73 (1.95%)	8.75 (1.71%)	8.90 (23)
18	8.65 (5.32%)	8.71 (4.59%)	8.73 (4.35%)	8.79 (3.64%)	8.80 (2.36%)	9.11 (24)
19	8.73 (6.87%)	8.79 (6.14%)	8.82 (5.78%)	8.88 (5.07%)	8.90 (4.83%)	9.33 (25)
20	8.96 (5.36%)	9.01 (4.77%)	9.03 (4.54%)	9.06 (4.19%)	9.08 (3.81%)	9.44 (26)

21	9.72 (3.08%)	9.76 (2.66%)	9.78 (2.45%)	9.82 (2.03%)	9.89 (1.31%)	10.02 (29)
22	10.02 (4.59%)	10.08 (3.97%)	10.2 (2.74%)	10.3 (1.65%)	10.4 (0.77%)	10.48 (30)

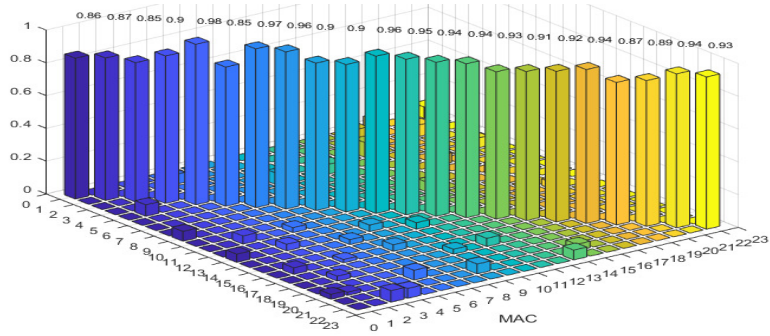

(a)

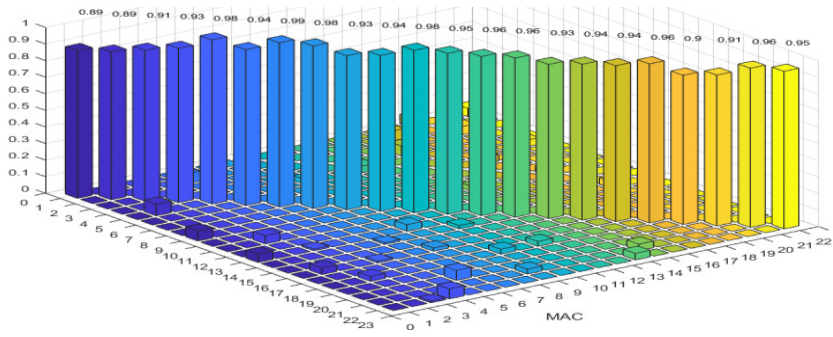

(b)

Figure 6-23–MAC values of mode shapes (a) before model updating (b) after model updating (ODIPSO)

The results presented in Table 6.16 and Figure 6-23 indicate that after model updating the achieved correlation between numerical and experimental modal analysis results is remarkable.

- Natural frequencies of modes obtained by numerical model and measurement do perfectly match except for transverse mode 3 (FEM mode), which is probably due to the boundary conditions in the transverse direction.

- The MAC values after model updating improved considerably (Figure 6-23). This demonstrates a close correspondence between the mode shapes of FEM and measurement.

- After model updating, the FEM is employed to consider other modes (numerical modes 11-22) that do not belong to the objective function. Table 6.16 and Figure 6-23 show that the model updating also reduces the discrepancy between the numerical and experimental results of other modes.

- The results demonstrate the superiority of ODIPSO algorithm over PSO, IPSO, and ODIPSO in terms of accuracy. This can be explained based on two main reasons:

1. Because ODIPSO employs IPSO to make particles of PSO more flexible.

2. OD is employed to arrange and only select the best quality particles for the next steps, this strategy helps to control the search space and to increase the effectiveness of ODIPSO.

Table 6.17 presents the initial estimated values of the uncertain parameters based on experience or estimated according to Ref. [110]. After model updating, uncertain parameters of the bridge are obtained as shown in Table 6.18

Table 6.17 – The range of variation of the uncertain parameters

	k_1	k_2	k_3	k_4	k_5	k_6	k_7	k_8	E
Lower	1,0	1,0	1,0	1,0	1,0	1,0	7	7	1,94
Upper	3,0	3,0	3,0	3,0	3,0	3,0	9	9	2,2

Table 6.18 – Values of uncertain parameters before and after updating

	k_1	k_2	k_3	k_4	k_5	k_6	k_7	k_8	E
Initial values	1,5	1,5	1,5	1,5	1,5	1,5	8,5	8,5	2,05
PSO	1,47	1,58	1,52	1,63	1,72	1,46	8,0	7,8	2,09
ODPSO	1,45	1,67	1,56	1,68	1,76	1,43	7,8	7,6	2,10
IPSO	1,41	1,69	1,57	1,72	1,82	1,38	7,5	7,4	2,12
ODIPSO	1,39	1,72	1,59	1,75	1,84	1,35	7,4	7,2	2,13

Note: unit of $k_1, k_2, k_3, k_4, k_5, k_6$ is $\times 10^{10}$N/m, unit of k_7, k_8 is $\times 10^7$ N/m, unit of E is $\times 10^5$ MPa

6.4 Chuong Duong bridge

6.4.1. Bridge description

This section will deal with simulations of damages (single and multiple) and the capability of different methods to find the simulated damages. An old large-scale steel truss bridge is employed. Chuong Duong Bridge (Figure 6-24) was built in 1983 across the Red River, connecting Hoan Kiem district with Long Bien district in Hanoi (Vietnam). The bridge consists of 11 simple spans with almost equal length (90m). Due to a long exploitation period of dense traffic flow and heavy loads with less maintenance, the bridge has been severely degraded with many damages appearing in truss members. Hence, a preliminary numerical model is needed for a proper design of the measurement campaign.

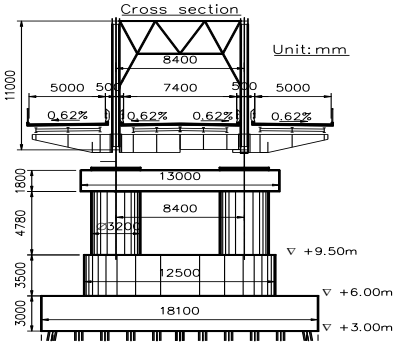

(a) (b)

Figure 6-24– Chuong Duong bridge; (a) General layout; (b) Cross-section of the bridge

Truss members consist of bottom lateral bracing, top lateral bracing, struts, diagonal chords, vertical chords, top chords, bottom chords shown in Table 6.19, and Figure 6.25 a [111].

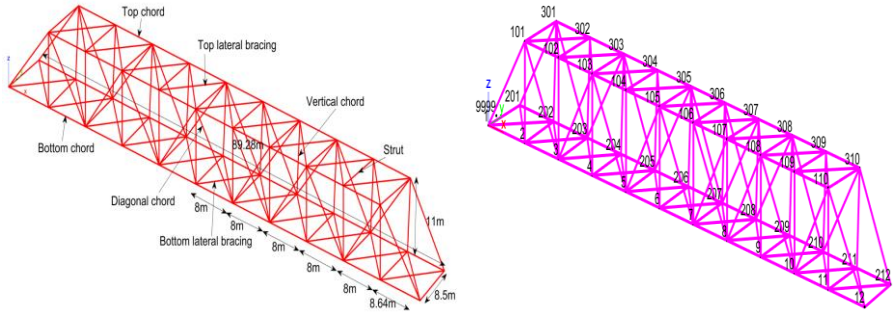

(a) Truss members (b) FEM

Figure 6.25. (a) Truss members, (b) FEM of Chuong Duong bridge

Table 6.19 – Cross-sectional properties of truss members

Truss members	Area (m^2)	Moment of inertia I_y (m^4)	Moment of inertia I_z (m^4)
Bottom lateral bracing	0,0080	0,00036	0,00065

Top lateral bracing	0,0081	0,00038	0,00071
Struts	0,067	0,01368	0,02194
Diagonal chords	0,067	0,01368	0,02194
Vertical chords	0,067	0,01368	0,02194
Top chords	0,067	0,01368	0,02194
Bottom chords	0,067	0,01368	0,02194

Note: I_y is the moment of inertia of the weak axis (the same direction with global Y), I_z is the moment of inertia of the strong axis (the same direction with global Z).

6.4.2. FEM

A FEM of the span on piers $P1$ and $P2$ (Figure 6.25 b) is built using the Stabil toolbox of MATLAB [95]. This model consists of 45 nodes and 146 beam elements with six DOFs at each node including translational displacements in X, Y, and Z - axes and the rotational displacements around X, Y and Z - axes. Pier $P1$ uses a pin bearing that only allows rotational displacements, whereas $P2$ applies a roller one that allows translational and rotational displacements.

The X-axis coincides with the longitudinal direction, while the Z-axis corresponds to the vertical direction and the Y-axis is in the horizontal axis of the bridge.

Modal analysis is performed by using a baseline model to generate input and output data for the network. The architecture network includes 3 layers (one input layer, one hidden layer, and one output layer). Input data consists of natural frequencies of the first fifteen modes as shown in Table 6.20, whereas output data includes damage locations and levels.

Table 6.20 – Natural frequencies of the first fifteen modes.

Modes	Natural frequencies (Hz)	Modes	Natural frequencies (Hz)	Modes	Natural frequencies (Hz)
1	1,23	6	6,21	11	8,89
2	2,41	7	7,78	12	9,58
3	4,19	8	8,03	13	9,99
4	4,26	9	8,24	14	10,22
5	4,59	10	8,84	15	10,83

The number of neuron in the hidden layer heavily influences the results of the process of training the network. It is assumed that the choice

of how many neurons depends on the specific problems that need to be solved. Hence, the number of neuron in the hidden layer is selected differently for each specific case by using iterations to determine the most optimal solution for the network. The data is split into three datasets including 70% for training, 15% for validation, and 15% for test.

To evaluate the effectiveness of the proposed method, both single and multiple damages are taken into account. The effect of noise is also assessed for all cases with a level of 2 % for natural frequencies. A computer with an Intel I7 Processor 1.91 GHz and 16GB RAM is employed to conduct all calculation tasks. To compare with ANNCS1, CS, ANN, and ANNCS2 are also applied to identify damages in the beam. For CS, the population number is 200 and the probability of detecting an alien egg is 0.25. ANN, ANNCS1, and ANNCS2 employ the Levenberg-Marquardt (LM) backpropagation algorithm to train the network.

6.4.3. Damage detection

6.4.3.1. Single damages

The stiffness of the elements decreases from 0% to 50% with an interval of 1%. Because the considered bridge is a large-scale model with numerous elements as well as DOFs, to reduce computational time, only truss members on one plane are employed for damage detection. The number of input data used to train the network is calculated as Eq. (6.1).

$$N_{s1} = n_e * n_s \tag{6.1}$$

Where n_e is the number of considered elements, n_s is the number of damage scenarios occurring at one element. Totally, there are 2100 samples (N_{s1}=$n_e * n_s = 42 * 50 = 2100$) are used for input data.

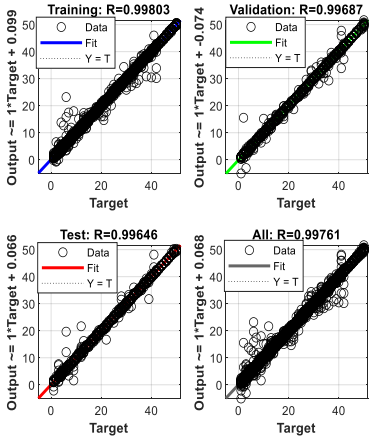

(a)

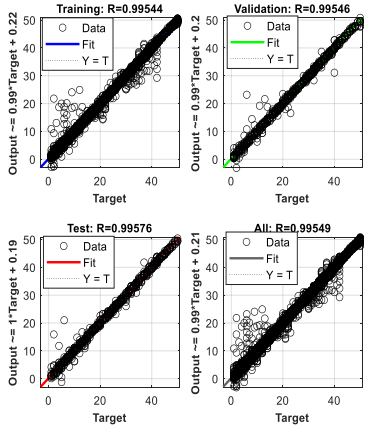

(b)

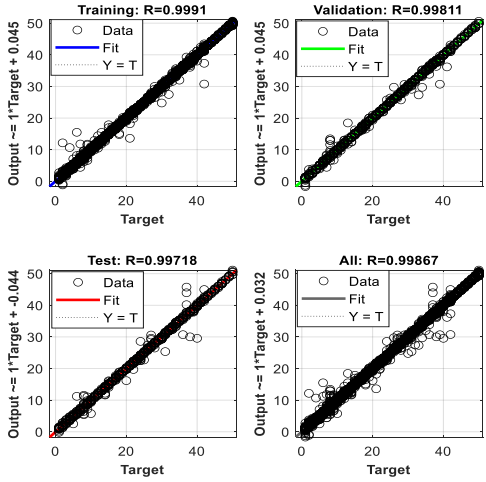

(c)

Figure 6-26. Regression values: (a) ANN; (b) ANNCS2; (c) ANNCS1

Figure 6-26 shows that the regression values of all cases are higher than 0.99 and the data in the datasets including training, evaluation, and test are along the target line (the 45-degree line). With linear regression models, the regression values (R) always range from 0 to 1. If the R is close to the upper bound (1), calculated and target results are exactly equivalent. This demonstrates that the network is trained successfully.

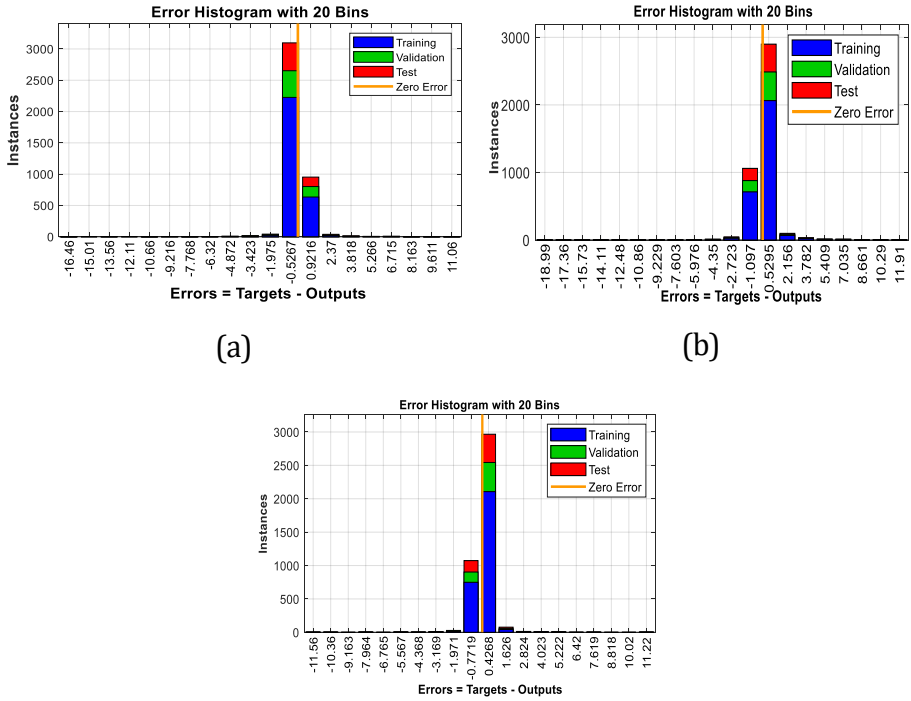

Figure 6-27. Error histogram: (a) ANN; (b) ANNCS2; (c) ANNCS1

Figure 6-27 indicates the histogram of the errors of the calculated and the desired outputs. The total data of the histogram is divided into 20 samples. While the *Y*-axis represents the number of sample, the *X*-axis denotes the error value. The zero-error line locates the position where calculated and target results are analogous. As observed in Figure 6-28 most of the errors of datasets are close to the zero-error line.

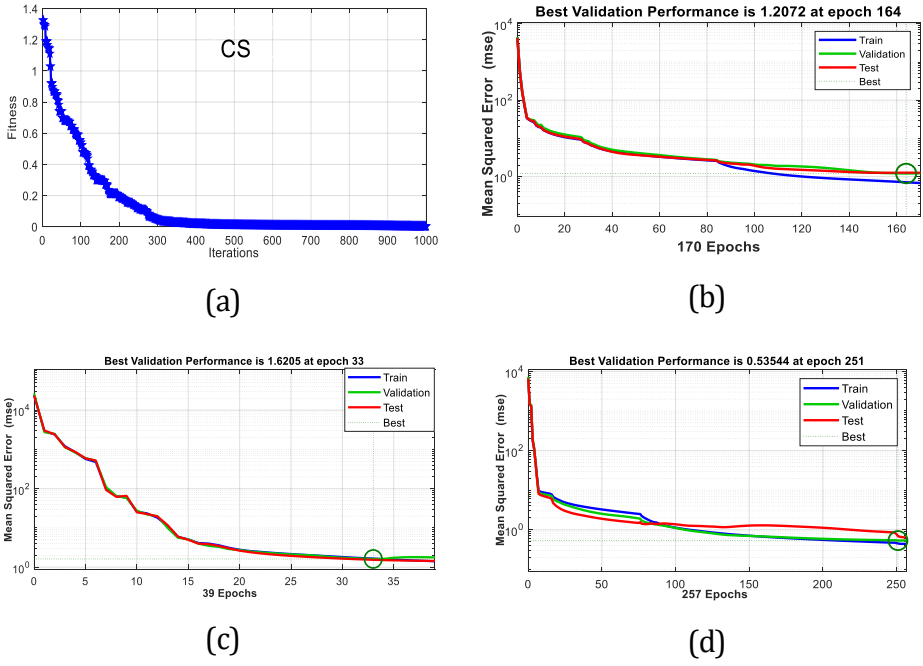

Figure 6-28. Tolerance: (a) CS; (b) ANN; (c) ANNCS2; (d) ANNCS1

Table 6.21 – Performance indices of algorithms – single damages.

Algorithms	MSE-values	*R*- Values	Total CPU time (second - s)
CS			41245
ANN	1.1056	0.997	69
ANNCS2	1.8475	0.995	539
ANNCS1	0.4822	0.998	135

As observed in Figure 6-29 and Table 6.21, ANNCS1 is superior to ANNCS2, and ANN in terms of MSE-values and *R*-values. ANN applies the GD technique to train the network that significantly reduces

computational time. However, the accuracy is reduced because the network gets stuck in local minima. ANNCS2 applies CS to determine the starting point for the network, but the network still gets stuck in local minima in the process of training the network. In some cases, ANNCS2 may provide worse results than ANN and becomes counterproductive if the process of finding the starting point of CS transfers the network to the other side of the global best. ANNCS2 also has no strategy to deal with this issue in the process of training the network since ANN and CS work independently. To deal with this problem, ANNCS2 can adjust some parameters of CS and network architecture of ANN but this solution is time-consuming. ANNCS1 contains the advantages of both ANN of CS. ANN is used to speed up convergence and improve the performance of the network through each iteration and CS is applied to help the network to escape from local minima. Hence, the results have the highest accuracy.

In terms of computational time, ANN, ANNCS2, and ANNCS1 spend 69 s, 539 s, and 135 s to find the optimal solution, whereas CS spends too much time on this process (41245 s). Because the application of the vectorization technique helping to reduce the dimension of data, ANNCS1 spends less time on training the network than ANNCS2. The process of looking for the best solution for CS is time-consuming since CS seeks global solutions based on stochastic search techniques. Moreover, CS has to adjust many parameters in each iteration, which is the main reason for the huge increase in computational cost.

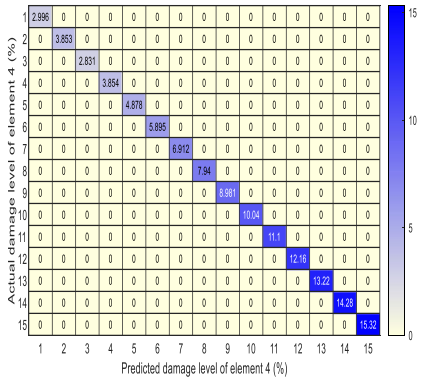

(a)

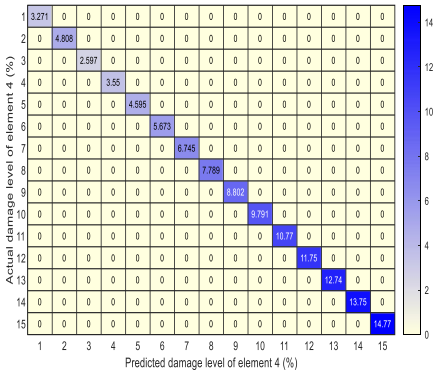

(b)

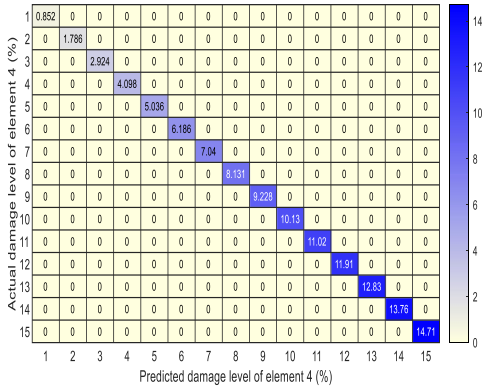

(c)

Figure 6-29. Damage level identification at element 4: (a) ANN; (b) ANNCS2; (c) ANNCS1

Figure 6-29 shows the result of detecting damage levels at element 4 using ANN, ANNCS2, and ANNCS1. While *Y*-axis represents the actual damage levels of element 4 (%), the *X*-axis denotes the predicted damage levels corresponding to the *Y*-axis, and the diagonal line represents

calculated values. ANNCS1 shows a high accuracy when detecting damage levels (at element 4) exactly. ANN and ANNCS2 predict wrongly damage levels of element 4 for some cases. For example, ANN and ANNCS2 determine 3% and 3.2% of damage happening at element 4, respectively compared to the actual damage of 1% happening at element 4.

6.4.3.2. Multiple damages

- 2 damaged elements.

Damages are generated at 2 random elements at the same time. The damage level is assigned from 0% to 50% with an interval of 1% for each element. The number of data sample is calculated as Eq (6.2).

$$N_{s2} = n_s * \frac{n_e!}{(n_e - 2)! * 2!} \tag{6.2}$$

With ! is factorial. n_e= 42; n_s= 50, the number of data sample (N_{s2}) is 43050

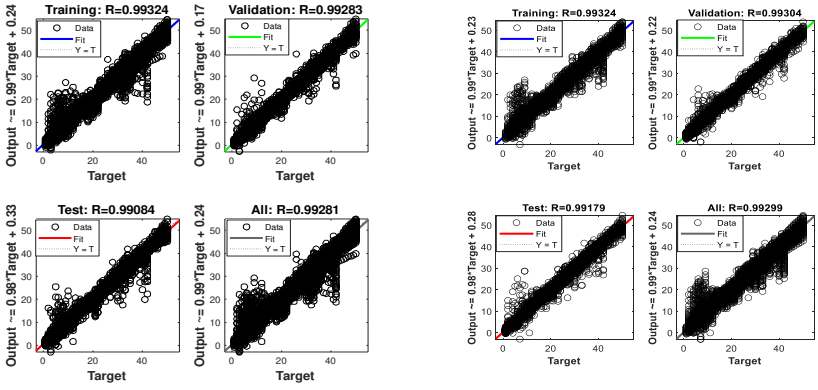

(a) (b)

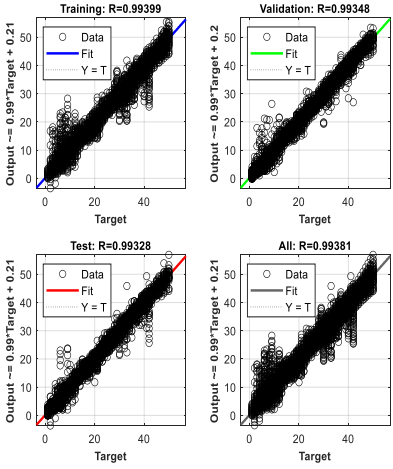

(c)

Figure 6-30. Regression values: (a) ANN; (b) ANNCS2; (c) ANNCS1

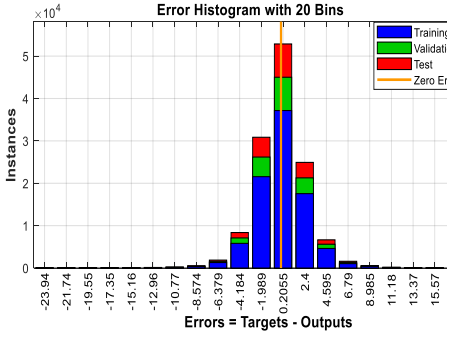

(a)

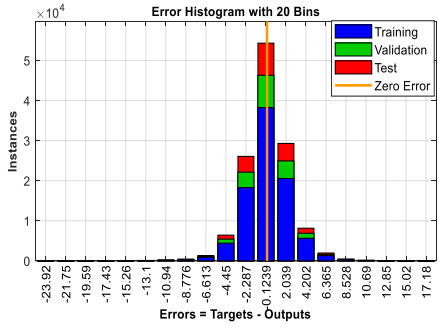

(b)

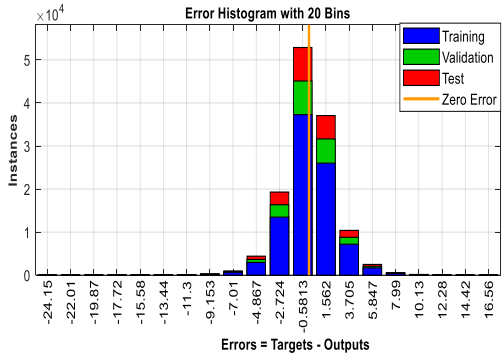

(c)

Figure 6-31. Error histogram: (a) ANN; (b) ANNCS2; (c) ANNCS1

Figure 6-30 shows that R – values of the network using ANN, ANNCS2, and ANNCS1 are 0.993, 0.993, and 0.994, respectively. Datasets of training, validation, and test are along the regression line. Figure 6-31 indicates that errors between calculated and desired values are close to the zero error line. Obtained results demonstrate that a good agreement between calculated and real outputs is achieved.

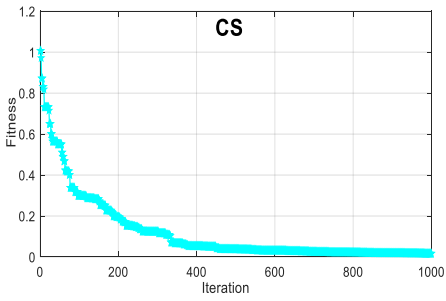

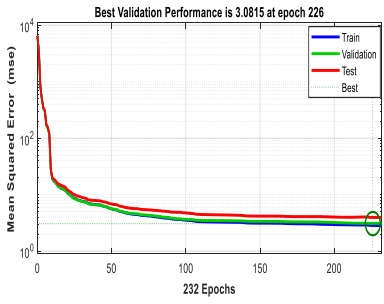

(a) (b)

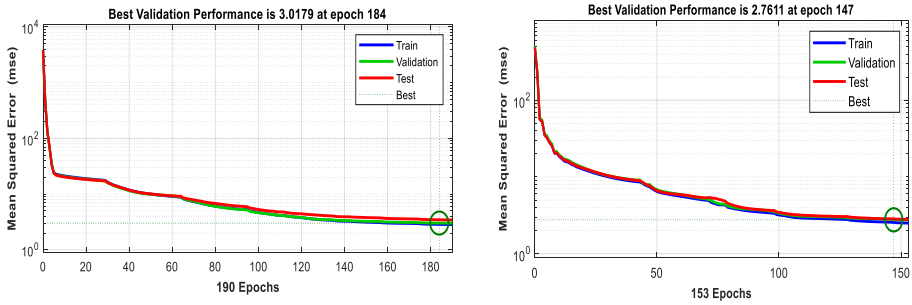

(c) (d)

Figure 6-32.Tolerance: (a) CS; (b) ANN; (c) ANNCS2; (d) ANNCS1

Table 6.22**.** Performance indices of algorithms – 2 damaged elements.

Algorithms	MSE-values	*R*- Values	Total CPU time (second-s)
CS			42539
ANN	3.2134	0.993	1550
ANNCS2	3.0503	0.993	3911
ANNCS1	2.6298	0.994	1703

Table 6.22 and Figure 6-32 show that ANNCS1 surpasses ANN, and ANNCS2 in terms of accuracy. MSE – value is calculated by ANNCS1 is lowest, at 2.6298, compared to 3.2134, and 3.0503 provided by ANN, and ANNCS2, respectively. In terms of computational time, ANN, ANNCS2, and ANNCS1 spend 1550 s, 3911 s, and 1703 s, respectively to determine the best solution, whereas CS expends 42539s for this process.

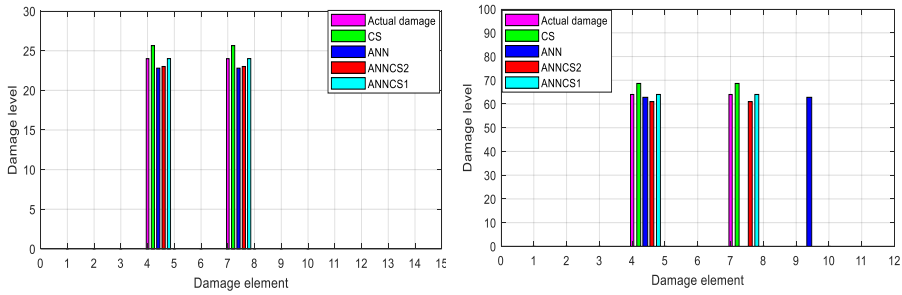

Figure 6-33. Damage detection results in in element 4 and element 7 using CS, ANN, ANNCS2, and ANNCS1: (a) 24%; (b) 64% damage.

Figure 6-33 shows that CS, ANNCS2, ANNCS1 can accurately identify the damage location and severity of element 4 and element 7. There are some errors when using ANN to detect the damages of elements. ANN detects 62% of damage happening at element 9. However, the real damage occurs at element 7 (64% of damage). The accuracy of damage level identification provided by ANNCS1 outperforms that of ANNCS2, CS, and ANN.

- 3 damaged elements.

Damages are generated at 3 random elements at the same time. The damage level is assigned from 0% to 50% with an interval of 1% for each element. The number of data sample is calculated as Eq (6.3).

$$N_{s3} = n_s * \frac{n_e!}{(n_e - 3)! * 3!} \tag{6.3}$$

n_e = 42; n_s = 50, The number of data sample (N_{s3}) is 574000.

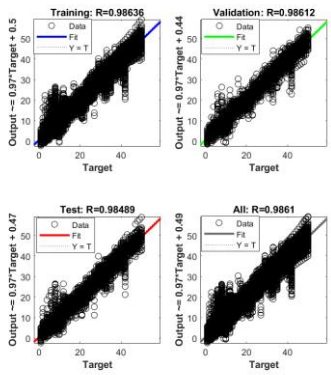

(a)

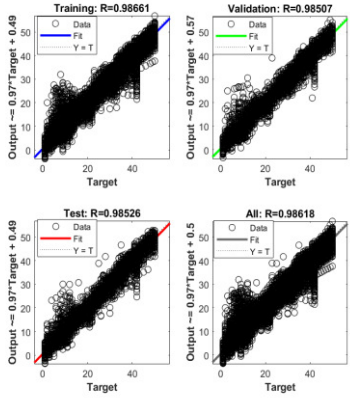

(b)

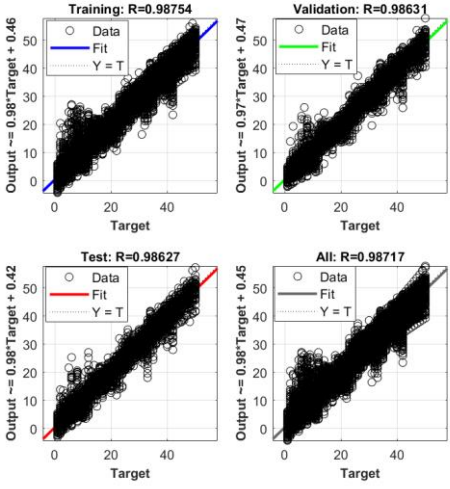

(c)

Figure 6-34. Regression values: (a) ANN; (b) ANNCS2; (c) ANNCS1

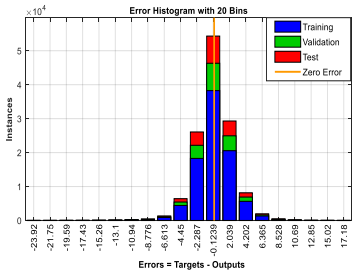

(a)

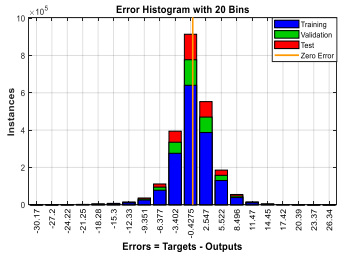

(b)

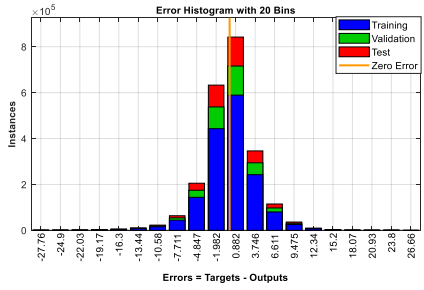

(c)

Figure 6-35. Error histogram: (a) ANN; (b) ANNCS2; (c) ANNCS1

Figure 6-34 shows *R*-values calculated by ANN, ANNCS2, and ANNCS1 higher than 0.986. The deviation between calculated and desired outputs (errors) also distributes close to the zero-error line (Figure 6-35).

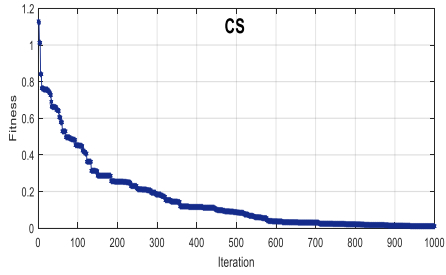

(a)

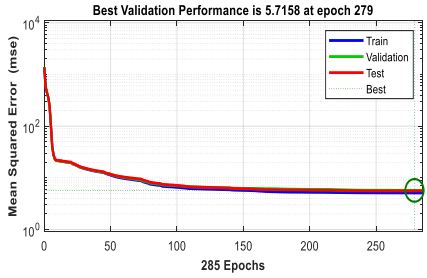

(b)

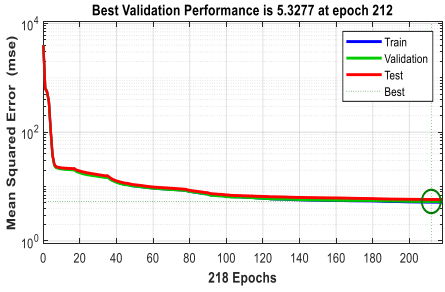

(c)

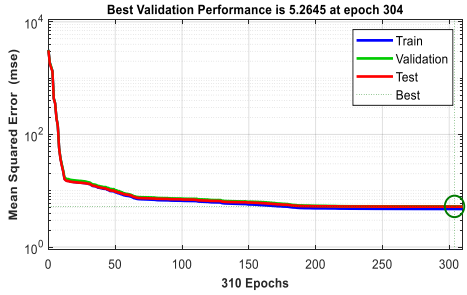

(d)

Figure 6-36. Tolerance: (a) CS; (b) ANN; (a) ANNCS2; (b) ANNCS1

Table 6.23 –Performance indices of algorithms – 3 damaged elements.

Algorithms	MSE-values	*R*- Values	Total CPU time (second -s)
CS			42568
ANN	5.6919	0.986	9102
ANNCS2	5.2626	0.986	13218
ANNCS1	4.8885	0.987	9513

Figure 6-36 and Table 6.23 show that ANNCS1 outperforms ANN and ANNCS2 in terms of accuracy. Regarding the CPU time, CS expends 42568s on looking for the global best, compared to only 9102 s, 13218 s, and 9513 of ANN, ANNCS2, and ANNCS1, respectively

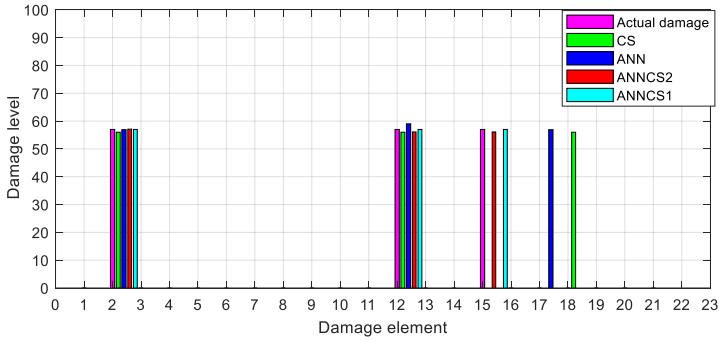

Figure 6-37. Damage detection results at elements 2, 12, and 15 using CS, ANN, ANNCS2, and ANNCS1: 57% damage

Figure 6-37 shows that ANNCS2, ANNCS1 can accurately identify the damage location and level of all elements. The accuracy of ANNCS1 outperforms that of ANNCS2. For instance, ANNCS1 predicts 57% damage of elements 2, 12, and 15, whereas ANNCS2 predicts 55% of damage occurring at those elements. ANN and CS detect damage location of elements 15 inaccurately.

6.5 Conclusion of chapter 6.

To consider the effectiveness of the proposed approaches, both numerical models and measurements are employed in this chapter. The proposed methods are used for model updating of two truss bridges, in which uncertain parameters including stiffness of supports, the stiffness of truss joints, and material properties are taken into account. The model using the semi-rigid connection at the truss joint can present the most exactly the behavior of the Nam O bridge. ODIPSO outperforms ODPSO in terms of accuracy and extremely reduces computational time compared to PSO and IPSO

Moreover, the proposed methods ANNCS1, ANN, CS, and ANNCS2 are also applied to detect both single and multiple damages in a large-scale truss bridge. The obtained results show that ANNCS1 is superior to ANN, CS, and ANNCS2 in terms of accuracy as well as computational cost.

Chapter 7 Conclusions and Recommendations for Future Work

7.1 Conclusions

This thesis focuses on monitoring the health of large-scale truss bridges in which model updating and damage detection problems are dealt with. Moreover, novel algorithms are also proposed to remedy the disadvantages of traditional MO algorithms and ANN, help them become more effective and applicable to real problems. From obtained results, some main conclusions can be drawn.

- PSO not only provides a better accuracy between the numerical model and measurements but also reduces the computational cost compared to GA. A side conclusion of the considered application example is that the assumption of semi-rigid joints (using rotational springs) can most accurately represent the dynamic characteristics of the studied truss bridge.

- ODIPSO not only outperforms PSO, IPSO, and ODPSO in terms of accuracy but also dramatically reduces the computational time compared to PSO and IPSO.
- ANNCS1 is completely superior to CS, ANN, and another hybrid ANN in terms of accuracy and considerably reduces calculational costs compared to CS.
- The vectorization technique reduces the dimension of data. Hence, the computational time is significantly reduced.
- From the obtained results, some recommendations for the application of each algorithm used in this thesis for SHM can be extracted:

    1. MO algorithms such as GA, PSO, IPSO can look for the global best but this process is time-consuming. For example, PSO, IPSO spend more than 12 days on seeking the best solution for the Guadalquivir bridge (a five-span truss bridge). Therefore, it is not feasible to apply pure MO algorithms to deal with optimization problems of large-scale structures.
    2. ODPSO and ODIPSO can reduce computational time but it is still large (more than 2 days to update Guadalquivir bridge).
    3. ANN is beneficial to computational cost. Therefore, ANN can apply to detect damages in large-scale structures but the

accuracy of results is poor if the network is trapped in local minima.

4. ANNCS1 not only can look for the best solution with a high level of accuracy and but also gain the benefit of reducing computational time. Hence, ANNCS1 has the potential to be employed for large-scale structures. However, these positive results do not mean that ANNCS1 is perfect. It has to be admitted that, when used for damage assessment of large-scale structures, too many multiple damages scenarios are considered, it extremely increases the computational time and reduces the accuracy of ANNCS1. The same applies for model updating with many updating aparameters.

7.2 Future Work

Although the obtained results from this research are positive, it must be admitted that the thesis requires further research as well as improvement of some of the aspects of the proposed methods. From the conducted research and the derived conclusions, main recommendations for further research are proposed

- In this thesis, structural damage identification of the proposed method is solely employed for a numerical model of a large-scale bridge. In this case, the effects of other factors such as noise and

temperature are not fully taken into account. Further research is needed to employ the proposed method in case of real damage to existing bridges.

- With potential capacity, numerous optimization algorithms such as Teaching Learning Based Optimization (TLBO) Algorithm, Salp Swarm Algorithm (SSA), and so forth have been proposed in recent years that possibly deal with drawbacks of traditional MO algorithms such as GA, PSO, and CS and contain enormous advantages. Hence, it is worth applying these state-of-the-art optimization algorithms for the SHM problem in the next research.

- In this thesis, to obtain data from measurement, traditional sensors were employed (wired sensors used for Nam O and My Thuan bridge, and wireless sensors used for Guadalquivir bridge). The installation of such high-cost sensors is time-consuming. Besides, because of the restricted number of sensors, the amount of obtained data is limited. This leads to a reduction in the accuracy of results (numerous higher modes are missing). Optimal sensor placement should be taken into account if the number of sensor is too few. This plays a vital role in obtaining as much structural behavior information as possible. On the other hand, advanced equipment and technology such as fiber Bragg

grating sensors… should be employed to increase the quality of the measured data for the upcoming research.

- It is commonly acknowledged that ANN has been proven its capacity for optimization problems or structural damage detection. However, because the structure of ANN is simple and without self-selecting characteristics, the capacity to deal with big data is limited. Damage detection of real bridges may generate a large amount of data. In this case, the use of ANN is no longer be useful. Therefore, it is necessary to employ other models of AI, typically, deep learning (DL), which has been commonly applied for many fields such as bioinformatics, drug design, medical image analysis and so on. The advantage of DL is that this model can take advantage of the ability to self-extract data features from the convolutional class and the trained classifier at the same time. Simultaneous learning of features and classifiers can help each other to find suitable parameters for feature vectors. With such outstanding advantages, the DL model is a promising candidate for the SHM of large-scale bridges.

Publications

- **Articles related to the present thesis**

1. **Tran-Ngoc, H.,** Khatir, S., De Roeck, G., Bui-Tien, T., Nguyen-Ngoc, L. and Abdel Wahab, M., 2018. Model updating for Nam O bridge using particle swarm optimization algorithm and genetic algorithm. *Sensors*, *18*(12), p.4131 (Q2; IF=3.031).
2. **Tran-Ngoc, H.**, He, L., Reynders, E., Khatir, S., Le-Xuan, T., De Roeck, G., Bui-Tien, T. and Wahab, M.A., 2020. An efficient approach to model updating for a multispan railway bridge using orthogonal diagonalization combined with improved particle swarm optimization. *Journal of Sound and Vibration*, p.115315. (Q1; IF=3.655).
3. **Tran-Ngoc, H.,** Khatir, S., Le-Xuan, T., De Roeck, G., Bui-Tien, T. and Wahab, M.A., 2020. A novel machine-learning based on the global search techniques using vectorized data for damage detection in structures. *International Journal of Engineering Science*, *157*, p.103376. (Q1; IF=8.843).

- **Other publications**

1. **Tran-Ngoc, H.,** Khatir, S., De Roeck, G., Bui-Tien, T. and Wahab, M.A., 2019. An efficient artificial neural network for damage detection in bridges and beam-like structures by improving training parameters using cuckoo search algorithm. *Engineering Structures*, *199*, p.10963. (Q1; IF=3.548).

2. **Tran-Ngoc, H.**, Khatir, S., Le-Xuan, T., De Roeck, G., Bui-Tien, T. and Wahab, M.A., 2021. Finite element model updating of a multispan bridge with a hybrid metaheuristic search algorithm using experimental data from wireless triaxial sensors. *Engineering with Computers*, pp.1-19. (Q1; IF=7.963).

3. **Tran-Ngoc, H.**, Khatir, S., Ho-Khac, H., De Roeck, G., Bui-Tien, T. and Wahab, M.A., 2021. Efficient Artificial neural networks based on a hybrid metaheuristic optimization algorithm for damage detection in laminated composite structures. *Composite Structures*, *262*, p.113339. (Q1; IF=5.083).

4. **Hoa, T.N.**, Khatir, S., De Roeck, G., Long, N.N., Thanh, B.T. and Wahab, M.A., 2020. An efficient approach for model updating of a large-scale cable-stayed bridge using ambient vibration measurements combined with a hybrid metaheuristic search algorithm. *Smart Structures and Systems*, *25*(4), pp.487-499. (Q1; IF = 3.342).

5. Nguyen, D.H., **Tran-Ngoc, H.**, Bui-Tien, T., De Roeck, G. and Wahab, M.A., 2020. Damage detection in truss bridges using transmissibility and machine learning algorithm: Application to Nam O bridge. *Smart Structures and Systems*, *26*(1), pp.35-47.

6. Dang, H.V., Raza, M., **Tran-Ngoc, H.**, Bui-Tien, T. and Nguyen, H.X., 2021. Connection stiffness reduction analysis in steel bridge via deep CNN and modal experimental data. *Structural Engineering and Mechanics*, *77*(4), p.495.

7. Khatir, S., Khatir, T., Boutchicha, D., Le Thanh, C., **Tran-Ngoc, H.**, Bui, T.Q., Capozucca, R. and Abdel-Wahab, M., 2020. An efficient hybrid TLBO-PSO-ANN for fast damage identification in steel beam structures using IGA. *Smart Structures and Systems*, *25*(5), pp.605-617.

8. Khatir, S., Boutchicha, D., Le Thanh, C., **Tran-Ngoc, H.**, Nguyen, T.N. and Abdel-Wahab, M., 2020. Improved ANN technique combined with Jaya algorithm for crack identification in plates using XIGA and experimental analysis. *Theoretical and Applied Fracture Mechanics*, p.102554.

9. Dang, H.V., **Tran-Ngoc, H.,** Nguyen, T.V., Bui-Tien, T., De Roeck, G. and Nguyen, H.X., 2020. Data-driven structural health monitoring using feature fusion and hybrid deep learning. *IEEE Transactions on Automation Science and Engineering.*

10. Nguyen-Ngoc, L., **Tran, H.**, Bui-Tien, T., Mai-Duc, A., Abdel Wahab, M., X Nguyen, H. and De Roeck, G., 2021. Damage detection in structures using Particle Swarm Optimization combined with Artificial Neural Network. *Smart Structures and Systems*, *28*(1), pp.1-12.

11. Khatir, S., Tiachacht, S., Le Thanh, C., **Tran-Ngoc, H.**, Mirjalili, S. and Wahab, M.A., 2021. A new robust flexibility index for structural damage identification and quantification. *Engineering Failure Analysis*, *129*, p.105714.

- **Conferences**

1. **Tran-Ngoc, H.**, Nguyen-Ngoc, L., Ho-Khac, H., Le-Thuc, A., De Roeck, G., Bui-Tien, T. and Wahab, M.A., 2020, July. Application of Improved Artificial Neural Network to Stiffness Reduction Analysis of Truss Joints in a Railway Bridge. In *Fracture, Fatigue and Wear* (pp. 139-152). Springer, Singapore.

2. **Tran-Ngoc, H.,** Ho-Khac, H., Le-Xuan, T., Nguyen-Tran, H., De Roeck, G., Bui-Tien, T. and Wahab, M.A., 2020, December. Model Updating for a Railway Bridge Using a Hybrid Optimization Algorithm Combined with Experimental Data. In *Proceedings of 1st International Conference on Structural Damage Modelling and Assessment* (pp. 19-30). Springer, Singapore.

3. **Tran-Ngoc, H.**, Khatir, S., De Roeck, G., Bui-Tien, T. and Wahab, M.A., 2020. Damage assessment in beam-like structures using cuckoo search algorithm and experimentally measured data. In *Proceedings of the 13th International Conference on Damage Assessment of Structures* (pp. 380-385). Springer, Singapore.

4. **Tran-Ngoc, H.**, Khatir, S., De Roeck, G., Bui-Tien, T., Nguyen-Ngoc, L. and Wahab, M.A., 2019, October. Stiffness identification of truss joints of the nam o bridge based on vibration measurements and model updating. In *International conference on arch bridges* (pp. 264-272). Springer, Cham.

5. Lan Nguyen-Ngoc, **Hoa Tran-Ngoc**, Hieu Nguyen-Tran, Binh Nguyen-Duc, Dang Nguyen-Le-Minh, Thanh Bui-Tien, M.A.Wahab. "Damage Detection in Structures using Artificial Neural Networks and Genetic Algorithms". The third International Conference on Sustainability in Civil Engineering (ICSCE 2020). (ISBN: 978-604-76-2284-9)

6. Ho, V.L., **Tran, N.H.**, De Roeck, G., Bui, T.T. and Wahab, M.A., 2018, August. System Identification Based on Vibration Testing of a Steel I-Beam. In *International Conference on Numerical Modelling in Engineering* (pp. 254-268). Springer, Singapore.

References

1. Friswell, M. and Mottershead, J.E., 2013. *Finite element model updating in structural dynamics* (Vol. 38). Springer Science & Business Media.
2. Maeck, J., Peeters, B. and De Roeck, G., 2001. Damage identification on the Z24 bridge using vibration monitoring. *Smart materials and structures*, *10*(3), p.512.
3. Teughels, A. and De Roeck, G., 2005. Damage detection and parameter identification by finite element model updating. *Revue européenne de génie civil*, *9*(1-2), pp.109-158.
4. Adeli, H., 2001. Neural networks in civil engineering: 1989–2000. *Computer-Aided Civil and Infrastructure Engineering*, *16*(2), pp.126-142.
5. Reynders, E. and De Roeck, G., 2008. Reference-based combined deterministic–stochastic subspace identification for experimental and operational modal analysis. *Mechanical Systems and Signal Processing*, *22*(3), pp.617-637.
6. Deng, L. and Cai, C.S., 2010. Bridge model updating using response surface method and genetic algorithm. *Journal of Bridge Engineering*, *15*(5), pp.553-564.

7. Ho, V.L., Tran, N.H., De Roeck, G., Bui, T.T. and Wahab, M.A., 2018, August. System identification based on vibration testing of a steel I-beam. In *International Conference on Numerical Modelling in Engineering* (pp. 254-268). Springer, Singapore.

8. Nguyen-Ngoc, L., Tran, H., Bui-Tien, T., Mai-Duc, A., Abdel Wahab, M., X Nguyen, H. and De Roeck, G., 2021. Damage detection in structures using Particle Swarm Optimization combined with Artificial Neural Network. *Smart Structures and Systems*, *28*(1), pp.1-12.

9. Dang, H.V., Raza, M., Tran-Ngoc, H., Bui-Tien, T. and Nguyen, H.X., 2021. Connection stiffness reduction analysis in steel bridge via deep CNN and modal experimental data. *Structural Engineering and Mechanics*, *77*(4), pp.495-508.

10. Dang, H.V., Tran-Ngoc, H., Nguyen, T.V., Bui-Tien, T., De Roeck, G. and Nguyen, H.X., 2020. Data-driven structural health monitoring using feature fusion and hybrid deep learning. *IEEE Transactions on Automation Science and Engineering*.

11. Tran, H., Khatir, S., De Roeck, G., Nguyen, L., Bui, T.T. and Abdel Wahab, M., 2020. An efficient approach for model updating of a large-scale cable-stayed bridge using ambient vibration measurements combined with a hybrid metaheuristic search algorithm. *Smart Structures and Systems*, *25*(4), pp.487-499.

12. Tran, N.H. and Bui, T.T., 2019. Damage detection in a steel beam structure using particle swarm optimization and experimentally measured results. *Science Journal of Transportation*, (9), pp.3-9.

13. Khatir, S., Tiachacht, S., Le Thanh, C., Tran-Ngoc, H., Mirjalili, S. and Wahab, M.A., 2021. A new robust flexibility index for structural damage identification and quantification. *Engineering Failure Analysis*, *129*, p.105714.

14. Nguyen, D.H., Tran-Ngoc, H., Bui-Tien, T., De Roeck, G. and Wahab, M.A., 2020. Damage detection in truss bridges using transmissibility and machine learning algorithm: Application to Nam O bridge. *Smart Structures and Systems*, *26*(1), pp.35-47.

15. Tran-Ngoc, H., Khatir, S., Le-Xuan, T., De Roeck, G., Bui-Tien, T. and Wahab, M.A., 2021. Finite element model updating of a multispan bridge with a hybrid metaheuristic search algorithm using experimental data from wireless triaxial sensors. *Engineering with Computers*, pp.1-19.

16. Tran-Ngoc, H., Khatir, S., Ho-Khac, H., De Roeck, G., Bui-Tien, T. and Wahab, M.A., 2021. Efficient Artificial neural networks based on a hybrid metaheuristic optimization algorithm for damage detection in laminated composite structures. *Composite Structures*, *262*, p.113339.

17. Gillich, G.R., Furdui, H., Wahab, M.A. and Korka, Z.I., 2019. A robust damage detection method based on multi-modal analysis in

variable temperature conditions. *Mechanical Systems and Signal Processing*, *115*, pp.361-379.

18. Tran-Ngoc, H., Khatir, S., De Roeck, G., Bui-Tien, T. and Wahab, M.A., 2020. Damage assessment in beam-like structures using cuckoo search algorithm and experimentally measured data. In *Proceedings of the 13th International Conference on Damage Assessment of Structures* (pp. 380-385). Springer, Singapore.
19. Gillich, G.R., Nedelcu, D., Malin, C.T., Biro, I. and Wahab, M.A., 2020. Efficient algorithm for frequency estimation used in structural damage detection. In *Proceedings of the 13th International Conference on Damage Assessment of Structures* (pp. 283-300). Springer, Singapore.
20. Gillich, G.R., Praisach, Z.I., Abdel Wahab, M., Gillich, N., Mituletu, I.C. and Nitescu, C., 2016. Free vibration of a perfectly clamped-free beam with stepwise eccentric distributed masses. *Shock and Vibration*, *2016*.
21. Khatir, S., Boutchicha, D., Le Thanh, C., Tran-Ngoc, H., Nguyen, T.N. and Abdel-Wahab, M., 2020. Improved ANN technique combined with Jaya algorithm for crack identification in plates using XIGA and experimental analysis. *Theoretical and Applied Fracture Mechanics*, *107*, p.102554.
22. Tran-Ngoc, H., Khatir, S., De Roeck, G., Bui-Tien, T., Nguyen-Ngoc, L. and Wahab, M.A., 2019, October. Stiffness identification of truss

joints of the nam o bridge based on vibration measurements and model updating. In *International conference on arch bridges* (pp. 264-272). Springer, Cham.

23. Jung, D.S. and Kim, C.Y., 2013. Finite element model updating on small-scale bridge model using the hybrid genetic algorithm. *Structure and Infrastructure engineering*, *9*(5), pp.481-495.
24. Zare Hosseinzadeh, A., Ghodrati Amiri, G. and Koo, K.Y., 2016. Optimization-based method for structural damage localization and quantification by means of static displacements computed by flexibility matrix. *Engineering Optimization*, *48*(4), pp.543-561.
25. Yildiz, A.R., 2013. Cuckoo search algorithm for the selection of optimal machining parameters in milling operations. *The International Journal of Advanced Manufacturing Technology*, *64*(1), pp.55-61.
26. Na, C., Kim, S.P. and Kwak, H.G., 2011. Structural damage evaluation using genetic algorithm. *Journal of Sound and Vibration*, *330*(12), pp.2772-2783.
27. Khatir, S., Belaidi, I., Khatir, T., Hamrani, A., Zhou, Y.L. and Wahab, M.A., 2017. Multiple damage detection in composite beams using Particle Swarm Optimization and Genetic Algorithm. *Mechanics*, *23*(4), pp.514-521.

28. Khatir, S., Dekemele, K., Loccufier, M., Khatir, T. and Wahab, M.A., 2018. Crack identification method in beam-like structures using changes in experimentally measured frequencies and Particle Swarm Optimization. *Comptes Rendus Mécanique*, *346*(2), pp.110-120.
29. Qin, S., Zhou, Y.L., Cao, H. and Wahab, M.A., 2018. Model updating in complex bridge structures using kriging model ensemble with genetic algorithm. *KSCE Journal of Civil Engineering*, *22*(9), pp.3567-3578.
30. Liu, T., Zhang, Q., Zordan, T. and Briseghella, B., 2016. Finite element model updating of Canonica Bridge using experimental modal data and genetic algorithm. *Structural Engineering International*, *26*(1), pp.27-36.
31. Zordan, T., Briseghella, B. and Liu, T., 2014. Finite element model updating of a tied-arch bridge using Douglas-Reid method and Rosenbrock optimization algorithm. *Journal of Traffic and Transportation Engineering (English Edition)*, *1*(4), pp.280-292.
32. Khatir, S., Wahab, M.A., Boutchicha, D., Capozucca, R. and Khatir, T., 2018, August. Optimization of IGA Parameters Based on Beam Structure Using Cuckoo Search Algorithm. In *Numerical Modelling in Engineering* (pp. 380-389). Springer, Singapore.

33. Xu, H.J., Liu, J.K. and Lu, Z.R., 2016. Structural damage identification based on cuckoo search algorithm. *Advances in Structural Engineering*, *19*(5), pp.849-859.
34. Perera, R., Ruiz, A. and Manzano, C., 2009. Performance assessment of multicriteria damage identification genetic algorithms. *Computers & Structures*, *87*(1-2), pp.120-127.
35. Panigrahi, S.K., Chakraverty, S. and Mishra, B.K., 2013. Damage identification of multistory shear structure from sparse modal information. *Journal of computing in civil engineering*, *27*(1), pp.1-9.
36. Lovbjerg, M., Rasmussen, T.K. and Krink, T., 2001, July. Hybrid particle swarm optimiser with breeding and subpopulations. In *Proceedings of the genetic and evolutionary computation conference* (Vol. 2001, pp. 469-476). San Francisco, USA.
37. Higashi, N. and Iba, H., 2003, April. Particle swarm optimization with Gaussian mutation. In *Proceedings of the 2003 IEEE Swarm Intelligence Symposium. SIS'03 (Cat. No. 03EX706)* (pp. 72-79). IEEE.
38. Baskar, S. and Suganthan, P.N., 2004, June. A novel concurrent particle swarm optimization. In *Proceedings of the 2004 Congress on Evolutionary Computation (IEEE Cat. No. 04TH8753)* (Vol. 1, pp. 792-796). IEEE.

39. Clerc, M., 1999, July. The swarm and the queen: towards a deterministic and adaptive particle swarm optimization. In *Proceedings of the 1999 congress on evolutionary computation-CEC99 (Cat. No. 99TH8406)* (Vol. 3, pp. 1951-1957). IEEE.
40. Wang, X.H. and Li, J.J., 2004, August. Hybrid particle swarm optimization with simulated annealing. In *Proceedings of 2004 International Conference on Machine Learning and Cybernetics (IEEE Cat. No. 04EX826)* (Vol. 4, pp. 2402-2405). IEEE.
41. Parsopoulos, K.E. and Vrahatis, M.N., 2002. Initializing the particle swarm optimizer using the nonlinear simplex method. *Advances in intelliGhent systems, fuzzy systems, evolutionary computation*, *216*, pp.1-6.
42. Qin, S., Zhang, Y., Zhou, Y.L. and Kang, J., 2018. Dynamic model updating for bridge structures using the kriging model and PSO algorithm ensemble with higher vibration modes. *Sensors*, *18*(6), p.1879.
43. Shirazi, M.N., Mollamahmoudi, H. and Seyedpoor, S.M., 2014. Structural damage identification using an adaptive multi-stage optimization method based on a modified particle swarm algorithm. *Journal of Optimization Theory and Applications*, *160*(3), pp.1009-1019.
44. Tran-Ngoc, H., He, L., Reynders, E., Khatir, S., Le-Xuan, T., De Roeck, G., Bui-Tien, T. and Wahab, M.A., 2020. An efficient approach to

model updating for a multispan railway bridge using orthogonal diagonalization combined with improved particle swarm optimization. *Journal of Sound and Vibration*, *476*, p.115315.

45. Mohapatra, P., Chakravarty, S. and Dash, P.K., 2015. An improved cuckoo search based extreme learning machine for medical data classification. *Swarm and Evolutionary Computation*, *24*, pp.25-49.
46. Marichelvam, M.K., Prabaharan, T. and Yang, X.S., 2014. Improved cuckoo search algorithm for hybrid flow shop scheduling problems to minimize makespan. *Applied Soft Computing*, *19*, pp.93-101.
47. Zhou, Y., Zheng, H., Luo, Q. and Wu, J., 2013. An improved cuckoo search algorithm for solving planar graph coloring problem. *Applied Mathematics & Information Sciences*, *7*(2), p.785.
48. Omari, M.A., Almagableh, A., Sevostianov, I. and Yaseen, A.B., 2020. Modeling of the viscoelastic properties of thermoset vinyl ester nanocomposite using artificial neural network. *International Journal of Engineering Science*, *150*, p.103242.
49. Qin, P., Shen, Y., Zhu, J. and Xu, H., 2005. Dynamic analysis of hydrodynamic bearing–rotor system based on neural network. *International Journal of Engineering Science*, *43*(5-6), pp.520-531.
50. Rahmanpanah, H., Mouloodi, S., Burvill, C., Gohari, S. and Davies, H.M., 2020. Prediction of load-displacement curve in a complex

structure using artificial neural networks: A study on a long bone. *International Journal of Engineering Science*, *154*, p.103319.

51. Schmidhuber, J., 2015. Deep learning in neural networks: An overview. *Neural networks*, *61*, pp.85-117.
52. Nguyen-Thanh, V.M., Nguyen, L.T.K., Rabczuk, T. and Zhuang, X., 2019. A surrogate model for computational homogenization of elastostatics at finite strain using the HDMR-based neural network approximator. *arXiv preprint arXiv:1906.02005*.
53. Nguyen, L.C. and Nguyen-Xuan, H., 2020. Deep learning for computational structural optimization. *ISA transactions*, *103*, pp.177-191.
54. Hwang, H.J., Baek, J.W., Kim, J.Y. and Kim, C.S., 2019. Prediction of bond performance of tension lap splices using artificial neural networks. *Engineering Structures*, *198*, p.109535.
55. Mangalathu, S., Heo, G. and Jeon, J.S., 2018. Artificial neural network based multi-dimensional fragility development of skewed concrete bridge classes. *Engineering Structures*, *162*, pp.166-176.
56. Fathalla, E., Tanaka, Y. and Maekawa, K., 2018. Remaining fatigue life assessment of in-service road bridge decks based upon artificial neural networks. *Engineering Structures*, *171*, pp.602-616.

57. Dackermann, U., Li, J. and Samali, B., 2013. Identification of member connectivity and mass changes on a two-storey framed structure using frequency response functions and artificial neural networks. *Journal of Sound and Vibration*, *332*(16), pp.3636-3653.
58. Park, J.H., Kim, J.T., Hong, D.S., Ho, D.D. and Yi, J.H., 2009. Sequential damage detection approaches for beams using time-modal features and artificial neural networks. *Journal of Sound and Vibration*, *323*(1-2), pp.451-474.
59. Kim, E.Y., Lee, Y.J. and Lee, S.K., 2012. Heath monitoring of a glass transfer robot in the mass production line of liquid crystal display using abnormal operating sounds based on wavelet packet transform and artificial neural network. *Journal of sound and vibration*, *331*(14), pp.3412-3427.
60. Zang, C. and Imregun, M., 2001. Structural damage detection using artificial neural networks and measured FRF data reduced via principal component projection. *Journal of sound and vibration*, *242*(5), pp.813-827.
61. Madan, A., 2005. Vibration control of building structures using self-organizing and self-learning neural networks. *Journal of sound and vibration*, *287*(4-5), pp.759-784.
62. Whitley, D., 1994. A genetic algorithm tutorial. *Statistics and computing*, *4*(2), pp.65-85.

63. Chen, G., Wang, H., Bezold, A., Broeckmann, C., Weichert, D. and Zhang, L., 2019. Strengths prediction of particulate reinforced metal matrix composites (PRMMCs) using direct method and artificial neural network. *Composite Structures*, *223*, p.110951.
64. Truong, T.T., Lee, S. and Lee, J., 2020. An artificial neural network-differential evolution approach for optimization of bidirectional functionally graded beams. *Composite Structures*, *233*, p.111517.
65. Stamopoulos, A.G., Tserpes, K.I. and Dentsoras, A.J., 2018. Quality assessment of porous CFRP specimens using X-ray Computed Tomography data and Artificial Neural Networks. *Composite Structures*, *192*, pp.327-335.
66. Rizzo, F. and Caracoglia, L., 2020. Artificial Neural Network model to predict the flutter velocity of suspension bridges. *Computers & Structures*, *233*, p.106236.
67. Hasançebi, O. and Dumlupınar, T., 2013. Linear and nonlinear model updating of reinforced concrete T-beam bridges using artificial neural networks. *Computers & Structures*, *119*, pp.1-11.
68. Chokshi, P., Dashwood, R. and Hughes, D.J., 2017. Artificial Neural Network (ANN) based microstructural prediction model for 22MnB5 boron steel during tailored hot stamping. *Computers & Structures*, *190*, pp.162-172.
69. Esteban, L.G., Fernández, F.G. and de Palacios, P., 2009. MOE prediction in Abies pinsapo Boiss. timber: Application of an

artificial neural network using non-destructive testing. *Computers & Structures*, *87*(21-22), pp.1360-1365.

70. Ma, J., Dong, S., Chen, G., Peng, P. and Qian, L., 2021. A data-driven normal contact force model based on artificial neural network for complex contacting surfaces. *Mechanical Systems and Signal Processing*, *156*, p.107612.
71. Kong, Y.S., Abdullah, S., Schramm, D., Omar, M.Z. and Haris, S.M., 2019. Optimization of spring fatigue life prediction model for vehicle ride using hybrid multi-layer perceptron artificial neural networks. *Mechanical Systems and Signal Processing*, *122*, pp.597-621.
72. Padil, K.H., Bakhary, N. and Hao, H., 2017. The use of a non-probabilistic artificial neural network to consider uncertainties in vibration-based-damage detection. *Mechanical Systems and Signal Processing*, *83*, pp.194-209.
73. Xing, Y.F., Wang, Y.S., Shi, L., Guo, H. and Chen, H., 2016. Sound quality recognition using optimal wavelet-packet transform and artificial neural network methods. *Mechanical Systems and Signal Processing*, *66*, pp.875-892.
74. Xie, S.L., Zhang, Y.H., Chen, C.H. and Zhang, X.N., 2013. Identification of nonlinear hysteretic systems by artificial neural network. *Mechanical Systems and Signal Processing*, *34*(1-2), pp.76-87.

75. Genlin, J., 2004. Survey on genetic algorithm [J]. *Computer Applications and Software*, *2*, pp.69-73.
76. Whitley, D. and Starkweather, T., 1990. Genitor II: A distributed genetic algorithm. *Journal of Experimental & Theoretical Artificial Intelligence*, *2*(3), pp.189-214.
77. Kennedy, J. and Eberhart, R., 1995, November. Particle swarm optimization. In *Proceedings of ICNN'95-international conference on neural networks* (Vol. 4, pp. 1942-1948). IEEE.
78. Yang, X.S. and Deb, S., 2009, December. Cuckoo search via Lévy flights. In *2009 World congress on nature & biologically inspired computing (NaBIC)* (pp. 210-214). Ieee.
79. Lu, Y., Liang, M., Ye, Z. and Cao, L., 2015. Improved particle swarm optimization algorithm and its application in text feature selection. *Applied Soft Computing*, *35*, pp.629-636.
80. Al-Bahrani, L.T. and Patra, J.C., 2018. A novel orthogonal PSO algorithm based on orthogonal diagonalization. *Swarm and Evolutionary Computation*, *40*, pp.1-23.
81. Yun-Lai, Z.H.O.U. and Wahab, M.A., 2017. Damage detection using vibration data and dynamic transmissibility ensemble with auto-associative neural network. *Mechanics*, *23*(5), pp.688-695.
82. Maity, D. and Saha, A., 2004. Damage assessment in structure from changes in static parameter using neural networks. *Sadhana*, *29*(3), pp.315-327.

83. Nguyen, V.V., Dackermann, U., Li, J., Alamdari, M.M., Mustapha, S., Runcie, P. and Ye, L., 2015. Damage identification of a concrete arch beam based on frequency response functions and artificial neural networks. *Electronic Journal of Structural Engineering*, *14*(1), pp.75-84.
84. Janssens, O., Slavkovikj, V., Vervisch, B., Stockman, K., Loccufier, M., Verstockt, S., Van de Walle, R. and Van Hoecke, S., 2016. Convolutional neural network based fault detection for rotating machinery. *Journal of Sound and Vibration*, *377*, pp.331-345.
85. Elshafey, A.A., Dawood, N., Marzouk, H. and Haddara, M., 2013. Crack width in concrete using artificial neural networks. *Engineering structures*, *52*, pp.676-686.
86. Cascardi, A., Micelli, F. and Aiello, M.A., 2017. An Artificial Neural Networks model for the prediction of the compressive strength of FRP-confined concrete circular columns. *Engineering Structures*, *140*, pp.199-208.
87. Khatir, S., Khatir, T., Boutchicha, D., Le Thanh, C., Tran-Ngoc, H., Bui, T.Q., Capozucca, R. and Abdel-Wahab, M., 2020. An efficient hybrid TLBO-PSO-ANN for fast damage identification in steel beam structures using IGA. *Smart Structures and Systems*, *25*(5), pp.605-617.

88. Rajendra, M., Jena, P.C. and Raheman, H., 2009. Prediction of optimized pretreatment process parameters for biodiesel production using ANN and GA. *Fuel*, *88*(5), pp.868-875.
89. Yazdanmehr, M., Anijdan, S.M. and Bahrami, A., 2009. Using GA–ANN algorithm to optimize soft magnetic properties of nanocrystalline mechanically alloyed Fe–Si powders. *Computational Materials Science*, *44*(4), pp.1218-1221.
90. Tran-Ngoc, H., Khatir, S., De Roeck, G., Bui-Tien, T. and Wahab, M.A., 2019. An efficient artificial neural network for damage detection in bridges and beam-like structures by improving training parameters using cuckoo search algorithm. *Engineering Structures*, *199*, p.109637.
91. Khatir, S., Tiachacht, S., Thanh, C.L., Bui, T.Q. and Wahab, M.A., 2019. Damage assessment in composite laminates using ANN-PSO-IGA and Cornwell indicator. *Composite Structures*, *230*, p.111509.
92. Azadeh, A., Mianaei, H.S., Asadzadeh, S.M., Saberi, M. and Sheikhalishahi, M., 2015. A flexible ANN-GA-multivariate algorithm for assessment and optimization of machinery productivity in complex production units. *Journal of Manufacturing Systems*, *35*, pp.46-75.
93. Choi, F.C., Li, J., Samali, B. and Crews, K., 2007. An experimental study on damage detection of structures using a timber

beam. *Journal of mechanical science and technology*, *21*(6), pp.903-907.

94. DjuriC, P.M., 1996. A model selection rule for sinusoids in white Gaussian noise. *IEEE Transactions on Signal Processing*, *44*(7), pp.1744-1751.
95. François, S., Schevenels, M., Dooms, D., Jansen, M., Wambacq, J., Lombaert, G., Degrande, G. and De Roeck, G., 2021. Stabil: An educational Matlab toolbox for static and dynamic structural analysis. *Computer Applications in Engineering Education*.
96. Duerr, D., 2006. Pinned connection strength and behavior. *Journal of structural engineering*, *132*(2), pp.182-194.
97. Saka, M.P., 1990. Optimum design of pin-jointed steel structures with practical applications. *Journal of Structural Engineering*, *116*(10), pp.2599-2620.
98. Luong, H.T., Zabel, V., Lorenz, W. and Rohrmann, R.G., 2017. Vibration-based model updating and identification of multiple axial forces in truss structures. *Procedia Engineering*, *188*, pp.385-392.
99. Dubina, D. and Zaharia, R., 1997. Cold-formed steel trusses with semi-rigid joints. *Thin-Walled Structures*, *29*(1-4), pp.273-287.
100. Csébfalvi, A., 2007. Optimal design of frame structures with semi-rigid joints. *Periodica Polytechnica Civil Engineering*, *51*(1), pp.9-15.

101. Pastor M, Binda M, Harčarik TJPE. Modal assurance criterion. 2012;48:543-

102. Vacher, P., Jacquier, B. and Bucharles, A., 2010, September. Extensions of the MAC criterion to complex modes. In *Proceedings of the international conference on noise and vibration engineering* (pp. 2713-2726).

103. Hjelmstad, K.D., Banan, M.R. and Banan, M.R., 1995. On building finite element models of structures from modal response. *Earthquake engineering & structural dynamics*, *24*(1), pp.53-67.

104. Reynders, E., Schevenels, M. and Roeck, G.D., 2014. A MATLAB Toolbox for Experimental and Operational Modal Analysis.

105. Reynders, E. and De Roeck, G., 2008. Reference-based combined deterministic–stochastic subspace identification for experimental and operational modal analysis. *Mechanical Systems and Signal Processing*, *22*(3), pp.617-637.

106. Peeters, B. and De Roeck, G., 1999. Reference-based stochastic subspace identification for output-only modal analysis. *Mechanical systems and signal processing*, *13*(6), pp.855-878.

107. Reynders E, Pintelon R, De Roeck GJMs, processing s. Uncertainty bounds on modal parameters obtained from stochastic subspace identification. 2008;22(4):948-69.

108. Bui, T., He, L. and De Roeck, G., 2012. Ambient Vibration Test of the Guadalquivir Railway Bridge. *Smart Structures*, pp.221-236

109. Fu, T.S., Ghosh, A., Johnson, E.A. and Krishnamachari, B., 2013. Energy-efficient deployment strategies in structural health monitoring using wireless sensor networks. *Structural Control and Health Monitoring*, *20*(6), pp.971-986.

110. Tran-Ngoc, H., Khatir, S., De Roeck, G., Bui-Tien, T., Nguyen-Ngoc, L. and Abdel Wahab, M., 2018. Model updating for Nam O bridge using particle swarm optimization algorithm and genetic algorithm. *Sensors*, *18*(12), p.4131.

111. Tran-Ngoc, H., He, L., Reynders, E., Khatir, S., Le-Xuan, T., De Roeck, G., Bui-Tien, T. and Wahab, M.A., 2020. An efficient approach to model updating for a multispan railway bridge using orthogonal diagonalization combined with improved particle swarm optimization. *Journal of Sound and Vibration*, *476*, p.115315.

Artificial Intelligence and Structural Health Monitoring.